Experimental investigation and analysis of the nonlinear response of turbulent swirl-stabilized flames

vorgelegt von
Sebastian Schimek,
Diplom-Ingenieur,
aus Berlin

Von der Fakultät V – Verkehrs- und Maschinensysteme
der Technischen Universität Berlin
zur Erlangung des akademischen Grades

Doktor der Ingenieurwissenschaften
– Dr.-Ing. –

genehmigte Dissertation

Promotionsausschuss:

Vorsitzender: Prof. Dr.-Ing. Roland Baar
Gutachter: Prof. Dr.-Ing. Christian Oliver Paschereit
Gutachter: Prof. Dr. Ephraim Gutmark
Gutachter: Prof. Dr. Nicolas Noiray
Tag der wissenschaftlichen Aussprache: 25. Mai 2016

Berlin 2016

Danksagung

Diese Dissertation ist während meiner Tätigkeit als wissenschaftlicher Mitarbeiter am Institut für Strömungsmechanik und Technische Akustik der Technischen Universität Berlin entstanden. Neben dem Projekt "Nichtlineare Flammentransferfunktionen", aus welchem die hier dargestellten Publikationen hervorgingen, habe ich am Fachgebiet für Experimentelle Strömungsmechanik in den letzten neun Jahren an vielen weiteren interessanten Projekten mitgewirkt, insbesondere auf dem Gebiet der Nassen Verbrennung. Mein Doktorvater, Prof. Dr.-Ing. Christian Oliver Paschereit, brachte mir stets großes Vertrauen entgegen und gewährte mir viele Freiheiten bei der Arbeit an diesen Projekten. Ich bin ihm nicht nur für die fachlichen Kenntnisse, die ich unter seiner Leitung erwerben konnte, zutiefst dankbar, sondern insbesondere auch für alles über das Wissenschaftliche hinaus, das er mir in dieser Zeit vermittelt hat. Ich freue mich sehr, dass ich auch weiterhin die Möglichkeit haben werde mit ihm zusammenzuarbeiten.
Ein besonderer Dank gilt auch den weiteren Gutachtern dieser Dissertation, Prof. Dr. Nicolas Noiray und Prof. Dr. Ephraim Gutmark, für die schnelle Begutachtung der Arbeit und die konstruktiven Fragen während der wissenschaftlichen Aussprache. Prof. Dr.-Ing. Roland Baar leitete auf erfreulich unkomplizierte Weise das Promotionsverfahren.
Für die finanzielle Förderung des Forschungsvorhabens "Nichtlineare Flammentransferfunktionen" möchte ich mich bei der Forschungsvereinigung Verbrennungskraftmaschinen e.V. (FVV, Frankfurt) bedanken. Das Vorhaben wurde von einem Arbeitskreis der FVV begleitet, welchem mein Dank für die stets angenehme Arbeitsatmosphäre und die große Unterstützung während der Bearbeitung des Projektes gebührt. Dr. Bruno Schuermans leitete den Arbeitskreis. Ich danke ihm dafür, dass er stets bei Fragen oder Problemen ein offenes Ohr hatte und mit seiner freundlichen Art beratend zur Seite stand. Seine Bereitschaft, ebenfalls als Gutachter in meinem Promotionsausschuss mitzuwirken, hätte ich sehr gerne in Anspruch genommen, wenn nicht terminliche Gründe im Weg gestanden hätten. Außerdem bedanke ich mich bei den hilfsbereiten Kollegen, die mich durch das gewissenhafte Korrekturlesen der Arbeit unterstützt haben: Joshua Gray, Dr. Kilian Oberleithner, Dominik Waßmer, Phoebe Kuhn und Georg Mensah.
Gerade in der Anfangsphase meiner Arbeit am Fachgebiet habe ich als sehr junger Mitarbeiter von meinen Kollegen Prof. Dr.-Ing. Jonas Moeck, Dr. Mirko Bothien, Dr. Arnaud Lacarelle und Daniel Guyot viel Unterstützung erfahren und durfte viel lernen. Insbesondere die bis heute fortwährende große geduldige Unterstützung durch Jonas, welche einen großen Einfluss auf meine wissenschaftlichen Arbeiten hatte und hat, möchte ich hervorheben. Die beiden weiteren Mitautoren meiner zweiten hier diskutierten Publikation,

Dr. Bernhard Cosic und Dr. Steffen Terhaar, haben mit mir über viele Stunden zugebracht, um die Messdaten zu analysieren und viele konstruktive Gespräche zu führen. Bei Dr. Kilian Oberleithner möchte ich mich nicht nur für die großartige Stabilitätsanalyse bedanken, sondern auch für seine große Geduld mit der er mir in vielen mehrstündigen Gesprächen alle meine Fragen zu diesem Thema beantwortet hat. Bei meinen Studenten Sascha Marder, Dr. Hanns Müller-Vahl, Ricardo Mevert und David Antes möchte ich mich für ihre fleißige Arbeit bedanken.
Bei einem Blick auf die wissenschaftlichen Mitarbeiter des Fachgebietes fällt es mir schwer Einzelne herauszuheben, da ich über die Jahre mit fast allen einmal einige Zeit zusammenarbeiten durfte, was nicht nur fachlich stets sehr erfreulich war, sondern meist auch darüber hinaus mehr als einen rein kollegialen Umgang darstellte. Es haben sich hier viele Freundschaften entwickelt, für die ich sehr dankbar bin. Euch alle hier aufzuzählen, würde wohl den Rahmen sprengen, daher möchte ich nur einige wenige nennen. Mit meinen Büropartnern Dr. Katharina Göckeler und Dr. Panagiotis Stathopoulos hatte ich nicht nur bei der täglichen Arbeit viel Spaß, sondern auch viele tolle Dinge abseits der Arbeit erleben. Für die unzähligen investierten Stunden in die Software für unsere Verbrennungsprüfstände möchte ich mich bei Kevin Thommes und David Holst bedanken. Durch ihre inzwischen langjährige Erfahrung im Umgang mit unseren Prüfständen war Phoebe Kuhn stets ein kompetenter Ansprechpartner bei Problemen mit unserem Equipment oder bei der Erweiterung neuer Komponenten - immer gut gelaunt und hilfsbereit. Navid Nayeri, der unser Fachgebiet zusammenhält war mir bei vielen strategischen Fragen im Umgang mit der Verwaltung und den einzelnen Abteilungen der Universität eine große Hilfe.
Ohne die große Unterstützung durch unser zuverlässiges Team im Sekretariat, Lilli Lindemann, Kristin Halboth, Sandy Meinecke und Maria Lück, das stets gute Laune verbreitet und für alle Fragestellungen Lösungsvorschläge parat hat, wäre ich wohl an so mancher bürokratischer Herausforderung gescheitert. In der Werkstatt des Fachgebietes haben mich während meiner Tätigkeit insbesondere Wilfried Postel, Axel Bendix, Manfred Ziehe, Horst Mettchen und Thorsten Dessin nicht nur dadurch unterstützt, dass sie die beauftragten Teile mit hoher Zuverlässigkeit und Genauigkeit gefertigt haben und durch ihr stetiges aktives Mitdenken so manchen konstruktiven Fehler von mir beseitigt haben, bevor das Teil gefertigt wurde. Insbesondere waren sie auch immer wieder geduldig dabei, Lösungen mitzuentwickeln und haben mir nebenbei viele Grundlagen in der Metallverarbeitung beigebracht. Zahlreiche Stunden hat Thorsten mich dabei unterstützt, die Zeichnungen für meinen Versuchsstand zu erstellen. Auch andere Projekte, wie den Bau der Brennkammer II oder des Energielabors, hätte ich ohne seine Unterstützung nicht in dieser Form realisieren können.
Alleine beim Bau des Energielabors haben wir ca. 8 km Kabel durch Studenten verlegen lassen, welche nach sorgfältig erstellten Listen und Plänen in etlichen Schaltschränken, Sensoren und Aktuatoren münden. Über meine gesamte Zeit am Fachgebiet ist das nur ein kleiner Teil dessen, wobei mich Heiko Stolpe, Felix Hase und Colin Muxlhanga unterstützt haben. Gerade bei Problemstellungen, die zwar weniger aufwändig, dafür aber deutlich komplexer waren, hat sich nicht selten gezeigt, dass Heiko ein unverzichtbarer Teil unserer Arbeitsgruppe ist, dessen Engagement genauso wie bei Thorsten Dessin und Andy Göhrs nach Feierabend definitiv noch nicht am Ende ist. Dass Lösungen zuverlässig gefunden und umgesetzt werden, habe ich auch bei Andy Göhrs und Robert Bahnweg erfahren dürfen. Ohne die zahlreichen Umbauten und die Durchführung von Messungen durch Andy, wären

meine Ergebnisse in dieser Form an vielen Stellen wohl nicht zustandegekommen. Frau Pätzold und Nico Seifert danke ich für ihren hilfreichen Einsatz als Systemadministratoren. Zu guter Letzt danke ich meiner Familie, insbesondere meiner Frau Katharina, für ihre liebevolle Unterstützung. Besonders in den vergangenen Wochen hat sie mir den Rücken weitgehend freigehalten, sodass mein Fokus voll und ganz auf der Fertigstellung meiner Promotion liegen konnte.

Sebastian Schimek

Zusammenfassung

Um eine niedrige Schadstoffemission bei der Stromerzeugung zu realisieren, wird bei den meisten Gasturbinen die magere Vormischverbrennung genutzt. Jedoch neigt diese Verbrennungstechnologie zu thermoakustischen Instabilitäten. Diese entstehen infolge einer Wechselwirkung zwischen der instationären Wärmefreisetzung der Flamme und dem akustischen Feld in der Maschine und können sehr starke Druckschwankungen verursachen. Um einer Beschädigung der Gasturbine vorzubeugen, müssen diese daher vermieden werden. Dies führt häufig zu einer Einschränkung des Betriebsbereiches. Stand der Technik ist die Anwendung linearer Netzwerkmodelle bei der Entwicklung von Gasturbinenbrennkammern, um das mögliche Auftreten thermoakustischer Instabilitäten in Abhängigkeit des Betriebspunktes vorherzusagen. Aufgrund ihres linearen Charakters eignen sich diese Modelle jedoch nicht für Vorhersagen der auftretenden Druckamplituden. Diese sind notwendig, um zu beurteilen, ob eine bestimmte Instabilität tatsächlich eine Gefährdung für die Maschine darstellt oder temporär während des Betriebs toleriert werden kann. Hierfür ist die Erweiterung der Modelle um die amplitudenabhängige Flammenantwort, die sogenannte *flame describing function* notwendig.
Viele Mechanismen, welche für die Flammenantwort auf akustische Störungen verantwortlich sind, wurden in der Vergangenheit bezüglich ihres möglichen Anteils am nichtlinearen Verhalten der amplitudenabhängigen Flammenantwort untersucht. Hierzu zählen beispielsweise Schwankungen des Äquivalenzverhältnisses, Fluktuationen der Flammenoberfläche, Schwankungen der Drallzahl und die Anregung kohärenter Strukturen. Dennoch bleibt die quantitative Vorhersage von Nichtlinearitäten und Sättigungen der amplitudenabhängigen Flammenantwort eine Herausforderung.
In der vorliegenden Arbeit werden drei Publikationen zusammengefasst und erörtert, welche sich mit experimentellen Untersuchungen der amplitudenabhängigen Flammenantwort in einem atmosphärischen, drallstabilisierten, mageren Vormischbrenner mit hoher Reynoldszahl befassen. Die Flammenantwort auf akustische Anregung über einen breiten Frequenzbereich wurde mittels OH^* Chemolumineszenz gemessen. Akustische Anregungsamplituden, bis hin zu Geschwindigkeitsfluktuationen welche der Größenordnung der mittleren Geschwindigkeit im Brenner entsprechen, wurden hierbei verwendet. OH^* Chemolumineszenz-Bilder der Flamme und Strömungsfelder wurden für verschiedene Anregungsfälle untersucht. Hierbei wurde beobachtet, dass viele Sättigungen der amplitudenabhängigen Flammenantwort von Änderungen des gemittelten Strömungsfeldes und der mittleren Flammenform in der Brennkammer abgeleitet werden können. Systematische Änderungen des

mittleren Strömungsfeldes und der mittleren Flammenform bei wachsenden Anregungsamplituden, welche einen signifikanten Einfluss auf den Betrag und die Phase der Flammenantwort haben, wurden beobachtet. Bei einer hydrodynamischen linearen Stabilitätsanalyse wurde eine starke Korrelation zwischen der Sättigung der Verstärkung kohärenter Strukturen durch die Scherschichten in der Brennkammer und Sättigungen in der amplitudenabhängigen Flammenantwort gefunden.

Abstract

In order to meet low emission standards, modern gas turbines are mostly operated in lean premixed combustion mode. This technology is prone to thermoacoustic pulsations, which are an interaction of the unsteady heat release of the flame and the acoustic field in the engine. These instabilities are associated with high-amplitude pressure pulsations which have to be avoided. To prevent resulting damage of the gas turbine, operating conditions often have to be constricted. Linear network models are state of the art in the development process of gas turbine combustors for predicting the possible occurrence of thermoacoustic instabilities for certain operating conditions. Due to their linear nature, these methods are not capable of predicting the resulting finite pressure amplitudes associated with a certain instability. The amplitude dependent response of the flame to acoustic perturbations, the so-called flame describing function, has to be known in order to predict the occurring pressure spectra and estimate whether a certain thermoacoustic instability may harm the engine or can be temporally tolerated during operation.
Several mechanisms involved in the flame response to acoustic perturbations have been studied in the past regarding their possible responsibility for the occurrence of nonlinearities in the flame describing function, e.g., equivalence ratio oscillations, flame front fluctuations, swirl number fluctuations or the excitation of coherent structures. However, the quantitative prediction of saturations and nonlinearities of the flame describing function remains challenging.
The present work summarizes and discusses three publications experimentally investigating the flame describing function of an atmospheric swirl stabilized, lean, premixed combustor at high Reynolds numbers. The heat release response in terms of OH^* chemiluminescence fluctuations to acoustic forcing up to acoustic velocity fluctuations on the order of the mean flow velocity is investigated over a broad frequency range. OH^* chemiluminescence images and flow field measurements are analyzed for various forcing conditions. It is observed that several saturations in the flame describing function can be explained by means of average quantities of the flow field and the flame in the combustion chamber during oscillation. Systematic changes of the flow field and flame shape with increasing oscillation amplitudes are observed that have a significant influence on the gain and the phase of the flame describing function. A hydrodynamic linear stability analysis is carried out, which shows a strong correlation between the saturation of the amplification of coherent structures in the shear layers in the combustor flow and saturations in the flame describing function.

Contents

Nomenclature

Latin letters

$\dot{m}$	Mass flow rate
Re_t	Turbulent Reynolds number
A	Acoustic transfer matrix
a	Arbitrary quantitie
$A_{11}, A_{12}, A_{21}, A_{22}$	Elements of the acoustic transfer matrix
c	Speed of sound
E_a	Acoustic energy
F	Gain of flame describing function
f	Upstream traveling acoustic wave
F, G, H	Eigenfunctions of the axial, radial and azimuthal velocity
FDF	Flame describing function
g	Downstream traveling acoustic wave
I	Chemiluminescence intensity
k	Wave number
LHV	Lower heating value
M	Mach number
m	Azimuthal wave number
n	Unit vector
P	Eigenfunctions of pressure
p	Pressure
Q	Integrated heat release
q	Volumetric heat release

R	Reflection coefficient
r	Radius
T	Temperature
u	Velocity
V	Volume
x	Space variable
Z	Acoustic impedance

Greek letters

α	Axial wave number
Δ	Difference
γ	Ratio of specific heat capacities
∇	Nabla operator
ω	Angular frequency
ϕ	Equivalence ratio
ρ	Density
φ	Phase

Subscripts, superscripts and symbols

$(\cdot)'$	Fluctuations
$(\cdot)^c$	Coherent part
$(\cdot)^s$	Stochastic part
$(\cdot)_0$	Mean value
$(\cdot)_\theta$	Azimuthal component
$(\cdot)_d$	Downstream
$(\cdot)_r$	Radial component
$(\cdot)_u$	Upstream
$(\cdot)_x$	Axial component
$\hat{(\cdot)}$	Fourier transform
∞	Infinity
$\partial_{(\cdot)}$	Partial derivative with respect to $(\cdot)$

$\mathfrak{R}$	Real part

Abbreviations

FDF	Flame Describing Function
FTF	Flame Transfer Function
LDA	Laser Doppler Anemometry
MMM	Multi Microphone Method
PIV	Particle Image Velocimetry

Publications

$\mathfrak{A}$	Schimek, S., Moeck, J. P., and Paschereit, C. O., 2011. An Experimental Investigation of the Nonlinear Response of an Atmospheric Swirl-Stabilized Premixed Flame. *Journal of Engineering for Gas Turbines and Power* , 133(10), p. 101502.
$\mathfrak{B}$	Schimek, S., Cosic, B., Moeck, J. P., Terhaar, S., and Paschereit, C. O., 2014. Amplitude-dependent flow field and flame response to axial and tangential velocity fluctuations. *Journal of Engineering for Gas Turbines and Power*, 137(8), Dec., p. 081501.
$\mathfrak{C}$	Oberleithner, K., Schimek, S., and Paschereit, C. O., 2015. Shear flow instabilities in swirl-stabilized combustors and their impact on the amplitude dependent flame response: A linear stability analysis. *Combustion and Flame*, 162(1), Jan., pp. 8699.

Chapter 1

Introduction

Energy. Probably one of the most challenging tasks of the 21st century is the supply of the population and industry with energy - electricity and heat - while saving the environment from pollution, decelerating the depletion of fossil energy sources and moving our energy generation towards more renewable resources.

The increasing supply of renewable energies into the grid enhances the challenge of balancing the demand and generation of electrical power. Figure 1.1 (top) shows the demand of electrical energy and the generation from solar and wind on an example summer day in a grid. A strong challenge of changing the electrical power generation further to renewables is that their availability does not coincide with the demand in the grid, leading to a net load that has to be generated by different energy sources. The continuously growing share of renewables in the energy market will enhance this problem and lead to steeper gradients in the net energy as indicated by the so-called California Duck Curve (fig. 1.1 bottom). In order to deal with this problem, flexible fossil power generation will be needed until eventually other technologies are available in the future. Currently, gas turbines are the only energy conversion technology that is available in large-scale applications and is capable of providing sufficiently fast ramp-up times to compensate for the resulting mismatch.

In order to meet the requirements of ultra low emission gas turbines, modern combustion systems mostly rely on swirl stabilized, lean premixed combustion. A strong susceptibility of this type of combustion to thermoacoustic instabilities makes a detailed understanding of related processes indispensable. These instabilities arise from the interaction of the unsteady heat release in the flame and the acoustic field in the combustor. If the two mechanisms constructively interfere, high-amplitude pressure pulsations occur, which have a detrimental effect on the combustion process [1] and the engine life. For safe operation of gas turbines without the occurrence of thermoacoustic instabilities, the operational ranges must often be constricted.

Linear thermoacoustic models of premixed combustion systems have been widely used to predict the linear system stability (see Dowling and Stow [2] or Paschereit et al. [3]). These methods are state of the art and standardly applied in the development phase of gas turbine combustion chambers. Due to their linear character, these network models do not predict amplitudes of instable system oscillations, but only frequencies where the system is linearly

unstable. However, for an estimation of whether a certain instability is harmful for the engine or can be temporally tolerated during operation, the amplitude of the pressure pulsations must be known. The response of the flame to the acoustic field in a combustion chamber, mainly velocity fluctuations, at high amplitudes is of non-linear character, e.g., a saturation of the flame response. These effects mainly determine the finite oscillation amplitude of the system, the limit cycle. Several studies [4–7] showed that limit cycle amplitudes can be predicted if the amplitude-dependent acoustic flame transfer function, the so-called flame describing function [4, 5] is available from models or experimental or numerical data.

In order to investigate the response of flames to an acoustic field, a common approach is to measure the flame behavior when exposed to an artificial acoustic field, for example, generated by loudspeakers in a laboratory. Nonlinear effects, like saturation in the flame response of industrial-type swirl burners, are often assumed to set in at velocity oscillation amplitudes that are on the order of the mean flow [8, 9]. Therefore, one of the key challenges in the presented project was the design of a test rig with a forcing device providing forcing amplitudes on that order of magnitude over a broad frequency range in order to measure nonlinearities in the flame response.

Several mechanisms responsible for the linear flame response and observed in association with the occurrence of nonlinearities in the flame describing function have been identified in the past, e.g., equivalence ratio oscillations [10–12], flame front fluctuations [13, 14], swirl number fluctuations [15] or the excitation of coherent structures [9, 13, 16, 17]. However, the quantitative prediction of saturations and nonlinearities of the flame describing function remains challenging. Dowling [4] argued that the heat release may not become negative during an oscillation and modeled nonlinearities with symmetric limitation of the heat release with good agreement to experimental data. However, in practice, heat release fluctuations of amplitudes higher than 100% of the mean can be observed, for example, in the present measurement data, that are caused by a strongly non-sinusoidal flame response. Peracchio and Proscia [18] modeled the nonlinear flame response in terms of a limitation of equivalence ratio fluctuations. However, comprehensive models that are not based on a limitation of the heat release, but cope with hydrodynamic effects of the flow field or the dynamics of the flame front are currently not available.

The increase of the generation of coherent structures due to high amplitude forcing resulting in wrinkling of the flame front and their impact on the flame describing function have been studied by Armitage et al. [17]. Furthermore, vortices shed at the combustion chamber inlet are known to locally change the turbulent flame speed, leading to an upstream propagation of the flame and associated flame front oscillations [19]. The amplification of coherent structures can be predicted with linear hydrodynamic stability analysis, which is based on the eigenvalue problem of the Orr-Sommerfeld equation in conjunction with an eddy viscosity model. Although the linear hydrodynamic stability has been studied for several decades [20–23], it just recently became a focus of the combustion community. O'Connor and Lieuwen [24] emphasized the importance of the associated amplification of coherent structures on the flame response. Several studies investigating the hydrodynamic stability in combustor flows deal with the well-known single helical instability precessing vortex

core [25]. However, helical, skew-symmetric fluctuations do not change the global heat release of the flame [26] and, hence are not the scope of the present investigation.

In the scope of this thesis, a test rig was developed that meets the requirement of providing sufficiently high forcing amplitudes over the entire frequency regime investigated by combining four 18-inch subwoofers with a variable upstream impedance, enabling resonant forcing. The forcing characteristics were compared to simulations of a 1-D network model that was used in the design phase. The high-amplitude forcing capabilities of the test rig were used to assess the nonlinearity of the acoustic damping in the burner and at the outlet boundary condition [27].

Within two measurement campaigns the experimental data discussed within this document were collected. The resulting publications given in chapter 4 are in the following referred to as:

- $\mathfrak{A}$: Schimek, S., Moeck, J. P., and Paschereit, C. O., 2011. An Experimental Investigation of the Nonlinear Response of an Atmospheric Swirl-Stabilized Premixed Flame. *Journal of Engineering for Gas Turbines and Power* , 133(10), p. 101502. DOI:10.1115/1.4002946

- $\mathfrak{B}$: Schimek, S., Cosic, B., Moeck, J. P., Terhaar, S., and Paschereit, C. O., 2014. Amplitude-dependent flow field and flame response to axial and tangential velocity fluctuations. *Journal of Engineering for Gas Turbines and Power*, 137(8), Dec., p. 081501. DOI:10.1115/1.4029368

- $\mathfrak{C}$: Oberleithner, K., Schimek, S., and Paschereit, C. O., 2015. Shear flow instabilities in swirl-stabilized combustors and their impact on the amplitude dependent flame response: A linear stability analysis. *Combustion and Flame*, 162(1), Jan., pp. 8699. DOI:10.1016/j.combustflame.2014.07.012

In $\mathfrak{A}$, the nonlinear flame response to various forcing amplitudes over a broad frequency range is investigated. Several mechanisms associated with saturation are identified. It is observed that the main properties of the flame, i.e., the average flame shape, undergoes changes while the forcing amplitude increases. $\mathfrak{B}$ focuses on changes of the flow field under forcing. The interaction of coherent structures with the flame front and the occurrence of swirl number fluctuations are investigated. In accordance to the findings in $\mathfrak{A}$, systematic changes of the mean flow field with varying forcing amplitudes are identified. A linear hydrodynamic stability analysis is applied to the mean flow fields in $\mathfrak{C}$. The changes of the mean flow field are shown to result in significant changes of the amplification properties of the shear layers to coherent structures. A strong correlation between the hydrodynamic effects in the shear layers and the nonlinear flame response is identified.

The remainder of this document is structured as follows: In chapter 2 the fundamentals underlying the presented research are given. Chapter 3 roughly explains the applied measurement techniques. A detailed description of the setups used, is provided in the respective

publications which are given subsequently. Finally, the results of the publications are discussed and their importance for a step forward to a comprehensive understanding of the flame dynamics at high pulsation amplitudes is shown in chapter 5.

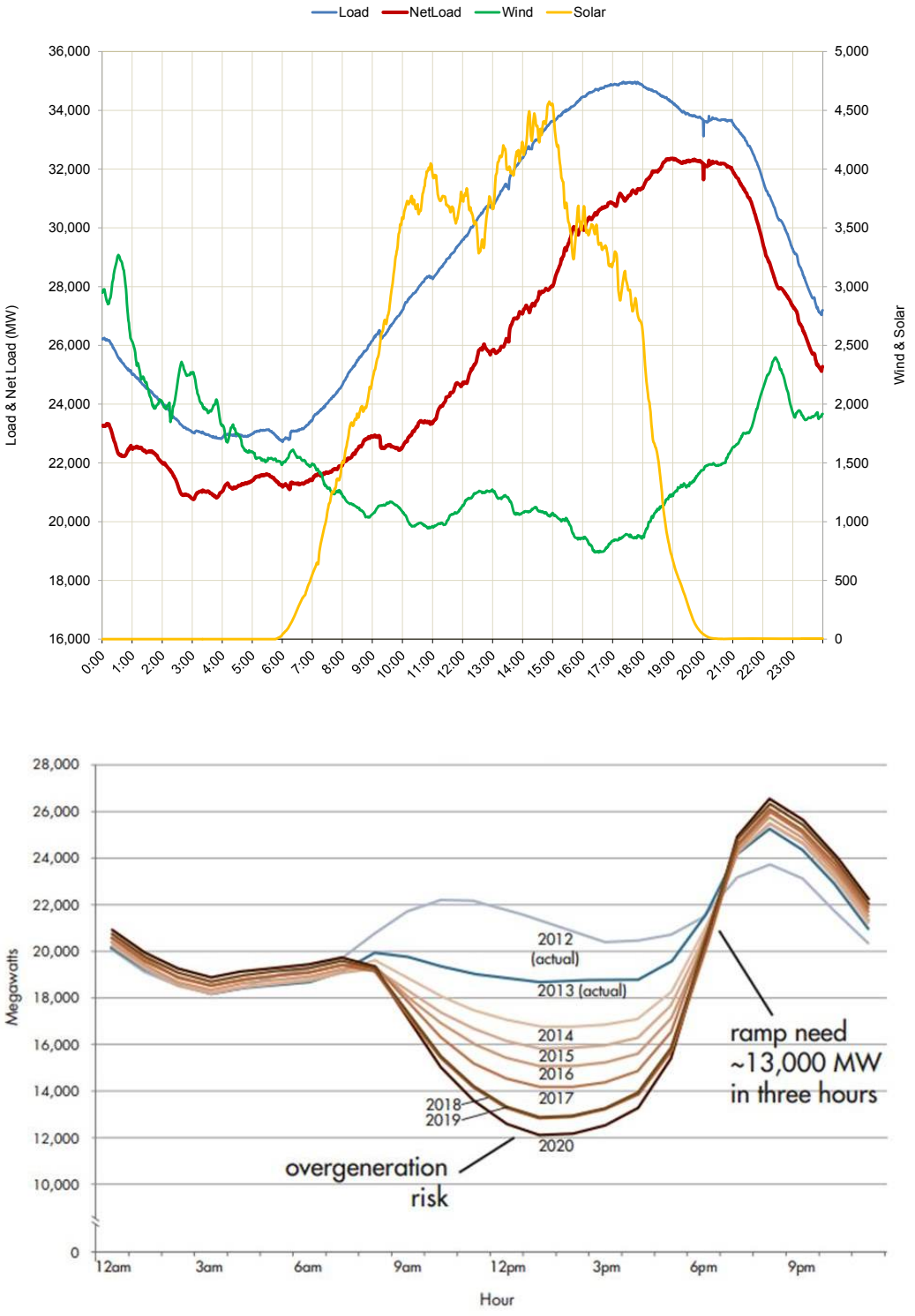

Figure 1.1: Top: Example fluctuation of electrical load and production of electricity from solar and wind power; bottom: California Duck curve - Increasing penetration of renewables in the energy market raise the need of flexible energy production; Source: California ISO

Chapter 2

Fundamentals

Thermoacoustic instabilities arise from the constructive interaction of the acoustic field in a combustor and the unsteady heat release of the flame. In order to understand, predict and avoid the resulting high amplitude pressure fluctuations, detailed knowledge of the acoustic properties of the confining system and the mechanisms leading to an unsteady heat release of the flame is crucial. Throughout this work the acoustic field in the combustor is considered to be one-dimensional. The resulting description of the acoustic properties is rather simple and, therefore, the fundamentals are only briefly introduced in the following. For a more detailed description of the acoustic fundamentals, see references [28–32]. Subsequently, the heat release response to perturbations is discussed.

Some references [28–30, 33] give a very good summary of the underlying mechanisms and were frequently consulted throughout the practical work and the writing of this thesis.

2.1 Acoustics

2.1.1 Wave equation

Rienstra and Hirschberg [31] give the following derivation for the wave equation. Linearizing the mass and momentum conservation equations in a quiescent fluid and neglecting body forces, source terms and viscous effects, one obtains the linear acoustic equations as

$$\partial_t \rho' + \rho_0 \nabla \cdot u' = 0 \tag{2.1}$$

$$\rho_0 \partial_t u' + \nabla p' = 0, \tag{2.2}$$

where ρ_0 is the mean density, and ρ', u', and p' are the fluctuations of density, velocity and pressure. Subtracting the time derivative of equation 2.1 from the divergence of equation 2.2, one obtains the acoustic wave equation

$$\partial_t^2 \rho' - \nabla^2 p' = 0. \tag{2.3}$$

The linearized constitutive equation, given by

$$p' = c^2 \rho', \tag{2.4}$$

where c is the speed of sound, leads to the (classic) wave equation

$$\partial_t^2 p' - c^2 \nabla^2 p' = 0 \tag{2.5}$$

and its Fourier transform, the Helmholtz equation

$$\omega^2 \hat{p} + c^2 \nabla^2 \hat{p} = 0, \tag{2.6}$$

with the angular frequency ω. A one-dimensional solution of equation 2.6 is d'Alembert's solution

$$\hat{p}(\omega, x) = \hat{f} e^{-ikx} + \hat{g} e^{ikx}, \tag{2.7}$$

with the Riemann invariants $\hat{f}(\omega, x)$ and $\hat{g}(\omega, x)$ giving the complex amplitudes of the upstream and downstream traveling waves, and the wave number $k = \omega/c$. The space variable x denotes the axial position in the one-dimensional duct. Thus, this equation is only valid for planar waves with wave lengths much longer than the diameter of the duct. This work neglects in the following the existence of higher modes (azimuthal and radial modes) as these decay very fast at the relatively low frequencies investigated throughout this work (cut-off modes) [31]. In the case of axial flow in the duct, equation 2.7 is extended to account for the influence of the Mach number M of the mean flow in the following way

$$\hat{p}(\omega, x) = \hat{f} e^{-ikx \frac{1}{1+M}} + \hat{g} e^{ikx \frac{1}{1-M}}. \tag{2.8}$$

An analogous representation of the acoustic field can be given by introducing the acoustic velocity $\hat{u}$:

$$\hat{u}(\omega, x) = \frac{1}{\rho c} (\hat{f} e^{-ikx \frac{1}{1+M}} - \hat{g} e^{ikx \frac{1}{1-M}}). \tag{2.9}$$

The present work deals with high acoustic amplitudes where acoustic velocity fluctuations on the order of magnitude of the mean velocity in a combustor are reached. However, the acoustic displacement is small compared to the acoustic wavelength, which allows for the use of the linear acoustic equations [31].

2.1.2 Boundary conditions

Equation 2.8 gives an infinite number of solutions for the planar acoustic field in an acoustic element, e.g., a duct. In order to determine the physically correct solution, boundary conditions have to be taken into account. The boundary condition can be expressed by the impedance $Z(\omega, x)$

$$Z = \frac{\hat{p}}{\hat{u} \cdot n}, \tag{2.10}$$

where n is the unit vector pointing outward normal to the boundary surface. At a closed end of a duct, the acoustic velocity is zero (velocity node), leading to an infinite impedance. On the other side at an open ended duct, the surrounding pressure is imposed and the acoustic pressure fluctuation becomes zero (pressure node), leading theoretically to an impedance of zero. For practical applications, approximations for various duct ends, such as unflanged ends [34, 35], flanged ends [35, 36], or ends consisting of an orifice [37, 38] can be found in literature.

Representing the acoustic field as the Fourier transform of complex upstream and downstream traveling waves $\hat{f}$ and $\hat{g}$, the boundary condition can be defined as a reflection coefficient R, relating the reflected and the incident wave to each other:

$$R(\omega) = \frac{\hat{g}(x,\omega)}{\hat{f}(x,\omega)}. \tag{2.11}$$

The reflection coefficient and impedance are related to each other as

$$R = \frac{Z-1}{Z+1} \quad and \quad Z = \frac{1+R}{1-R}. \tag{2.12}$$

2.2 1-D network modeling

In the acoustic analyis of combustion systems, it is common to separate the entire system into individual elements which are described as acoustic four-poles [1] (fig. 2.1). Each element is characterized by a frequency-dependent transfer matrix which relates the acoustic quantities on one side of the element to those corresponding to the other side of the element (here referred to as upstream and downstream). The acoustic field on the two sides of a four-pole element is often represented with either

- upstream and downstream traveling waves ($\hat{f}(x,\omega)$ and $\hat{g}(x,\omega)$)
- acoustic pressure and acoustic velocity ($\hat{p}(x,\omega)$ and $\hat{u}(x,\omega)$)

These representations are equivalent, which means they can be deduced from each other.

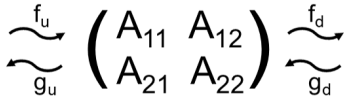

Figure 2.1: Acoustic element - represented as a four-pole element with upstream and downstream traveling waves.

Generally, for the thermodynamic analysis of single flames with the network modeling approach, it is assumed that it is sufficient to focus on planar acoustic waves, since the wavelength is large compared to all characteristic diameters (cut-off frequencies). This assumption must be taken with care, since especially the distance between the burner and the flame is very small and the decay of complex acoustical structures and higher dimensional interactions of two adjacent elements cannot be excluded. Under these assumptions,

a decomposition of a complex acoustic system into its basic components can be done.
Following the network approach, an acoustic element is characterized by a transfer matrix

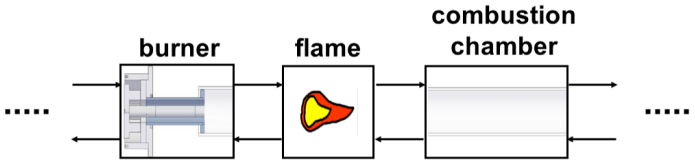

Figure 2.2: Network model, composed from basic acoustic elements

A, which relates acoustic pressure and velocity upstream and downstream of the element in the frequency domain

$$\begin{pmatrix} \hat{p}_2 \\ \hat{u}_2 \end{pmatrix} = \begin{pmatrix} A_{11} & A_{12} \\ A_{21} & A_{22} \end{pmatrix} \begin{pmatrix} \hat{p}_1 \\ \hat{u}_1 \end{pmatrix}. \tag{2.13}$$

The pressure is scaled with the characteristic impedance ρc (ρ denoting the density and c the speed of sound). An acoustic system can be represented by combining the corresponding transfer matrices of the individual elements (e.g., ducts, area discontinuities, etc.).

2.3 Heat release–acoustic interaction

Thermoacoustic instabilities result from a coupling of the unsteady heat release of the flame and the acoustic field in the combustor. Acoustic waves emitted by the flame due to unsteady heat release are reflected from the acoustic boundaries of the system. When the reflected waves interfere constructively with the flame, i.e., if the flame amplifies the acoustic waves, resonance of the system may occur.

2.3.1 Wave equation including unsteady heat release

The one-dimensional homogeneous wave equation 2.5 becomes inhomogeneous when extended by a source term which represents the unsteady heat release [2]:

$$\partial_t^2 p' - c^2 \partial_x^2 p' = (\gamma - 1)\partial_t q'. \tag{2.14}$$

γ is the ratio of the specific heat capacities and $q'(x,t)$ is the unsteady component of the volumetric heat release.

2.3.2 Flame response to acoustic perturbations – mechanisms

The acoustic field in a combustor as well as its interaction with the heat release oscillations are generally very well understood and can be solved analytically with the equations given above. The most complex part of modeling the thermoacoustic behavior of a combustor is the flame response to the acoustic field. Because of the variety of mechanisms involved

leading to the heat release fluctuations due to acoustic perturbations, only several distinct mechanisms are discussed in this section. A more detailed overview of thermoacoustic mechanisms can be found in Keller [39] or Lieuwen et al. [32]

Assuming a complete reaction of the fuel injected into a combustion chamber, the heat release is given by:

$$q = \dot{m}\phi LHV. \tag{2.15}$$

$\dot{m}$, ϕ, and LHV are the current mass flow of combustible mixture through the flame surface, the equivalence ratio of fuel and air and the lower heating value of the fuel. Assuming the latter to be constant, the linearized, normalized fluctuation of heat release can be derived from [40] equation 2.15 as

$$\frac{q'}{q} = \frac{\dot{m}'}{\dot{m}} + \frac{\phi'}{\phi}. \tag{2.16}$$

Several mechanisms of the interaction between fluctuations in the heat release and thermoacoustic instabilities have been extensively investigated in the past. According to Huang and Yang [41], instabilities with associated frequencies below 30-50 Hz are often associated with entropie wave or to blow off phenomena, which may occur when combustors are operated close to lean blow-out. For higher frequencies, the two mechanisms described by equation 2.16 are dominant, i.e., equivalence ratio fluctuations and fluctuations in the consumption rate of the combustible mixture. The latter are generally associated with flame front fluctuations. For transverse or azimuthal acoustic modes, also frequencies much higher than 1000 Hz may occur (high frequency instabilities). In this study, the occurrence of azimuthal modes is neglected.

2.3.2.1 Equivalence ratio fluctuations

In order to have the high mixing quality of fuel and oxidizer necessary for an efficient combustion with low emissions, the injection of gaseous fuel in gas turbine combustors is generally realized with high momentum through small holes or slots and often perpendicular with respect to the main flow. The high velocities in the fuel system and the resulting high pressure drop over the injector lead to a high impedance of the fuel system. At thermoacoustic instabilities or acoustic forcing, velocity fluctuations of the air mass flow at the fuel injectors cause fluctuations in the fuel concentration, since the fuel mass flow is rather constant due to the high stiffness of the fuel system.

Equivalence ratio fluctuations are known to be one of the dominant mechanisms of thermoacoustic instabilities. An increase of the equivalence ratio during a fraction of one oscillation increases on the one hand the local heat release directly, since the adiabatic flame temperature increases, and on the other hand, the laminar flame speed. Thus, the flame moves upstream and, therefore, increases the amount of gas that is combusted per unit time and, hence, also the heat that is released.

The frequency and amplitude of thermoacoustic oscillations governed by equivalence ratio fluctuations can be predicted very well [18]. Reasonable results can be even achieved by taking only the direct change of heat release into account and neglecting flame surface area fluctuations due to equivalence ratio fluctuations [42].

2.3.2.2 Flame front fluctuations

Acoustic perturbations may alter the heat release due to flame front fluctuations by several mechanisms. Velocity fluctuations at the combustion chamber inlet may result in coherent structures, i.e., vortices that are convected by the flow to the flame front. On the one hand, these vortices may lead to local flame extinction due to flame stretch in terms of strain rate and curvature [43]. On the other hand, vortices may locally increase the turbulence. This leads to an increase of the turbulent flame speed and a temporal propagation of the flame in the upstream direction [19]. Velocity fluctuations at the swirl generator of a combustor lead to two types of fluctuations downstream of the swirler: An axial velocity fluctuation, i.e., an acoustic wave that convects downstream with the speed of sound and a fluctuation of tangential velocity that can be regarded as a perturbation of the hydrodynamic field that convects with the speed of the main flow. Due to the different convection velocities, these two perturbations reach the flame separated by a time lag resulting in swirl number fluctuations that lead to flame front fluctuations [44, 45].

2.3.2.3 Flame Transfer Function (FTF) / Flame Describing Function (FDF)

Due to the complexity of the flame response to perturbations and the variety of mechanisms involved, analytical solutions for the stability of combustion systems generally do not exist. A general black box approach for the response of the flame to acoustic perturbations is given by the flame transfer function, which describes the linear response of the heat release to low amplitude acoustic perturbations. A more general formulation is introduced by the flame describing function, which is an amplitude dependent flame transfer function. The flame is treated as a compact acoustic element that is given by the ratio of the Fourier transforms of the normalized heat release rate fluctuations and the normalized velocity fluctuations at the combustor inlet

$$FDF(\omega, |u'|) = \frac{Q'/Q_{\text{mean}}}{u'/u_{\text{mean}}}, \tag{2.17}$$

where Q is the integral heat release of the flame. As the heat release rate cannot be measured directly, a common assumption is that the flame describing function can be regarded as the ratio of the normalized OH* chemiluminescence intensity fluctuation and the normalized velocity fluctuation

$$FDF(\omega, |u'|) = \frac{I'_{OH^*}/I_{OH^*\text{mean}}}{u'/u_{\text{mean}}}. \tag{2.18}$$

This implies a linear relation between the intensity of the OH* chemiluminescence and heat release. For technically premixed flames, this may introduce a significant error, as

equivalence ratio fluctuations can occur, which have a significant effect on the OH* chemiluminescence [19]. However, all configurations in this document, where this relation is used, are based on perfect premixing of fuel and air far upstream of the combustor, in order to avoid equivalence ratio fluctuations. For cases in which this is not guaranteed, only qualitative effects of the flame dynamics are investigated.

Generally, the flame describing function can be written as

$$FDF(\omega, |u'|) = F(\omega, |u'|)e^{i\varphi(\omega,|u'|)}, \tag{2.19}$$

where $F(\omega, |u'|)$ is the frequency and excitation amplitude dependent gain and $\varphi(\omega, |u'|)$, a frequency and excitation amplitude dependent phase. [4]

2.3.2.4 Rankine-Hugoniot relations

In order to integrate the experimentally obtained or modeled flame describing functions into acoustic network models, the Rankine-Hugoniot relations [46] for low Mach numbers can be applied in order to obtain the flame describing matrix:

$$\hat{p}_2 = \hat{p}_1 \tag{2.20a}$$

$$\hat{u}_2 = [1 + (\frac{T_2}{T_1} - 1)FDF(\omega)]\hat{u}_1. \tag{2.20b}$$

2.4 Acoustic energy balance

In the following section, the gain and the loss of acoustic energy over a compact flame are analyzed. Unsteady heat release of the flame adds acoustic energy to the system under particular conditions, given by the Rayleigh criterion. Assuming linearity of the entire system, the feedback between the acoustic field and the heat release might lead to infinite pulsation amplitudes which physically make no sense. Nonlinearities in the damping of the acoustic waves in the combustion system are briefly discussed before explaining the appearance of limit cycles due to nonlinearities in the flame response.

2.4.1 Rayleigh criterion

The change of acoustic energy due to unsteady heat release is given by [47]

$$\Delta E_a = \int_V \int_T p'(x,t)q'(x,t)dtdV. \tag{2.21}$$

$\Delta E_a > 0$ is a necessary condition for the growth of acoustic energy and the development of a thermoacoustic instability in the system. As can be easily seen, this can only hold true, if the phase difference of pressure fluctuations and heat release fluctuations is smaller than

90. In order to change the stability of a system, it is often sufficient to change the phase relation between pressure and heat release, for example, by adjusting the convective time lags in the flame.

2.4.2 Nonlinear damping

The damping of acoustic waves in combustion chambers is mainly attributed to viscous damping. In addition to damping caused by boundary layers, acoustic waves traveling through the combustor induce vortical structures at area discontinuities. In order to avoid thermoacoustic instabilities, Helmholtz dampers and acoustic liners [48] are frequently used to increase the damping of combustion chambers. The nonlinear behavior of dampers and vortical structures at area discontinuities have been recently studied [49]. In the following, the nonlinear behavior of the damping of the system is neglected and nonlinearities resulting in finite oscillation amplitudes are assumed to originate from the flame dynamics.

2.4.3 Limit cycles

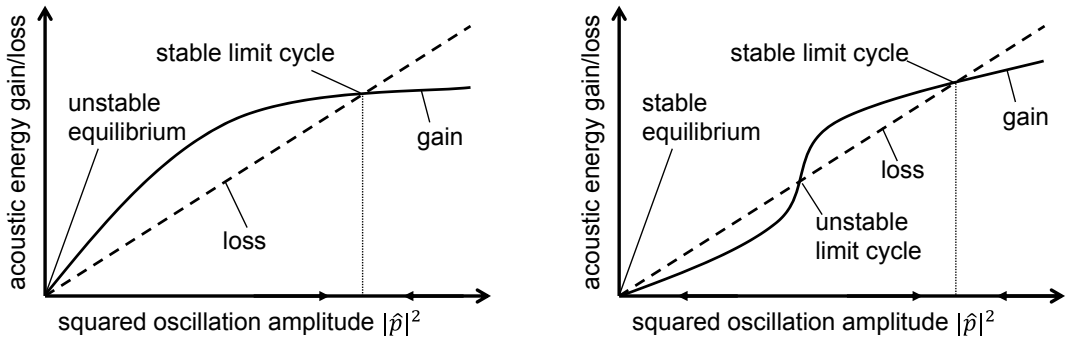

Figure 2.3: Acoustic energy balance, left: Supercritical instability, right: Subcritical instability

If ΔE_a is larger than the sum of acoustic losses in the combustion system, i.e., mainly viscous damping and losses at the system boundaries, the acoustic energy of the system grows and the oscillation amplitude rises - a self sustaining thermoacoustic instability establishes. Fig. 2.3 (left) gives the gain and loss of acoustic energy qualitatively as a function of the acoustic oscillation amplitude for linearly unstable operating conditions. For small oscillation amplitudes, the gain of acoustic energy is larger than the damping. Hence, perturbations increase exponentially until nonlinear mechanisms limit the growth. The loss of acoustic energy is considered to be linear. Due to saturation in the flame response, a balance of acoustic energy gain and loss is established at a finite oscillation amplitude, the limit cycle.

Figure 2.3 (right) displays the energy gain–loss balance for the case of a subcritical instability. For small oscillation amplitudes the gain of acoustic energy is smaller than the loss, and thus, the system is linearly stable and perturbations arising in the system decay.

The inflexion of the flame response results in further equilibrium points for the acoustic energy of the system. Large perturbations, e.g., of the flow field, may raise the system to a higher oscillation level and thus, to another limit cycle [50, 51]. As the system is linearly stable, these subcritical instabilities cannot be predicted by a linear system analysis. Some recent works emphasized the importance of subcritical instabilities by demonstrating that thermoacoustic systems are generally prone to exhibit significant transient growth [52, 53].

Saturation effects in the flame response of industrial-type swirl burners are often assumed to become significant at velocity oscillation amplitudes that are of the order of the mean flow [8, 9]. Therefore, it is necessary to provide forcing amplitudes of this magnitude over a broad frequency range in order to measure nonlinear effects in the flame response.

If the flame describing function of a flame is known, an acoustic network model describing the complete system can be used for the prediction of limit cycles [4, 5].

2.5 Hydrodynamic stability analysis

The linear local hydrodynamic stability analysis in the associated publications was carried out by Kilian Oberleithner. His thesis [54] gives a detailed overview of the fundamentals and techniques used for these calculations and is referred to here as a general reference for detailed information. Hence, the methodology is only briefly explained in the following.

The purpose of this technique is to show under which conditions perturbations emitted at the combustion chamber inlet are amplified or dampened while convecting along the shear layers to the reaction zone.

According to Hussain and Reynolds [55] each quantity $a(x,t)$ of the flow field (e.g., velocity, pressure, etc.) can be triple-decomposed as

$$a(x,t) = a_0(x) + a^{\mathrm{c}}(x,t) + a^{\mathrm{s}}(x,t), \tag{2.22}$$

where $a_0(x)$ is the time-averaged part, $a^{\mathrm{c}}(x,t)$, the coherent part and $a^{\mathrm{s}}(x,t)$, the stochastic part of the quantity. Generally, it is assumed that the length scales of the coherent parts are much larger than the scale of stochastic fluctuations. Furthermore, the coherent part that can be reconstructed from normal modes of the flow is defined to be periodic in time.

In the present analysis, a polar coordinate system is used and the coherent part of each velocity component and the pressure are decomposed by a normal mode Ansatz:

$$(v_x^{\mathrm{c}}, v_r^{\mathrm{c}}, v_\theta^{\mathrm{c}}, p^{\mathrm{c}}) = \Re\left\{(H, iF, G, P)\, e^{i(\alpha x + m\theta - \omega t)}\right\}, \tag{2.23}$$

where H, F, G and P are the complex eigenfunctions of the axial, radial and azimuthal velocity and the pressure, α is the complex axial wave number, ω the complex angular frequency and m the real azimuthal wave number. The local linear stability analysis is carried out at several axial locations separately. It is assumed that the flow is only weakly nonparallel, i.e., for the present investigations, the mean velocity in the radial and azimuthal

directions is neglected at each profile and only the axial velocity profile is taken into account for the stability analysis.

Similar to the derivation of the Orr-Sommerfeld equation, substituting the normal mode Ansatz 2.23 into the mass continuity and the Navier-Stokes equation and linearizing with respect to the mean flow, one obtains a set of four differential equations:

for continuity

$$\partial_r F + \frac{F}{r} + \frac{mG}{r} + \alpha H = 0 \tag{2.24a}$$

for the x-momentum

$$\frac{\partial_r^2 H}{\mathrm{Re}_t} + \frac{\partial_r H}{r\mathrm{Re}_t} + \left[i\omega - \frac{imV_\theta}{r} - i\alpha V_x - m^2 r^2 \mathrm{Re}_t\right] H \\ -i\partial_r V_x F - i\alpha P = \frac{\alpha^2 H}{\mathrm{Re}_t} \tag{2.24b}$$

for the r-momentum

$$\frac{i\partial_r^2 F}{\mathrm{Re}_t} + \frac{i\partial_r F}{r\mathrm{Re}_t} - \left[\omega - \frac{mV_\theta}{r} - \alpha V_x + \frac{i(m^2+1)}{r^2\mathrm{Re}_t}\right] F \\ -2\left[\frac{im}{r^2\mathrm{Re}_t} - \frac{V_\theta}{r}\right] G - \partial_r P = \frac{i\alpha^2 F}{\mathrm{Re}_t} \tag{2.24c}$$

for the θ-momentum

$$\frac{\partial_r^2 G}{\mathrm{Re}_t} + \frac{\partial_r G}{r\mathrm{Re}_t} + \left[i\omega - \frac{imV_\theta}{r} - i\alpha V_x - \frac{m^2+1}{r^2\mathrm{Re}_t}\right] G \\ - \left[i\partial_r V_\theta + \frac{2m}{r^2\mathrm{Re}_t} + \frac{iV_\theta}{r}\right] F - \frac{imP}{r} = \frac{\alpha^2 G}{\mathrm{Re}_t}, \tag{2.24d}$$

with the turbulent Reynolds number Re_t, which is determined from the fluid viscosity and an additional eddy viscosity, resulting from the small-scale fluctuations and being taken into account via the Boussinesq approximation.

In the present investigation, the amplification rate of perturbations in the combustor flow under acoustically forced conditions is analyzed. Hence, it is assumed that coherent structures are axisymmetric with $m = 0$. The boundary conditions are set to

$$F(\infty) = G(\infty) = H(\infty) = P(\infty) = 0 \tag{2.25a}$$

$$F(0) = G(0) = 0 \tag{2.25b}$$

$$H(0) \quad \text{and} \quad P(0) \quad \text{finite.} \tag{2.25c}$$

The so-called spatial stability analysis approach is applied, with a complex wave number α and real frequencies ω. In order to achieve a solution for the system of differential equations 2.24, the according dispersion relation is solved for each axial position x and each frequency ω using the Chebyshev spectral collocation methods and obtaining the

complex eigenvalue α and the complex eigenfunctions H, F, G and P. The imaginary part of the axial wave number α is the negative growth rate of perturbations at a certain axial location and frequency.

Chapter 3

Measurement Techniques

In the following, the measurement and post processing techniques used in the associated publications are briefly described. Since the techniques are not the focus of this thesis, but merely used as tools, only rough explanations are given. For more detailed information, the reader is referred to the references.

3.1 Multi Microphone Method (MMM)

In order to determine the planar acoustic field in ducts, the multi microphone method is used. Schuermans [29] gives a comprehensive overview and mathematical implementation of this technique. At several axial positions in the duct, microphones are mounted and the acoustic pressure fluctuations are measured. A least square fit of the Fourier transform is applied in order to determine the planar acoustic field in the duct. For the measurements described here, 3 to 5 microphones were mounted upstream and downstream of the combustor in order to identify the acoustic pressure and velocity fluctuations.

3.2 Particle Image Velocimetry (PIV)

Particle image velocimetry is a state of the art measurement technique that is extensively described in literature [56, 57]. It allows in the applied configuration for the measurement of two velocity components in a plane in the combustion chamber. The measurement plane is illuminated with a laser sheet twice and the reflection of seeding particles in the flow is captured with a camera. By cross correlating the two images, the velocity field is obtained. While the basic principle of this method is rather simple, advanced applications as well as post processing methods can become very complex depending on the exact specification of the measurement.

3.3 Laser Doppler Anemometry (LDA)

Laser Doppler anemometry is a well known measurement technique [57], that allows for pointwise highly time resolved two component velocity measurements. Two coherent laser beams are crossed, generating an interference pattern in a small measurement volume. Particles that are seeded into the flow and cross the volume reflect the light to a sensor. The intensity fluctuation of the light that results from the interference pattern can be analyzed using wavelet decomposition methods in order to determine the velocity component of the particle normal to the pattern. Using this principle with two laser beam pairs at different frequencies allows for two component velocity measurements.

3.4 OH* chemiluminescence

A direct measurement of the heat release in a flame is hardly possible. Hence, a measurement of the intensity of light emission of the flame at particular wavelengths is used as a surrogate. The OH-radical is an intermediate reaction species that occurs during the combustion process of natural gas and several other fuels. The excited radical emits light at a wavelength of around 308 nm. A photomultiplier equipped with a band-pass filter is applied in the measurements in order to capture the integral OH^* chemiluminescence at a high temporal resolution. An intensified CCD camera, also equipped with a band-pass filter, is used to measure the spatial distribution of the heat release in the flame. As stated in chapter 2, equivalence ratio fluctuations may have an influence on the OH^* chemiluminescence intensity, hence, a quantitative analysis of the heat release by the OH^* chemiluminescence is only valid for perfectly premixed operation conditions.

3.5 Phase-averaging

The camera used for recording the OH^* chemiluminescence images is capable of taking pictures with a repetition frequency of ≈ 5 Hz. In order to resolve the heat release fluctuations that occur at the much higher forcing frequencies, a triggering signal of the camera was recorded and a phase-average algorithm [58] is applied to the images in post processing. A Hilbert transformation of the reference signal is applied in order to determine the phase of the triggering signals of the camera relative to the oscillation of the reference signal.

3.6 Abel deconvolution

The camera used for the OH^* chemiluminescence images captures a line of sight integration of the OH^* chemiluminescence of the flame. In order to recover the radial distribution of the OH^* chemiluminescence from the projection, Abel deconvolution schemes [59, 60] were applied. Rotational symmetries have to be assumed for the application of this technique. Although the occurrence of non-rotational symmetric coherent structures was not a priori

precluded, this assumption is valid, since the phase averaging of the OH^* chemiluminescence images with respect to the forcing frequencies eliminates antisymmetric structures like precessing vortex core oscillations, if present, as long as they occur at a frequency other than the forcing frequency.

Chapter 4

Publications

The following pages include the publications, which are discussed in the subsequent chapter.

An Experimental Investigation of the Nonlinear Response of an Atmospheric Swirl-Stabilized Premixed Flame

Sebastian Schimek[1]
e-mail: sebastian.schimek@pi.tu-berlin.de

Jonas P. Moeck

Christian Oliver Paschereit

Chair of Fluid Dynamics,
Institute of Fluid Dynamics and Technical Acoustics,
Hermann-Föttinger-Institut,
Technische Universität Berlin,
10623 Berlin, Germany

Due to stringent emission restrictions, modern gas turbines mostly rely on lean premixed combustion. Since this combustion mode is susceptible to thermoacoustic instabilities, there is a need for modeling tools with predictive capabilities. Linear network models are able to predict the occurrence of thermoacoustic instabilities but yield no information on the oscillation amplitude. The prediction of the pulsation levels and hence an estimation whether a certain operating condition has to be avoided is only possible if information on the nonlinear flame response is available. Typically, the flame response shows saturation at high forcing amplitudes. A newly constructed atmospheric test rig, specifically designed for the realization of high excitation amplitudes over a broad frequency range, is used to generate extremely high acoustic forcing power with velocity fluctuations of up to 100% of the mean flow. The test rig consists of a generic combustor with a premixed swirl-stabilized natural gas flame, where the upstream part has a variable length to generate adaptive resonances of the acoustic field. The OH chemiluminescence response, with respect to velocity fluctuations at the burner, is measured for various excitation frequencies and amplitudes. From these measurements, an amplitude dependent flame transfer function is obtained. Phase-averaged OH* pictures are used to identify changes in the flame shape related to saturation mechanisms. For different frequency regimes, different saturation mechanisms are identified.* [DOI: 10.1115/1.4002946]

1 Introduction

One of the main issues in gas turbine development is the stability of the combustion process. By the implementation of lean premixed combustion, stringent emissions restrictions could be followed, but the combustion process was adversely affected, as it became more susceptible to thermoacoustic instabilities. These instabilities arise from the interaction of the unsteady heat release and the acoustic field in the engine. If the two mechanisms constructively interfere, high amplitude pressure pulsations occur, which have a detrimental effect on the combustion process [1]. Linear thermoacoustic models of premixed combustion systems have been widely used to predict linear system stability (see, e.g., Ref. [2] or Ref. [3]). However, for an estimation whether a certain instability is harmful for the engine, the amplitude of the pressure pulsations has to be known.

For linearly unstable operating conditions, the energy gain of the acoustic field due to thermoacoustic interactions is larger than the damping at small oscillation amplitudes. Hence, perturbations grow exponentially until nonlinear mechanisms start to become important. The dominant nonlinearity is commonly attributed to the flame response [4] and has been found to be mainly of saturation type. The loss mechanisms associated with visco-thermal damping and radiation from the boundaries can be, on the other hand, considered essentially linear. The variation of the energy gain and loss as a function of the oscillation amplitude is quantitatively shown in Fig. 1. Due to the saturation in the flame response, a balance of acoustic energy gain and loss is established at finite oscillation amplitude, the limit cycle. Clearly, to determine the amplitude of the limit cycle oscillation, the nonlinear dependence of the energy gain (essentially the flame transfer function) has to be known. If an amplitude dependent flame response—the flame describing function—is available, the oscillation amplitude can be estimated [4,5]. On the other hand, a premixed combustion system may exhibit strong thermoacoustic oscillations even if it is linearly stable [6,7]. These subcritical instabilities cannot be detected by a linear analysis. Opposed to linear instabilities, the existence of this type of oscillations can only be predicted if the nonlinear flame response is known.

Saturation effects in the flame transfer function of industrial-type swirl burners are often assumed to set in at velocity oscillation amplitudes that are of the order of the mean flow [8,9]. Therefore, it is necessary to realize a forcing mechanism which provides excitation amplitudes in that order of magnitude. The combustor test rig used for the investigations presented in this paper was specifically designed for the experimental investigation of nonlinear flame transfer functions. High forcing amplitudes are realized by using four high power woofers in combination with a variable upstream impedance—a trombone. As a first application, the high amplitude forcing capabilities of the test rig have been used to assess the nonlinearity of the acoustic damping in the burner and at the outlet boundary condition [10].

In the present investigation, the flame describing function (FDF) has been determined for a range of frequencies and forcing amplitudes at fixed operation conditions. OH* images from the flame have been recorded and used to gain information on the flame shape characteristics related to the saturation processes for different frequencies. Two excitation frequencies are investigated in detail.

2 Experimental Setup

The experimental setup that was used for the present investigations is an atmospheric combustor test rig shown schematically in Fig. 2. The burner that is mounted in the test rig consists of a swirl generator followed by an annular duct and an area discontinuity to

[1]Corresponding author.

Contributed by the International Gas Turbine Institute of ASME for publication in the JOURNAL OF ENGINEERING FOR GAS TURBINES AND POWER. Manuscript received May 18, 2010; final manuscript received May 27, 2010; published online April 25, 2011. Editor: Dilip R. Ballal.

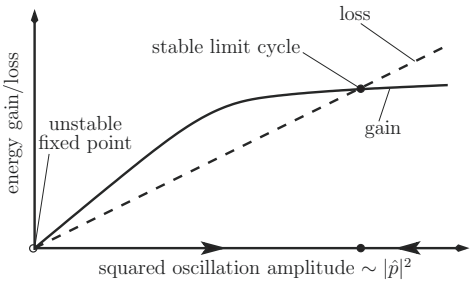

Fig. 1 Acoustic energy balance

the combustion chamber (Fig. 3, left). Figure 3 (right) shows a cut through the swirl generator, which was designed based on the movable block principle [11] to allow for a wide range of swirl numbers. The flow enters axially into this section and is then guided radially between fixed blocks and movable blocks into the inner tube. Between the blocks, there are two types of slots: (i) radial and (ii) mixed radial and tangential. By moving all blocks of one type, the sizes of the two slot types can be varied and thus the amount of tangential momentum which leads to a change in swirl intensity. The swirl number can be varied between 0 and approximately 2. All tests were run at a calculated swirl number [12] of approximately 1.2. Fuel (natural gas) is injected through 16 circumferentially distributed holes in the upstream plate of the swirl generator, near the root of the centerbody.

After passing the swirler, the flow enters an annular duct followed by an area expansion to the combustion chamber where a vortex breakdown is established. This leads to a recirculation zone and thus to a stabilization of the flame. The combustion chamber is made from silica glass to provide optical access for chemiluminescence measurements, i.e., integral OH^* emissions recorded with a photomultiplier and OH^* pictures acquired with an intensified charge coupled device (ICCD)-camera. The exhaust tube provides the possibility to change the downstream reflection coefficient by mounting an orifice. At the tube upstream of the swirl generator, an array of microphones is mounted (see Fig. 2). The axially distributed microphones allow to determine the plane acoustic field with the multimicrophone-method [13]. Using the burner transfer matrix without flame, which is known from preliminary tests [10], the velocity fluctuation at the combustion chamber inlet due to the acoustic field upstream of the combustor can be calculated. In this way, the amplitude dependence of the burner transfer matrix is not taken into account. This might introduce a slight error in the determined velocity fluctuation.

The main feature of the test rig, concerning the realization of high forcing amplitudes for amplitude dependent flame transfer function measurements, is the combination of four 18 in. (approximately 460 mm) woofers (B&C 18PS76, with a maximum electrical power of 600 W per speaker) with a variable upstream impedance of the combustor. To realize the latter, the length of the tube between the speakers and the burner inlet can be varied with a computer controlled traversing system. This mechanism allows to use the forcing of the woofers in resonance over the desired frequency range. The end of the trombone tube upstream of the loudspeakers is connected with a preheater supplying the combustion system with air preheated up to 500°C.

All tests presented in this paper were carried out with an air mass flow of 150 kg/h at a preheat temperature of 220°C with an equivalence ratio of ϕ=0.65. The test conditions for the present investigations were as follows. For different lengths of the upstream tube, a sweep in the frequency range of interest was used as a forcing signal. In this way, the resonance frequencies could be identified (Fig. 4). In a next step, these frequencies were used for a sinusoidal excitation with increasing amplitudes. For each amplitude, 500 pictures were acquired with the ICCD camera. A trigger pulse from the camera system is recorded and is used in

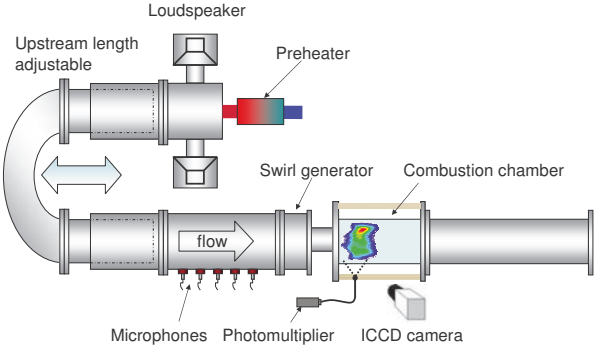

Fig. 2 Test rig overview

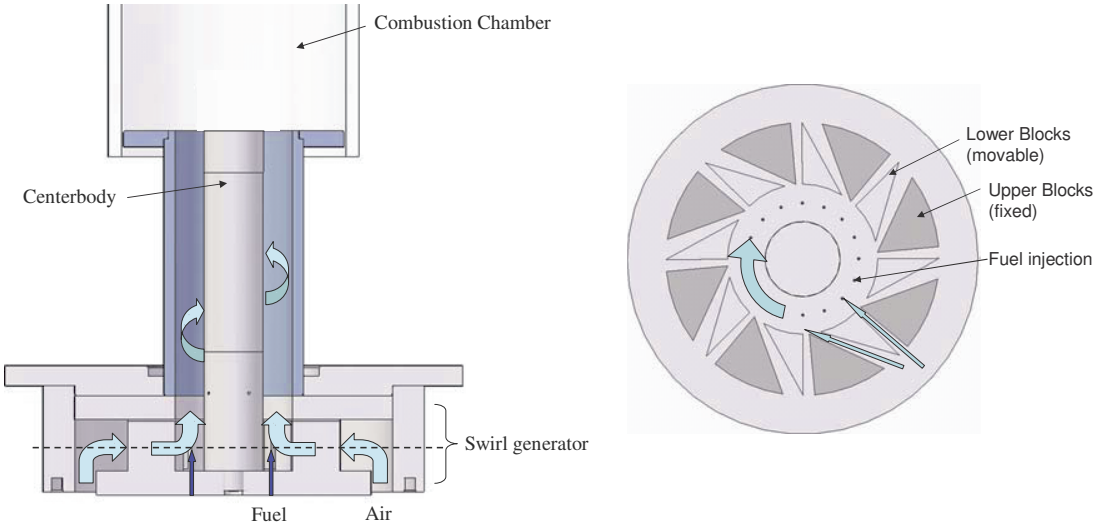

Fig. 3 Burner, left: swirl generator with annular duct and area jump to silica glass combustion chamber; right: cut through the movable block swirl generator

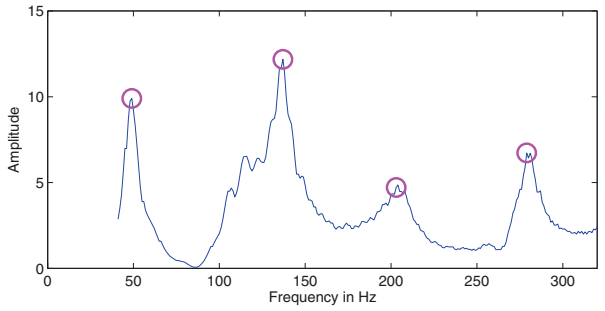

Fig. 4 Principle sketch of pressure fluctuation due to flame response to sweep excitation; resonant frequencies are used for monofrequent excitation

the post-processing to make a phase correlation for each image with the photomultiplier signal and perform a phase-locking average of the images [14]. The phase-averaged images correspond to the projection of an approximately axisymmetric intensity distribution. An Abel deconvolution scheme [15] was applied to the phase-averaged images to recover the radial intensity distribution from the projection.

3 Measurement Results

Figure 5 shows an Abel deconvoluted image of the flame in the unexcited case, embedded into a sketch of the combustor. The flow, entering as a swirling annular jet, forms an inner recirculation zone with a vortex breakdown and an outer recirculation zone, indicated by the arrows [16]. The reaction zone starts at the edge of the centerbody and grows downstream in the shear layer between the annular jet and the inner recirculation zone.

The flame describing function generally is given by the ratio of the Fourier transform of the normalized heat release fluctuation and normalized velocity fluctuation

$$F(\omega,|u'|)=\frac{Q'/Q_{\text{mean}}}{u'/u_{\text{mean}}} \tag{1}$$

As the heat release cannot be measured directly, a common assumption is that the flame describing function can be regarded as the ratio of the normalized OH* chemiluminescence fluctuation and the normalized velocity fluctuation

$$F(\omega,|u'|)=\frac{I'_{\text{OH}^*}/I_{\text{OH}^*\text{mean}}}{u'/u_{\text{mean}}} \tag{2}$$

This implies a linear relation between the intensity of the OH* chemiluminescence and heat release which may introduce a significant error for a nonideally premixed operation mode as equivalence ratio fluctuations can occur [17]. Anyway this relation is

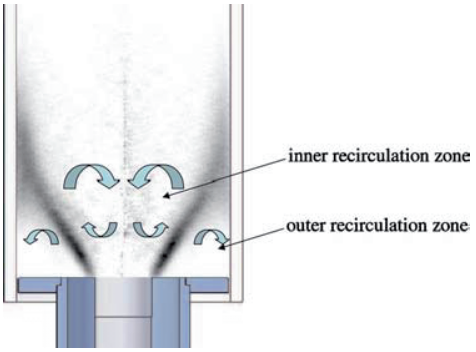

Fig. 5 Sketch of the combustion chamber and image of the flame

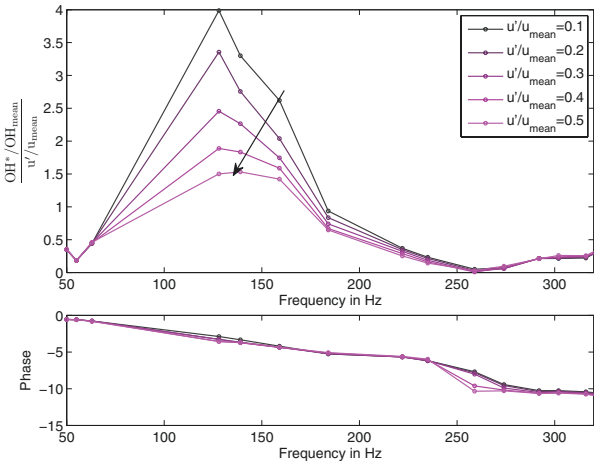

Fig. 6 Flame describing function for u'/u_{mean} = 0.1, 0.2, 0.3, 0.4, 0.5, arrow indicates increasing amplitudes

used to gain qualitative information about the saturation mechanisms in the flame. The flame describing function can be written as

$$F(\omega,|u'|)=G(\omega,|u'|)e^{i\Phi(\omega,|u'|)} \tag{3}$$

where G is a frequency and excitation amplitude dependent gain and Φ is a frequency and excitation amplitude dependent phase.

The measured flame describing function is shown in Fig. 6. Between 50 Hz and 65 Hz, a regime is obvious where the lines for different forcing amplitudes are equal and thus no dependence on the forcing amplitude, which means that the flame response is linear. In the range of 65–128 Hz, no data could be recorded, due to insufficient forcing amplitudes. For forcing frequencies 128 Hz, 139 Hz, and 158 Hz, the highest fluctuations in OH* chemiluminescence have been measured. Palies et al. [18] found that the transfer function gain shows the strongest nonlinear behavior in regions where it reaches its maximum, which is confirmed here. Further increasing the forcing frequency leads to decreasing values in the flame describing function, until at 259 Hz a minimum is reached. Up to that frequency, the nonlinearities decrease but are still clearly visible. Weakly nonlinear behavior is also visible in the region from 259 Hz to 320 Hz where the values increase for all forcing amplitudes shown.

The phase decreases monotonously corresponding to a time delay of 5.9 ms between the velocity fluctuation at the combustion

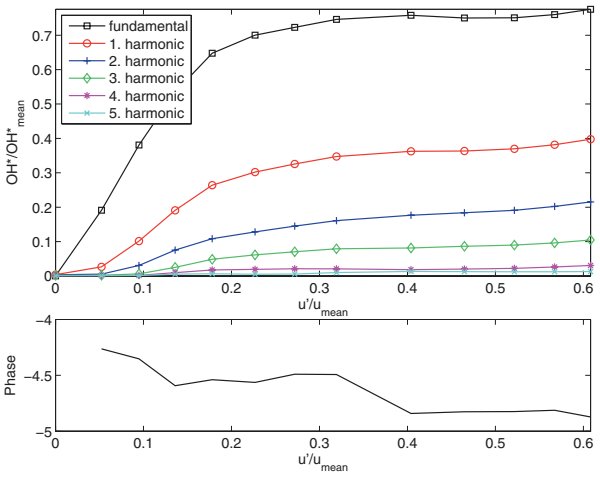

Fig. 7 OH* response at 128 Hz

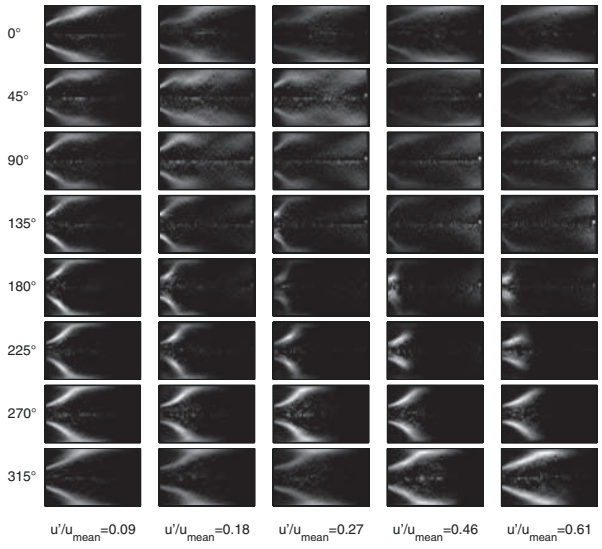

Fig. 8 OH* pictures of the flame at a forcing frequency of 128 Hz: phase-averaged, Abel deconvoluted, for increasing excitation amplitudes

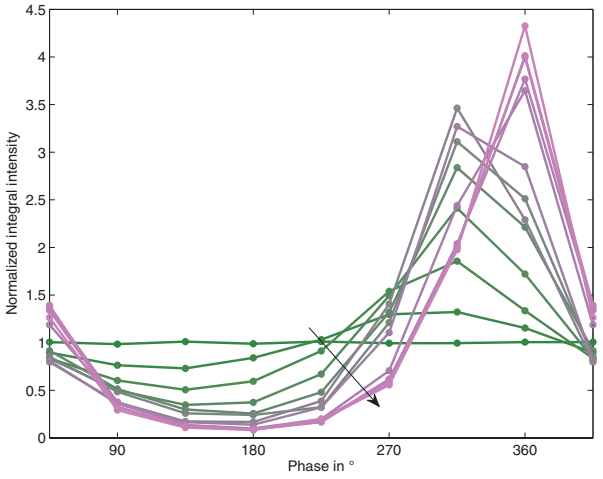

Fig. 9 OH* chemiluminescence intensity normalized with its mean value; averaged over the non-Abel deconvoluted flame images at 128 Hz for different forcing amplitudes; arrow indicates direction of increasing forcing amplitude

chamber inlet and the OH* response. The spread in phase at 259 Hz can be neglected as the magnitude is essentially zero. Another spread is obvious in the region of the highest values in the flame describing function (128 Hz, 139 Hz, and 158 Hz) and will be discussed later.

As described by Lohrmann et al. [19], two major forms of flame pulsation shapes could be found. The first one shows a pulsating reaction zone in the shear layer between the inner recirculation zone and the annular jet and appears at excitation frequencies lower than a critical frequency (here ≈200 Hz). Forcing at higher frequencies leads to a flame shape with a vortex propagating into the outer recirculation zone. In the following, the results for frequencies 128 Hz and 292 Hz will be discussed in detail.

4 Analysis of the Response at a Forcing Frequency of 128 Hz

Figure 7 shows the normalized OH* response related to the normalized velocity fluctuation at a forcing frequency of 128 Hz. A linear growth of the OH* chemiluminescence fluctuation due to the velocity fluctuations is visible up to $u'/u_{\text{mean}} \approx 0.17$. A further increase of the forcing amplitude leads to a saturation process that limits the OH* response. Significant growth of the first and the second harmonics, which indicates nonlinear heat release behavior, is visible, even at low forcing amplitudes, at which the saturation process is not apparent.

Figure 8 shows the images of the flame at a forcing frequency of 128 Hz with increasing forcing amplitudes. The OH* pictures are phase-averaged and Abel deconvoluted. Starting at the phases 180–225 deg, it is visible that the flame is concentrated at the burner mouth with increasing forcing amplitudes and vanishes further downstream. In the phases 270–315 deg, the reaction zone grows along the shear layer between the annular jet and the outer recirculation zone. In the following, phases 0–135 deg, the flame lifts off from the burner mouth and is convected downstream. Comparing the last two columns, a significant change in the flame form is absent, which agrees with the saturation characteristics observed in Fig. 7. The maximum of the fluctuating velocity at the combustion chamber inlet is reached at 45 deg, the minimum at 225 deg.

The phase-averaged pictures are spatially averaged to obtain an integral intensity of the OH* chemiluminescence, similar to the photomultiplier signal. Figure 9 shows the development of the intensity over one oscillation period for several forcing amplitudes. For low amplitudes, a sinusoidal oscillation is visible. For increasing amplitudes, the shape is changing through nonlinear distortion. The intensity is lower than the average for more than one half of the cycle with only small variations and is higher than the average for the rest of the cycle showing a sharp peak. This behavior confirms, on the one hand, the observations made in Fig. 8 with a long drift off of the flame and a fast re-ignition at the burner mouth and in the shear layer, on the other hand, the rise of the harmonics in Fig. 7 even at low forcing amplitudes. The average of the intensities over one oscillation period is a constant value and does not depend on the forcing amplitude (not shown here). As the spatially integrated intensity reaches nearly zero around 180 deg, and as the flame nearly vanishes for high amplitudes, the temporal extinction of the flame can be regarded as the dominant saturation process at 128 Hz.

To estimate the position of the flame, the center of mass (COM) of one-half of the Abel deconvoluted, phase-averaged pictures is calculated as follows:

$$\text{COM}_r = \frac{\overline{\int I(r,x)x\,dx}}{\overline{\int I(r,x)\,dx}}, \quad \text{COM}_x = \frac{\overline{\int I(r,x)r\,dr}}{\overline{\int I(r,x)\,dr}} \tag{4}$$

where I is the intensity distribution.

Figure 10 shows the movement of the COM in the upper half of the Abel deconvoluted images (Fig. 8) over one period at a forcing frequency of 128 Hz. The movement of the COM grows with increasing forcing amplitude. A saturation process of the movement of the COM is visible for high forcing amplitudes. The COM moves clockwise during one oscillation.

Averaging the COM over one oscillation period, the movement of the averaged flame position depending on the excitation amplitude can be obtained. These are shown in Fig. 11 for all frequencies considered. It is visible that the movement of the averaged flame position is dominant for 128 Hz, 139 Hz, and 159 Hz and nearly vanishes for most of the other frequencies. At the frequencies with high response, the averaged flame position moves 20–30 mm downstream and 6 mm in the radial direction. In Fig. 6, an

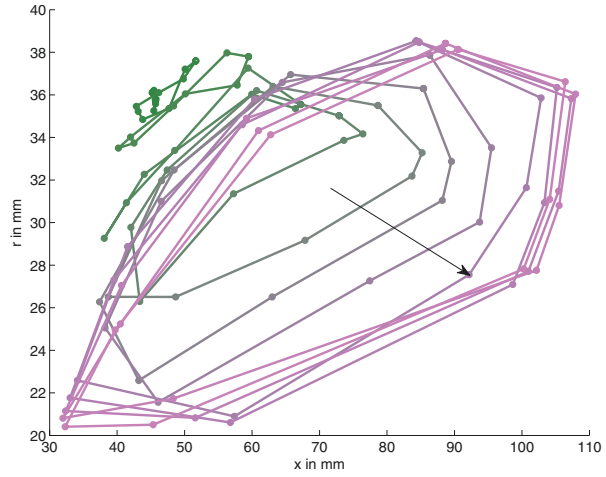

Fig. 10 Center of mass movement over one period at a forcing frequency of 128 Hz; arrow indicates direction of increasing forcing amplitude; saturation at four highest amplitudes visible; coordinates related to combustion chamber inlet

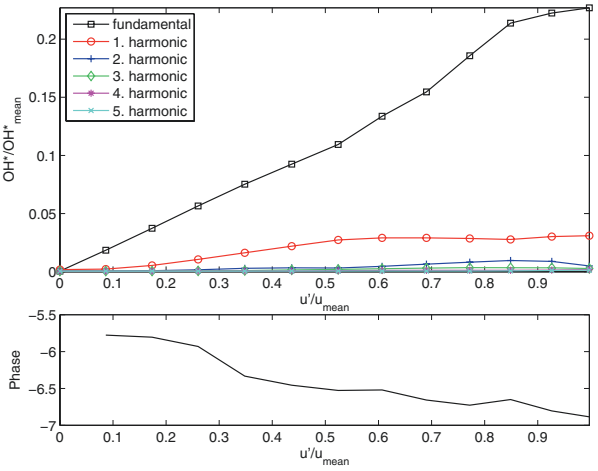

Fig. 12 OH* response at 292 Hz

increase in the phase lag for increasing excitation amplitudes has been observed. This can be explained with the movement downstream of the averaged flame position and thus an increased time delay depending on the forcing amplitude.

5 Analysis of the Response at a Forcing Frequency of 292 Hz

Figure 12 shows the normalized OH* response related to the normalized velocity fluctuation at a forcing frequency of 292 Hz. A region of linear growth of the OH* chemiluminescence fluctuation is visible up to $u'/u_{\text{mean}} \approx 0.55$. In the next region, the OH* chemiluminescence fluctuation shows a nonlinear behavior, growing stronger than in the proportional linear regime up to $u'/u_{\text{mean}} \approx 0.8$, and finally leading to a saturation process. This type of amplitude dependence of the transfer function gain is particularly important, since it can give rise to subcritical instabilities [6,7], which are not predicted by the linear system analysis. In contrast to the OH* response at 128 Hz, the saturation occurs at a larger value of u'/u_{mean}, whereas $\text{OH}^*/\text{OH}^*_{\text{mean}}$ is much smaller.

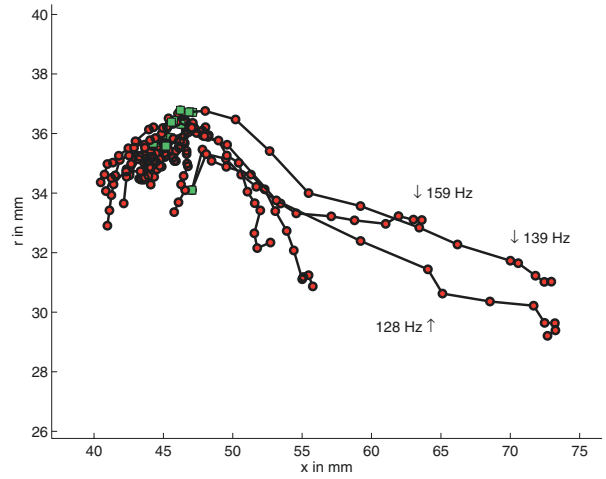

Fig. 11 Center of mass averaged over one period—each line for one frequency at different excitation amplitudes, starting at the squares

The first harmonic grows with the forcing amplitude but in a smaller manner than in Fig. 7. The second harmonic is nearly absent.

Figure 13 shows the phase-averaged, Abel deconvoluted OH* images, taken at a forcing frequency of 292 Hz. Starting from a phase of 90 deg, it can be observed that the flame is sucked close to the annular combustion chamber inlet (135 deg). The reaction zone forms a vortex in the outer recirculation zone at a phase of 225 deg. These outer branches of the flame are convected downstream in the following phases 270–45 deg as the annular jet grows, until the flame reaches the original position of the shear layer between the annular jet and the inner recirculation zone again at 90 deg. The maximum of the fluctuating velocity at the combustion chamber inlet is reached at 105 deg, the minimum at 285 deg.

Figure 14 shows the development of the intensity over one oscillation period for several forcing amplitudes at 292 Hz. In contrast to Fig. 9, a sinusoidal behavior is visible not only for small amplitudes, but also for forcing corresponding to a velocity fluctuation of up to $u'/u_{\text{mean}} \approx 1$. A saturation in the fluctuation amplitude is visible for the two cases with the highest forcing

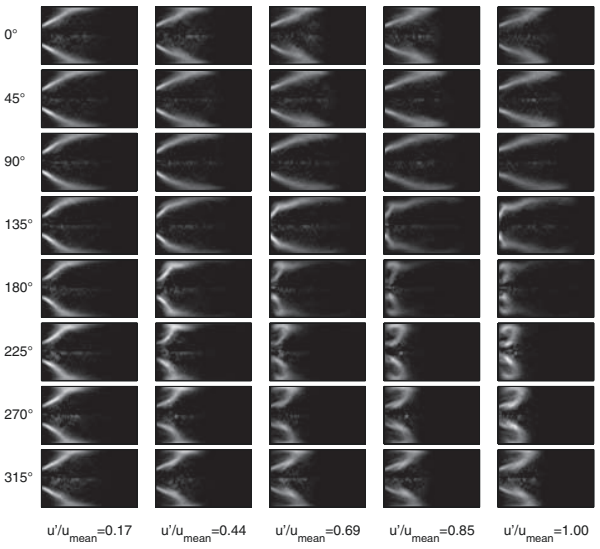

Fig. 13 OH* pictures of the flame at a forcing frequency of 292 Hz: phase-averaged, Abel deconvoluted, for increasing excitation amplitudes

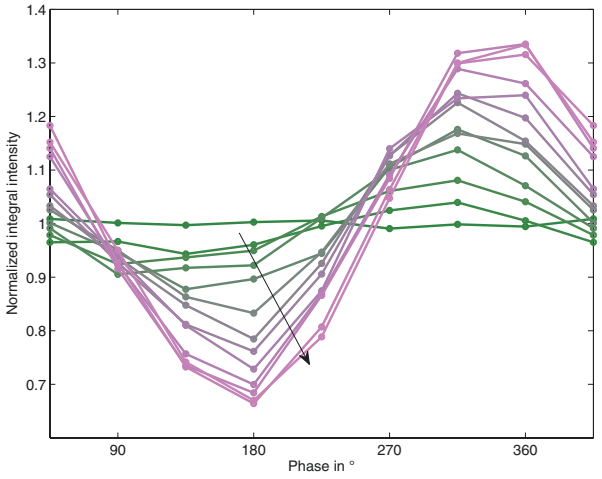

Fig. 14 OH* chemiluminescence intensity—for each excitation amplitude normalized with its mean value; averaged over the non-Abel deconvoluted flame images at 292 Hz; arrow indicates direction of increasing forcing amplitude

amplitudes in good agreement with Fig. 12. The low amplitude of the higher harmonics can be confirmed in this case, too.

6 Self-Excited Instability

Since the flame was unstable with an open exhaust tube at the operating conditions chosen here, all results presented so far have been measured with an orifice at the exhaust tube, changing the downstream reflection coefficient and suppressing the instability. The orifice was removed in order to measure the amplitude of a limit cycle of the self-excited instability. Neither the frequency nor the amplitude changed considerably depending on the position of the traversing system. This independence on the upstream reflection coefficient confirms a strong saturation in the region of the limit cycle. Figure 15 shows a spectrum and a time trace of the instability. In the latter, temporal extinction as found in Fig. 9 is visible, as the OH* chemiluminescence reaches nearly zero in the minimum. The spectrum shows a saturation at $OH^*/OH^*_{mean} \approx 1.3$ at a frequency of 173 Hz. The OH* response of the two frequencies closest to this point, for which a flame describing function has been determined, is shown in Fig. 16 (top and middle). Although a combustion chamber inlet velocity fluctuation of more than $u'/u_{mean}=0.5$ was realized, the regime of saturation where the limit cycle in the self-excited instability is situated could not be reached. Figure 16 (bottom) shows the OH* response at a forcing frequency of 50 Hz, where the resonance in the upstream tube of the trombone allows a forcing amplitude of up to $u'/u_{mean}=1.8$, and a saturation of the OH* response is visible at $u'/u_{mean} \approx 1.5$. Here, as well as in the instability case, it becomes clear that a forcing amplitude of much more than $u'/u_{mean}=0.5..1$ is necessary to measure the saturation behavior at all relevant frequencies.

7 Summary and Outlook

The flame describing function has been determined in a frequency range of 50–320 Hz. The phase-averaged, Abel deconvoluted OH* images of the flame have been used to gain information on the flame shape behavior at saturation processes at different frequencies. For low frequencies (up to 235 Hz), partial extinction has been found to be the dominant mechanism leading to a saturation in the OH* response of the flame. A shift in the phase for high excitation amplitudes has been identified to be related to a movement of the average flame position. For excitation frequencies higher than 270 Hz, a vortex, propagating into the outer recirculation zone, in the flame shape could be found. It is shown that forcing amplitudes of $u'/u_{mean}=0.5..1$ are not sufficient for several frequencies to measure a saturation process in the flame response.

In future work, modeling of pulsation amplitudes from the flame describing function and the acoustic boundaries is planed. Phase-averaged particle image velocimetry measurements will be done to gain detailed information on the interaction of the flow field and the flame.

Acknowledgment

Financial support from the Research Association for Combustion Engines (FVV) is gratefully acknowledged.

Nomenclature

COM_r = radial coordinate center of mass
COM_x = axial coordinate center of mass
F = flame describing function
G = gain of flame describing function
I = intensity distribution
I'_{OH^*}/I_{OH^*mean} = normalized OH* chemiluminescence intensity
Q'/Q_{mean} = normalized heat release fluctuation
r = radial coordinate

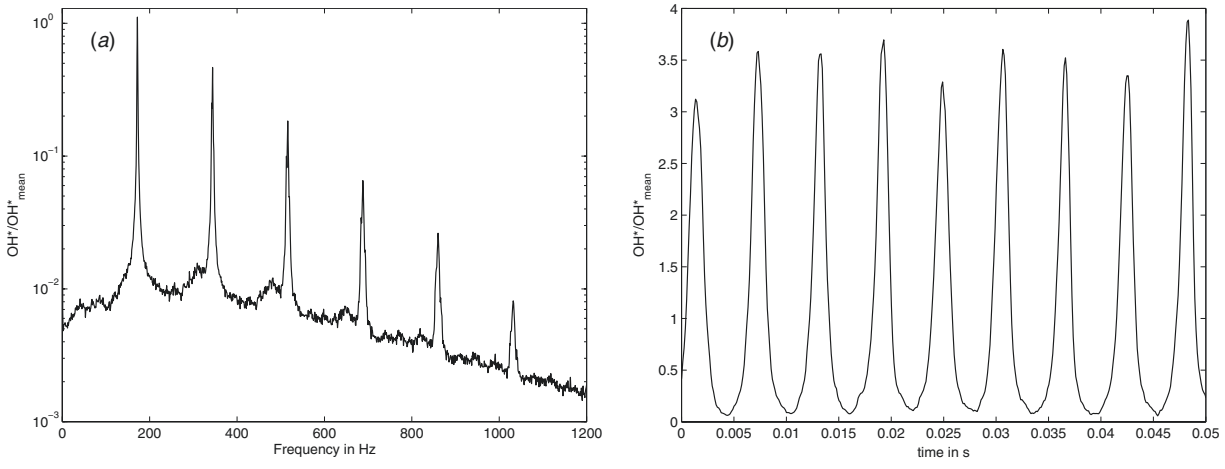

Fig. 15 Photomultiplier signal of a self-excited instability at 173 Hz

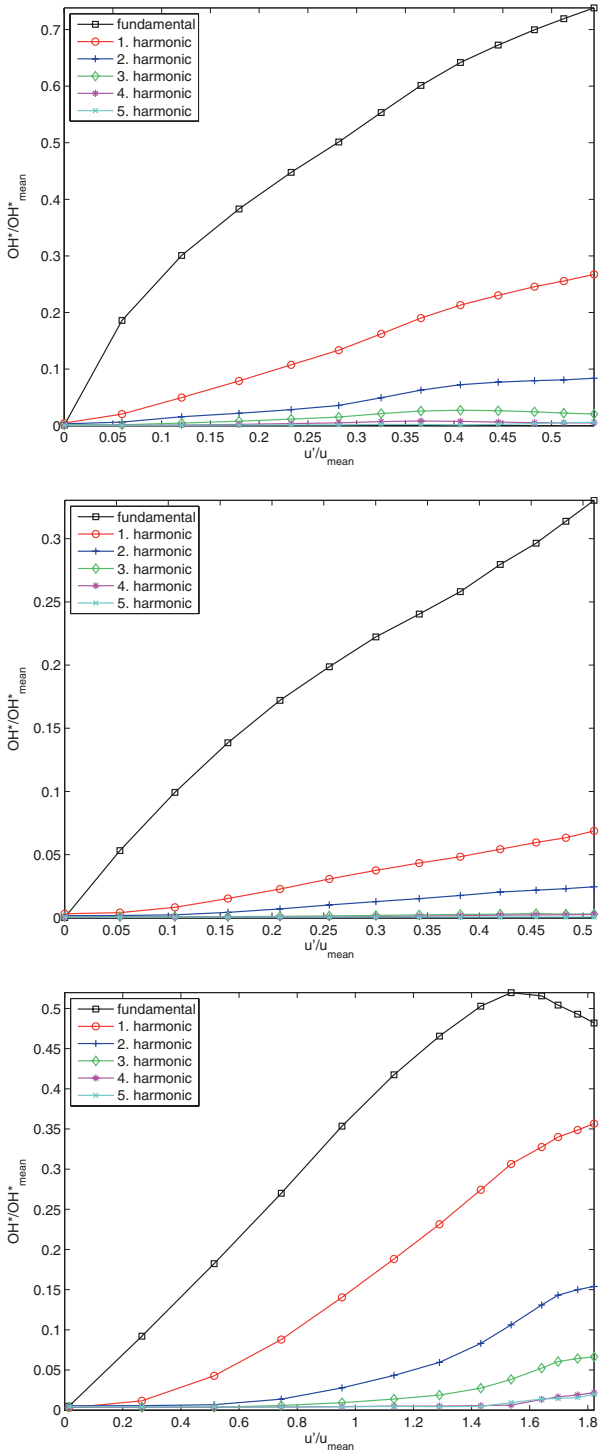

Fig. 16 Normalized OH* response at 159 Hz (top), 184 Hz (middle), and 50 Hz (bottom)

u' = velocity fluctuation
u'/u_{mean} = normalized velocity fluctuation
x = axial coordinate
ϕ = equivalence ratio
Φ = phase angle of flame describing function
ω = angular frequency

References

[1] Lieuwen, T. C., and Yang, V., eds., 2005, *Combustion Instabilities in Gas Turbine Engines* (Progress in Astronautics and Aeronautics, Vol. 210), AIAA, Reston, VA.

[2] Dowling, A. P., and Stow, S. R., 2003, "Acoustic Analysis of Gas Turbine Combustors," J. Propul. Power, **19**(5), pp. 751–764.

[3] Paschereit, C. O., Schuermans, B., Bellucci, V., and Flohr, P., 2005, "Implementation of Instability Prediction in Design: Alstom Approaches," *Combustion Instabilities in Gas Turbine Engines* (Progress in Astronautics and Aeronautics, Vol. 210), T. Lieuwen and V. Yang, eds., AIAA, Reston, VA, pp. 445–480.

[4] Dowling, A. P., 1997, "Nonlinear Self-Excited Oscillations of a Ducted Flame," J. Fluid Mech., **346**, pp. 271–290.

[5] Noiray, N., Durox, D., Schuller, T., and Candel, S., 2008, "A Unified Framework for Nonlinear Combustion Instability Analysis Based on the Flame Describing Function," J. Fluid Mech., **615**, pp. 139–167.

[6] Lieuwen, T. C., 2002, "Experimental Investigation of Limit-Cycle Oscillations in an Unstable Gas Turbine Combustor," J. Propul. Power, **18**(1), pp. 61–67.

[7] Moeck, J. P., Bothien, M. R., Schimek, S., Lacarelle, A., and Paschereit, C. O., 2008, "Subcritical Thermoacoustic Instabilities in a Premixed Combustor," AIAA Paper No. 2008-2946.

[8] Bellows, B. B., Bobba, M. K., Forte, A., Seitzmann, J. M., and Lieuwen, T., 2007, "Flame Transfer Function Saturation Mechanisms in a Swirl-Stabilized Combustor," Proc. Combust. Inst., **31**, pp. 3181–3188.

[9] Balachandran, R., Ayoola, B. O., Kaminski, C. F., Dowling, A. P., and Mastorakos, E., 2005, "Experimental Investigation of the Nonlinear Response of Turbulent Premixed Flames to Imposed Inlet Velocity Oscillations," Combust. Flame, **143**(1–2), pp. 37–55.

[10] Schimek, S., Moeck, J. P., and Paschereit, C. O., 2009, "Design of a Combustion Test Rig With High Amplitude Forcing Capabilities for Nonlinear Flame Transfer Function Measurements," *Proceedings of the 16th International Congress on Sound and Vibration*.

[11] Leuckel, W., 1967, "Swirl Intensities, Swirl Types and Energy Losses of Different Swirl Generating Devices," Technical Report Document No. G02/a/16.

[12] Schneider, C., 2004, "Über die Charakterisierung von Turbulenzstrukturen in verdrallten Strömungen," Ph.D. thesis, TU Darmstadt, Hessen, Deutschland.

[13] Paschereit, C. O., Schuermans, B., Polifke, W., and Mattson, O., 2002, "Measurement of Transfer Matrices and Source Terms of Premixed Flames," ASME J. Eng. Gas Turbines Power, **124**(2), pp. 239–247.

[14] Güthe, F., and Schuermans, B., 2007, "Phase-Locking in Post-Processing for Pulsating Flames," Meas. Sci. Technol., **18**(9), pp. 3036–3042.

[15] Yuan, Z.-G., 1995, "The Filtered Abel Transform and Its Application in Combustion Diagnostics," NASA Report No. NASA/CR2003-212121.

[16] Thumuluru, S. K., and Lieuwen, T., 2009, "Characterisation of Acoustically Forced Swirl Flame Dynamics," *Proceedings of the Combustion Institute*, Vol. 32, pp. 2893–2900.

[17] Schuermans, B., Bellucci, V., Guethe, F., Meili, F., Flohr, P., and Paschereit, C. O., 2004, "A Detailed Analysis of Thermoacoustic Interaction Mechanisms in a Turbulent Premixed Flame," ASME Paper No. GT2004-53831.

[18] Palies, P., Durox, D., Schuller, T., Morenton, P., and Candel, S., 2009, "Dynamics of Premixed Confined Swirling Flames," C. R. Mec., **337**, pp. 395–405.

[19] Lohrmann, L., Büchner, H., Zarzalis, N., and Krebs, W., 2003, "Flame Transfer Function Characteristics of Swirl Flames for Gas Turbine Applications," ASME Paper No. GT2003-38113.

Sebastian Schimek[1]
Hermann-Föttinger-Institut,
Technische Universität Berlin,
Müller-Breslau-Str. 8,
Berlin 10623, Germany
e-mail: Schimek@tu-berlin.de

Bernhard Cosić
Hermann-Föttinger-Institut,
Technische Universität Berlin,
Müller-Breslau-Str. 8,
Berlin 10623, Germany

Jonas P. Moeck
Hermann-Föttinger-Institut,
Technische Universität Berlin,
Müller-Breslau-Str. 8,
Berlin 10623, Germany

Steffen Terhaar
Hermann-Föttinger-Institut,
Technische Universität Berlin,
Müller-Breslau-Str. 8,
Berlin 10623, Germany

Christian Oliver Paschereit
Hermann-Föttinger-Institut,
Technische Universität Berlin,
Müller-Breslau-Str. 8,
Berlin 10623, Germany

Amplitude-Dependent Flow Field and Flame Response to Axial and Tangential Velocity Fluctuations

The current paper investigates the nonlinear interaction of the flow field and the unsteady heat release rate and the role of swirl fluctuations. The test rig consists of a generic swirl-stabilized combustor fed with natural gas and equipped with a high-amplitude forcing device. The influence of the phase between axial and azimuthal velocity oscillations is assessed on the basis of the amplitude and phase relations between the velocity fluctuations at the inlet and the outlet of the burner. These relations are determined in the experiment with the multimicrophone-method and a two component laser Doppler velocimeter (LDV). Particle image velocimetry (PIV) and OH-chemiluminescence measurements are conducted to study the interaction between the flow field and the flame. For several frequency regimes, characteristic properties of the forced flow field and flame are identified, and a strong amplitude dependence is observed. It is found that the convective time delay between the swirl generator and the flame has an important influence on swirl-number oscillations and the flame dynamics in the low-frequency regime. For mid and high frequencies, significant changes in the mean flow field and the mean flame position are identified for high forcing amplitudes. These affect the interaction between coherent structures and the flame and are suggested to be responsible for the saturation in the flame response at high forcing amplitudes.* [DOI: 10.1115/1.4029368]

Introduction

To meet the requirements of ultra low emissions, modern gas turbines mostly rely on lean premixed combustion. A strong susceptibility of this combustion mode to thermoacoustic instabilities makes a detailed understanding of the underlying physical mechanisms necessary. These instabilities arise from the interaction of the unsteady heat release rate in the flame and the acoustic field in the combustor. If the two mechanisms constructively interfere, high-amplitude pressure pulsations occur, which have a detrimental effect on the combustion process and the engine life time [1].

Linear thermoacoustic models of premixed combustion systems have been widely used to predict linear system stability (see Ref. [2] or Ref. [3]). Traditional network modeling techniques are based on small-amplitude input–output relations in frequency domain. They can thus be only used to predict system stability or instability and the associated oscillation frequencies. However, to assess whether a certain instability has to be avoided, the amplitude of the pressure pulsations has to be known.

For linearly unstable operating conditions, the energy gain of the acoustic field due to the interaction with the unsteady heat release rate in the flame is larger than the damping at small oscillation amplitudes. Hence, perturbations increase exponentially until nonlinear mechanisms limit the growth. The dominant nonlinearity is commonly attributed to the flame response [4] and has been found to be essentially of saturation type. The loss mechanisms are, on the other hand, often considered to be linear, as they are associated with viscothermal damping and sound radiation from the boundaries. The variation of the energy gain and loss as a function of the oscillation amplitude is qualitatively shown in Fig. 1. Due to saturation in the flame response, a balance of acoustic energy gain and loss is established at a finite oscillation amplitude, the limit cycle. To estimate the amplitude of the limit cycle oscillation, the nonlinear dependence of the energy gain, which is determined by the amplitude dependence of the flame response, must be known.

Saturation effects in the flame response of industrial-type swirl burners are often assumed to become significant at velocity oscillation amplitudes that are of the order of the mean flow [5,6]. Therefore, it is necessary to provide forcing amplitudes of this

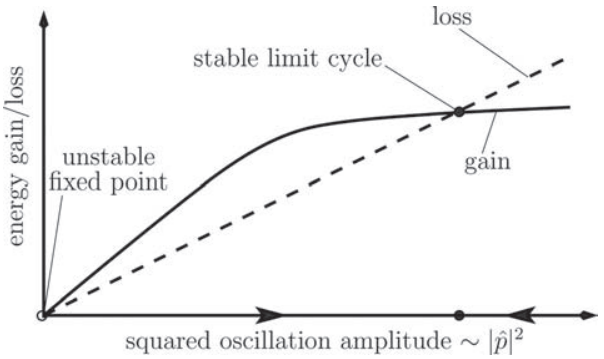

Fig. 1 Acoustic energy balance and supercritical instability

[1]Corresponding author.

Contributed by the Combustion and Fuels Committee of ASME for publication in the Journal of Engineering for Gas Turbines and Power. Manuscript received September 3, 2014; final manuscript received October 9, 2014; published online January 28, 2015. Editor: David Wisler.

magnitude over a broad frequency range in order to measure nonlinear effects in the flame response.

The amplitude-dependent flame transfer function, commonly referred to as the flame describing function [4,7], is defined as

$$F(\omega, |u'|) = \frac{Q'/Q_{\text{mean}}}{u'/u_{\text{mean}}} \tag{1}$$

where Q' and u' are the Fourier transforms of the fluctuations in heat release rate and combustion chamber inlet velocity, respectively, ω is the angular oscillation frequency, and $|u'|$ denotes the fundamental velocity fluctuation amplitude. As the heat release rate cannot be measured directly, a common assumption is that the flame describing function can be represented as the ratio of normalized fluctuations in OH*-chemiluminescence and combustor inlet velocity

$$F(\omega, |u'|) = \frac{\text{OH}^*/\text{OH}^*_{\text{mean}}}{u'/u_{\text{mean}}} \tag{2}$$

This implies a linear relation between the light emission intensity of excited OH radicals and the heat release rate, which is a reasonable assumption for perfectly premixed conditions [8]. The flame describing function can be alternatively expressed as

$$F(\omega, |u'|) = G(\omega, |u'|)e^{i\phi(\omega,|u'|)} \tag{3}$$

where G is the frequency and amplitude-dependent gain and ϕ is a frequency and amplitude-dependent phase. If the flame describing function is available, the oscillation amplitude of the combustion system can be estimated using extensions of the traditional network modeling techniques [4,7].

Various mechanisms have been shown to be responsible for heat release rate fluctuations induced by velocity perturbations, e.g., equivalence ratio oscillations [9–11], flame front fluctuations [12–14], or excitation of fluid mechanical instabilities [6,12,15]. An axial fluctuation of the combustion chamber inlet velocity can result in the generation of vortices at the inner and/or outer edge of the annular combustion chamber inlet. Armitage et al. [16] identified increased vortex generation and the associated flame front wrinkling due to shed vortices convected along the inner and outer shear layers to result in saturation of the flame response at high forcing amplitudes.

Entrainment of gases from the outer or inner recirculation zones is a mechanism associated with vortex shedding. The resulting enhancement of the mixing of fresh gas in the annular jet with hot exhaust gas and radicals from the recirculation zones can result in ignition of the jet upstream of the main reaction zone and cause an oscillating flame front. Vortices shed from the combustion chamber inlet may also result in a locally increased turbulence level and thus augment the burning velocity; this may enable the flame to propagate into the vortex core [8]. As the increase in burning velocity due to turbulent fluctuations is limited, this mechanism saturates at increased forcing amplitudes.

Based on the measurement data used in the present paper, Oberleithner et al. [17] conducted a hydrodynamic stability analysis of the reacting flow field. A strong correlation of saturations in the amplification of flow disturbances due to shear layer instabilities and the saturation of the flame response were identified for the mid frequency regime.

Palies et al. [18] demonstrated that mode conversion occurs in a swirl generator, which has a strong impact on the flame response. An axial velocity fluctuation upstream of the swirl generator results in an axial and a tangential velocity fluctuation downstream, subject to different transport velocities. The axial fluctuation is an acoustic wave, traveling with the speed of sound, whereas the tangential fluctuation is a vortical perturbation of the hydrodynamic field, and thus travels with a speed at the order of the flow velocity. The resulting time lag at the combustion chamber inlet between the two velocity fluctuations results in disturbances in swirl and hence in flame angle (FA) fluctuations. This may have a strong effect on the flame shape and position.

Following the results available in the literature, the interaction of hydrodynamic structures and the heat release rate of the flame is of crucial importance for the understanding of the flame response saturation mechanisms. Hence, the aim of this study is to shed some light onto the flow field–heat release interaction using phase-averaged and spatially resolved flow field and heat release rate data. After a brief description of the experimental apparatus, PIV and OH* camera measurement results are discussed. Several saturation mechanisms are identified, which are summarized at the end of the study.

Experimental Setup

The atmospheric combustor test rig used for the present investigation is shown schematically in Fig. 2. Figure 3 shows the burner, which consists of a swirl generator followed by an annular duct and an area discontinuity to the combustion chamber. The

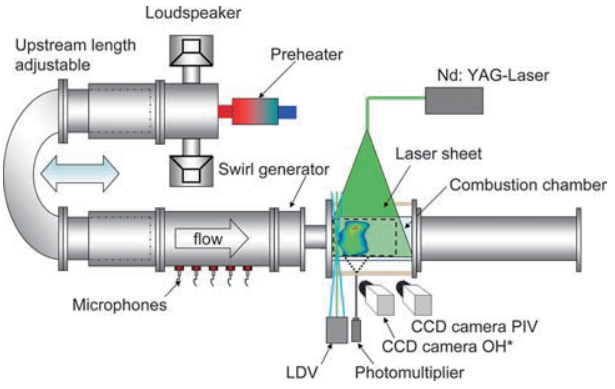

Fig. 2 Test rig overview with measurement devices

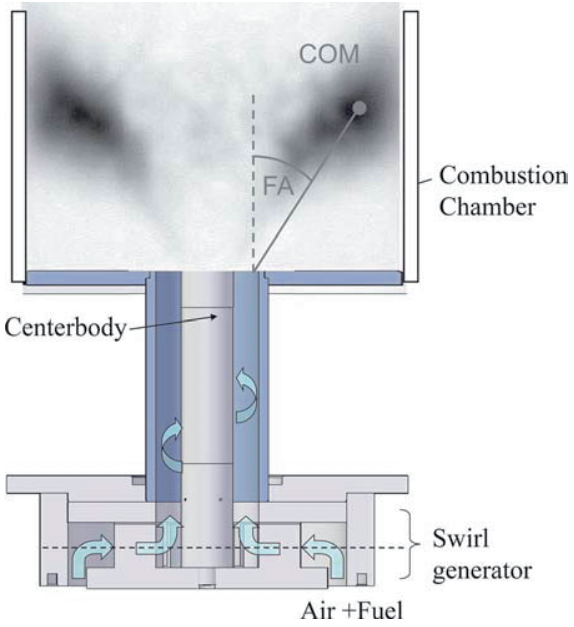

Fig. 3 Burner, swirl generator with annular duct, and area jump to silica glass combustion chamber; flame angle (FA) and center of mass (COM) are indicated

center of mass (COM) and the FA are indicated. The FA is defined as the angle between the combustor axis and the line between the COM of the OH* chemiluminescence distribution and the middle of the annular combustor inlet (Fig. 4) and will be used later in this paper. Figure 4 shows a cut through the swirl generator, which was designed based on the movable block principle [19] in order to allow for a variation of the swirl number. The flow enters axially into this section and is then guided radially between the fixed blocks, mounted on the downstream plate of the swirler, and the movable blocks, mounted on the upstream plate of the swirler, into the inner annular duct. Between the blocks, there are two types of slots: (i) radial and (ii) mixed radial and tangential. By turning the upstream plate of the swirler and thereby moving all blocks of one type, the sizes of the two slot types can be varied and thus the amount of tangential momentum. This leads to a change in swirl intensity. Schneider [20] gives a theoretical (geometrical) swirl number in an annular setup like the one used here based on Leuckels [19] analytic derivation for a movable block swirler. The theoretical swirl number used in the present investigation is 0.7.

The combustor was operated in a perfectly premixed mode, with natural gas injected far upstream of the combustor, near the loudspeakers (see Fig. 2), with an equivalence ratio of $\varphi = 0.7$. Due to the large distance between fuel injection and combustion chamber ($\approx$2 m), a homogeneous mixture of fuel and air is assumed. The combustor is operated at a Reynolds number of 37,000, based on the hydraulic diameter of the annular duct downstream of the swirler and the bulk velocity therein. After passing the swirler, the flow enters the annular duct followed by an area expansion to the combustion chamber, where vortex breakdown is established. This leads to a recirculation zone and thus to a stabilization of the flame. The combustion chamber is made from silica glass in order to provide optical access for chemiluminescence and laser optical measurements (i.e., integral OH* emissions recorded with a photomultiplier, OH*-chemiluminescence images acquired with an ICCD-camera, PIV, and LDV measurements).

The exhaust tube can be equipped with an orifice at the downstream end in order to prevent self-excited thermoacoustic instabilities, which are present in the test rig at certain operating conditions when using an unobstructed combustor outlet. At the tube upstream of the swirl generator, an array of microphones is mounted (see Fig. 2). The axially distributed microphones allow to determine the plane acoustic field with the multimicrophone-method [21].

The main feature of the test rig, concerning the realization of high forcing amplitudes for measurements of the nonlinear flame response, is the combination of four 18-in. woofers (B&C 18PS76), with a maximum electrical power of 600 W per speaker with a variable upstream impedance of the combustor. To realize the latter, the length of the tube between the speakers and the burner inlet can be varied with a computer controlled traversing system. This mechanism allows the forcing of the woofers to be used in resonance over the desired frequency range. For different lengths of the upstream tube, a sine sweep between 50 and 500 Hz was used as a forcing signal. Resonance frequencies were identified and subsequently used for sinusoidal excitation with increasing amplitudes.

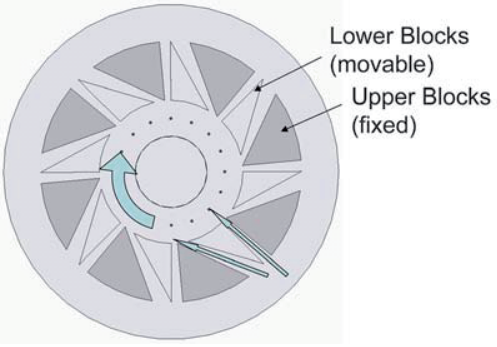

Fig. 4 Burner, cut through the movable block swirl generator

OH*-chemiluminescence was measured in two ways. A photomultiplier with a band-pass filter centered at 307 nm was used to detect the time-resolved global OH*-chemiluminescence intensity in order to allow for an estimation of the heat release rate fluctuations. Simultaneously, an intensified CCD camera, also equipped with a band-pass filter centered at 307 nm, was used to gain information on the phase-resolved spatial distribution of the heat release rate. This camera was operated at a low temporal resolution ($\approx$5 Hz) compared to the oscillation frequencies of the flame. For every case presented, 500 pictures were acquired. A trigger pulse from the camera system was recorded and was used in a postprocessing step to perform a phase correlation for each image with respect to the excitation signal. In this way, a phase-conditioned average of the images can be achieved [22]. The phase-averaged images correspond to the projection of an approximately axisymmetric intensity distribution. An Abel deconvolution scheme [23] was applied to the phase-averaged images to recover the radial intensity distribution from the projection.

The amplitude-dependent burner transfer function was obtained by a combination of the multimicrophone-method [21] and two-component LDV measurements. This allows for a characterization of the downstream response of the burner in terms of axial and azimuthal velocity fluctuations as a function of the oscillation frequency and the amplitude on the upstream side. The velocity fluctuation in the annular jet at the combustion chamber inlet was measured with a two-component LDV system. It allows for highly time-resolved, simultaneous measurements of two velocity components, in the present case axial and tangential, at one point in the middle of the radial extent of the annular jet, approximately 7 mm downstream of the combustion chamber inlet.

PIV measurements were made for various forcing frequencies and amplitudes in the reacting flow field; the flow was seeded with aluminum oxide particles. An Nd:YAG laser (see Fig. 2) was used with a pulse separation of $\approx$6 μs, in order to obtain the flow field in the axial and radial directions in a plane through the center axis of the combustor.

Measurement Results

This section starts with an analysis of the measurement results for the amplitude-dependent response of the burner. Subsequently, the flame describing function is discussed. For specific frequencies, the interaction between the flow field oscillations and the corresponding fluctuations in the heat release rate distribution are presented.

Burner Transfer Function. Figure 5 shows the acoustic transfer function of the burner. The axial describing function, relating fluctuations in axial velocity at the swirler inlet to fluctuations in axial velocity at the combustion chamber inlet, shows moderate saturation for low forcing frequencies. For frequencies higher than 150 Hz, no saturation occurs for the frequencies and amplitudes investigated. Generally, the gain for the response of the axial component decreases with increasing frequency up to 250 Hz and remains approximately constant for higher frequencies. The phase exhibits only a slight frequency dependence and no considerable effect of the forcing amplitude.

The azimuthal burner describing function, which relates fluctuations in axial velocity at the swirler inlet to fluctuations in azimuthal velocity at the combustion chamber inlet, is shown in Fig. 6. The phase decreases continuously, corresponding to a time lag of $\approx$4.4 ms, which is associated with the convective time from the swirl generator to the combustor inlet, and is amplitude independent. The spread at 254 Hz is due to a vanishing magnitude and hence irrelevant. The magnitude of the azimuthal describing function decreases up to 150 Hz. For frequencies higher than

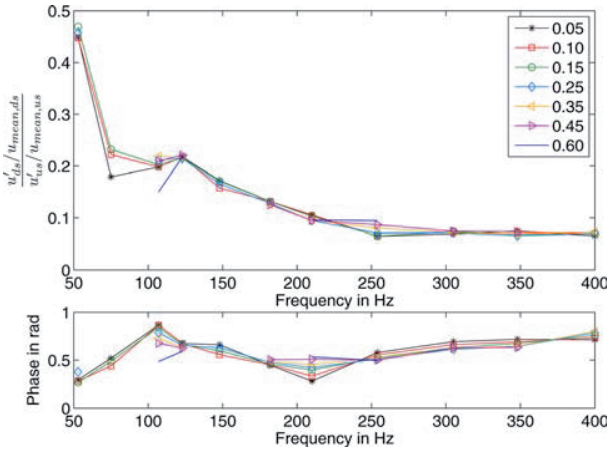

Fig. 5 Acoustic burner describing function, gain, and phase of the transfer function relating axial velocity fluctuations at the swirler inlet to axial velocity fluctuations at the combustion chamber inlet. Symbols indicate the forcing level in terms of the normalized acoustic velocity amplitude ($|u'|/\bar{u}$) at the combustion chamber inlet.

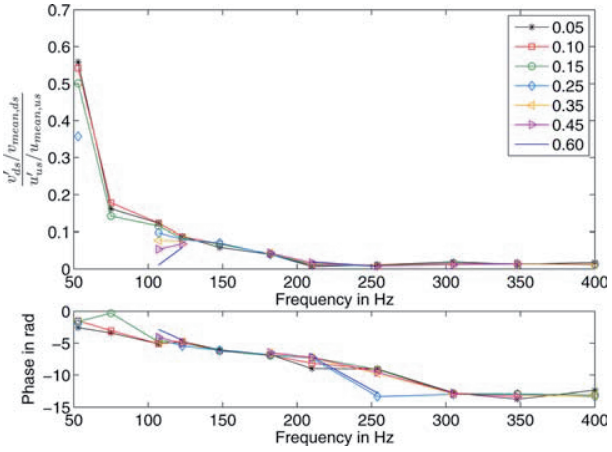

Fig. 6 Acoustic burner describing function, gain, and phase of the transfer function relating axial velocity fluctuations at the swirler inlet to azimuthal velocity fluctuations at the combustion chamber inlet. Symbols indicate the forcing level in terms of the normalized acoustic velocity amplitude ($|u'|/\bar{u}$) at the combustion chamber inlet.

200 Hz, the gain is about one order of magnitude lower than the gain of the axial describing function. Hence, azimuthal velocity fluctuations do not have a considerable influence at these higher frequencies.

Amplitude Dependence of the Flame Response and Interaction With the Flow Dynamics. Figure 7 presents the flame describing function. The phase is decreasing continuously with increasing frequency. For frequencies higher than 200 Hz, a weak amplitude dependence of the phase can be observed. The slope of the phase is associated with a time lag of 4.4 ms. The equivalence with the convective time delay of the azimuthal burner describing function appears to be a coincidence.

It is often assumed that the flame response to velocity perturbations is mostly related to two mechanisms which are convectively transported to the flame front [8]: equivalence ratio fluctuations, which do not have an influence in the present setup due to the long mixing length, and vortex shedding at the area discontinuity at the combustion chamber inlet. One oscillation period at 254 Hz,

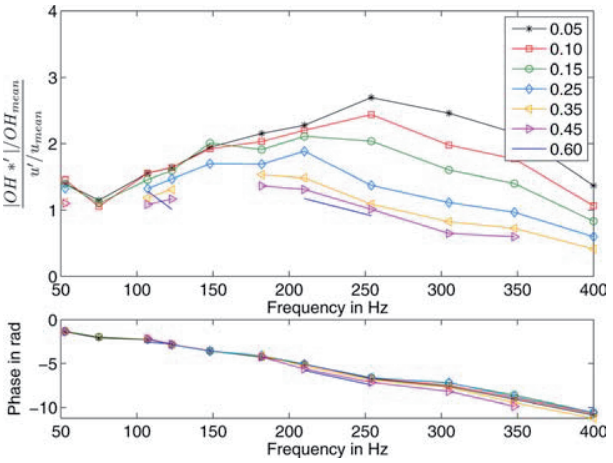

Fig. 7 Flame describing function for various forcing amplitudes. Symbols indicate the forcing level in terms of the normalized acoustic velocity amplitude ($|u'|/\bar{u}$) at the combustion chamber inlet.

which is the frequency with the highest gain in the flame transfer function, corresponds to ≈4 ms. This is in good agreement with the time delay calculated from the slope of the phase of 4.4 ms and indicates that one mechanism is clearly dominating the flame response almost over the entire frequency range investigated. In the linear regime, the gain of the flame describing function decreases at lower frequencies until a minimum is attained at about 75 Hz. The larger gain at 53 Hz indicates the occurrence of another mechanism determining the flame response in that frequency regime. Saturation in the flame response can be observed over almost the entire frequency range for increasing forcing amplitudes.

Forcing at 53 Hz. Figure 8 consists of two columns, each showing the Abel-deconvoluted radially weighted OH*-chemiluminescence images of the flame at six of eight equidistant phases of one oscillation period and the associated flow field at a forcing frequency of 53 Hz. On the left side of each image, the flow field is displayed as a vector plot visualizing regions of high velocity, on the right side as streamlines revealing vortical structures. The solid line indicates the inner region of reversed axial flow. Each column corresponds to one normalized forcing amplitude, left 0.22 and right 0.33, in the linear regime of the flame response (see Fig. 9).

Although a normalized forcing amplitude of almost 0.5 was reached, a clear saturation of the describing function could not be observed at 53 Hz. Generally, the oscillation of the flame front and the flow field at the two forcing amplitudes examined here are qualitatively similar but show the phenomena discussed in the following with varying intensity.

For 53 Hz, the gain of the axial and the azimuthal burner describing functions (Figs. 5 and 6) is almost equal. The phase between the axial and azimuthal fluctuations at the combustion chamber inlet is approximately π. This results in a strong fluctuation of the ratio between azimuthal and axial velocity, i.e., in the swirl number and hence in the FA. While the flame is moving downstream, phases 4–8, the intensity of the OH* chemiluminescence increases, whereas it decreases in the other phases of the oscillation cycle, when the flame moves upstream.

For $|u'|/\bar{u} = 0.22$, a strong axial fluctuation of the flame position due to FA fluctuations is already visible. In phase 4, the axial inlet velocity is at its maximum and the azimuthal one at its minimum. A pocket with low azimuthal and high axial momentum is formed at the combustion chamber inlet and starts convecting along the annular jet, leading to a deformation of the inner recirculation zone and a bend of the flame front in phase 6. In the

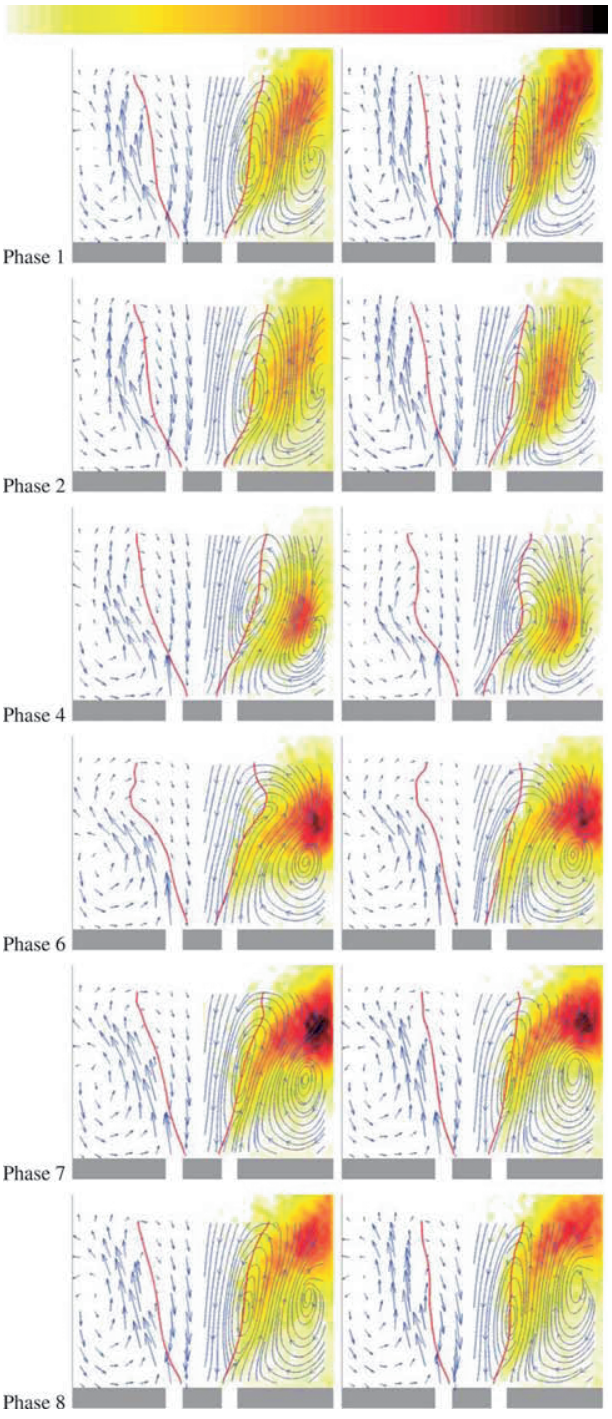

Fig. 8 Two columns corresponding to $u'/\bar{u} = 0.22$ (left) and 0.33 (right) at 53 Hz. Each row corresponds to one of eight equidistant phases of the forcing period. Each individual picture shows the OH* image of the flame and the corresponding phase-averaged flow field.

following two phases, it convects to the downstream end of the reaction zone and stretches the flame brush in the axial direction. The heat release rate reaches a maximum at phase 7. The impact of the pocket with maximum azimuthal momentum on the flame, which is generated at phase 8, is less obvious due to the lower heat release rate at phases 2–4.

Figure 10 shows the total displacement of the COM of the OH*-chemiluminescence images in axial direction, Δx_{COM},

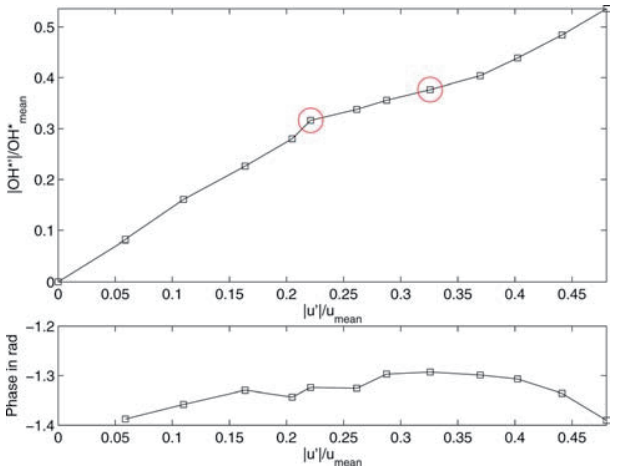

Fig. 9 Amplitude-dependent flame response at 53 Hz

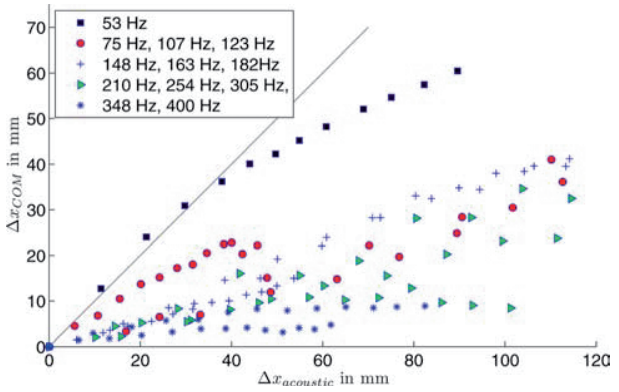

Fig. 10 Axial displacement of the COM of the OH*-chemiluminescence images versus acoustic displacement in the annular jet; straight line indicates equal acoustic and com displacements

plotted against the acoustic displacement in the annular jet for various frequencies. The total acoustic displacement is defined as

$$\Delta x_{\mathrm{acoustic}} = \frac{u'_{\mathrm{jet}}}{\pi f} \tag{4}$$

with the absolute velocity fluctuation amplitude in the annular jet u'_{jet}. At a forcing frequency of 53 Hz, the displacement of the COM of the OH*-chemiluminescence intensity is as high as the acoustic displacement up to 40 mm. The change in the slope for higher displacements than 40 mm can be also observed as a slight change in the slope of the amplitude-dependent flame response in Fig. 9 at a normalized forcing amplitude of 0.2. The slope of the curve for 53 Hz in Fig. 10 is significantly higher than for other forcing frequencies. The strong fluctuation of the swirl number and hence the FA leads to an increased axial fluctuation of the flame position. In the earlier studies [13] for other operating conditions, it has been found that at similar axial flame movements, parts of the reaction zone were torn apart from the main reaction zone during saturation of the corresponding describing function.

Forcing at 123 Hz. Figure 11 shows the Abel-deconvoluted images of the flame and the flow field at a forcing frequency of 123 Hz at normalized forcing amplitudes of $|u'|/\bar{=}0.19$ corresponding to the linear regime and 0.77 where the flame response significantly changes the slope (see Fig. 12). A comparison of the

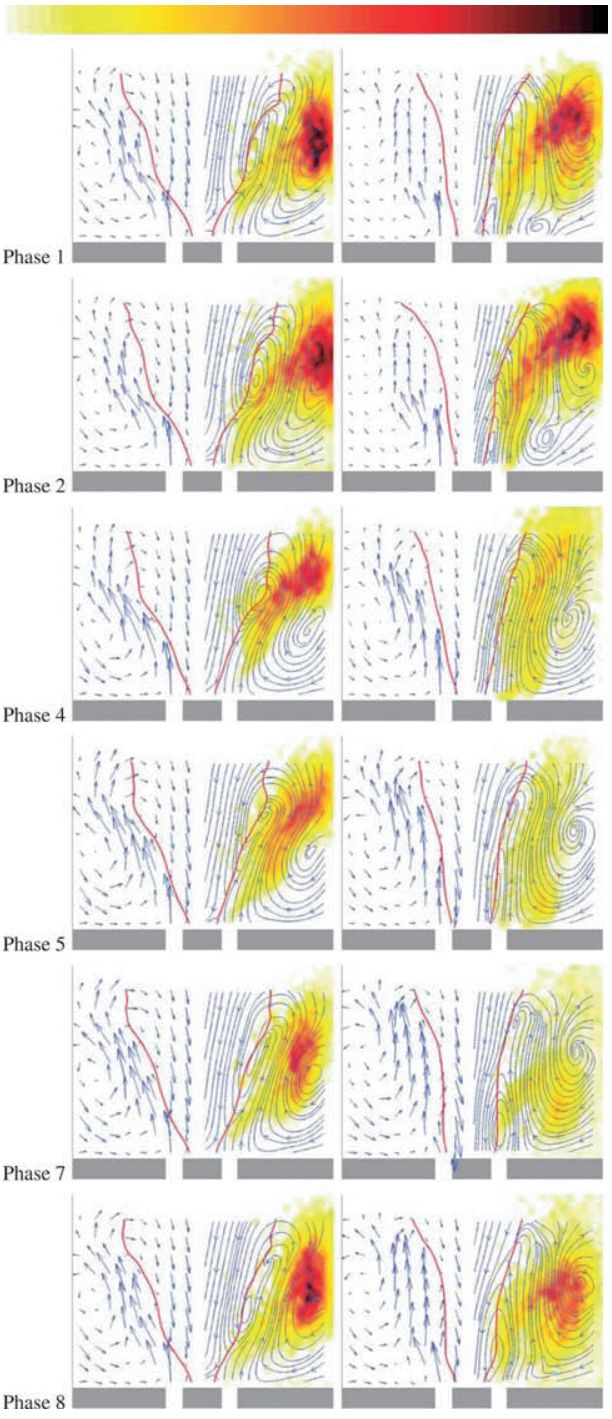

Fig. 11 Two columns corresponding to $|u'|/\bar{u} = 0.19$ (left) and 0.77 (right) at 123 Hz. Each row corresponds to one of eight equidistant phases of the forcing period. Each individual picture shows the OH* image of the flame and the corresponding phase-averaged flow field.

phase response of the burner describing functions (Figs. 5 and 6) shows that the axial and tangential fluctuations are approximately in phase at the combustion chamber inlet at a forcing frequency of 123 Hz; hence, swirl fluctuations are rather small.

The first column of Fig. 11 shows only small fluctuations in the flame location for forcing at 123 Hz compared to forcing at 53 Hz with a similar amplitude. The axial oscillation of the flame position due to the strong swirl number fluctuations in the previous

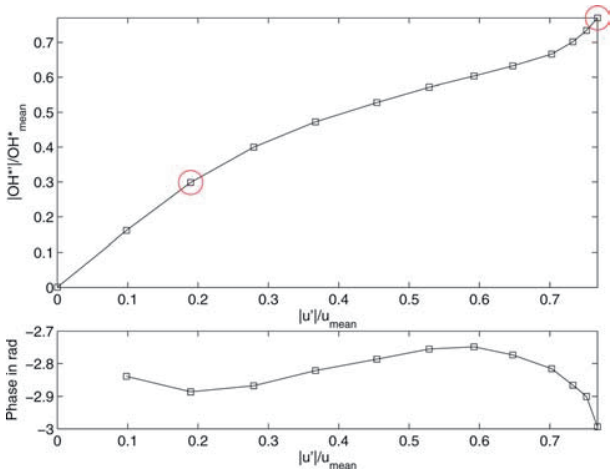

Fig. 12 Amplitude-dependent flame response at 123 Hz

case is completely absent. The flame is anchored in the inner shear layer of the annular jet and fluctuates in intensity due to the fluctuation of unburned gas transport to the flame front. The maximum of the axial velocity is in phase 2, where a deflection of the flame front can be observed.

In phase 1, a vortex is generated at the outer edge of the combustion chamber inlet and sheds in phase 2 (right column). The vortex travels downstream along the shear layer in the subsequent phases. A thin flame brush in the unburned gas in the outer shear layer, which is apparent in phase 7 but can be even seen in earlier phases, is ignited. It starts in phase 4 and increases continuously in strength, while the axial jet velocity decreases. The flame brush moves downstream in the outer shear layer as the axial velocity increases in the subsequent phases and moves through the annular jet, igniting fresh gas in the inner shear layer. Note that ignition of the flame starts in the outer shear layer of the jet and the flame flashes from downstream into the inner shear layer, traveling upstream while the axial velocity is increasing.

With increasing forcing amplitude, vortices shed at the outer edge of the combustion chamber inlet gain intensity. These vortices lead to an increased entrainment from the outer recirculation zone which thickens the shear layer. As the flow is confined, the increased thickness of the shear layer narrows the inner recirculation zone and leads to a decreased FA for all phases compared to the lower-amplitude forcing case. This results in a vortex in the inner shear layer that is visible over almost the entire oscillation period, one half nozzle diameter downstream of the inner edge of the combustion chamber inlet. Note that the axial extent of the flame increases for the higher forcing amplitude.

Forcing at 254 Hz. Figure 13 shows Abel-deconvoluted images of the flame and the flow field for a forcing frequency of 254 Hz. The normalized forcing amplitudes $|u'|/\bar{u} = 0.12$ and 0.75 correspond to the end of the linear and to the saturated regime of the flame describing function, respectively (see Fig. 14). Please note that the flame describing function shows two saturation regimes at forcing amplitudes of $|u'|/\bar{u} \approx 0.2$ and $|u'|/\bar{u} \approx 0.7$, respectively.

The burner describing function (Fig. 6) exhibits a vanishing azimuthal fluctuation amplitude compared to the magnitude of the axial fluctuation for frequencies larger than 200 Hz. Therefore, any fluctuation in the azimuthal velocity is neglected in the following discussion.

In phase 6, the axial velocity is at a minimum. In the left column, a flame brush develops upstream of the main reaction zone. The reacting pocket convects along the annular jet, becoming stronger in the subsequent phases until it hits the main reaction zone at phase 4.

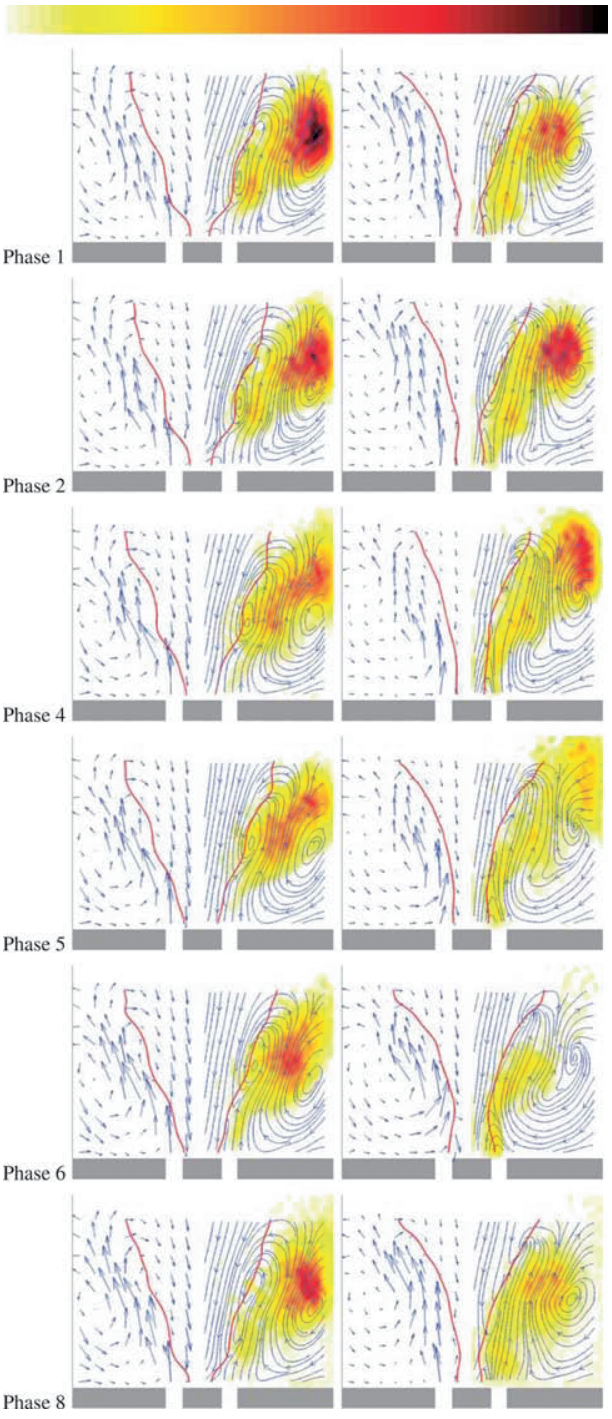

Fig. 13 Two columns corresponding to $|u'|/\bar{u} = 0.12$ (left) and 0.75 (right) at 254 Hz. Each row corresponds to one of eight equidistant phases of the forcing period. Each individual picture shows the OH* image of the flame and the corresponding phase-averaged flow field.

For the higher forcing amplitude, again, the inner recirculation zone is narrowed significantly, resulting in a decreased FA. Figure 15 shows the FAs for 254 Hz and various other forcing frequencies plotted against the normalized forcing amplitude. The FA decreases significantly for all frequencies investigated with increasing forcing amplitude. The flow field data confirm that the inner recirculation zone is narrowed significantly for increased forcing amplitudes (not shown). A plausible explanation is that

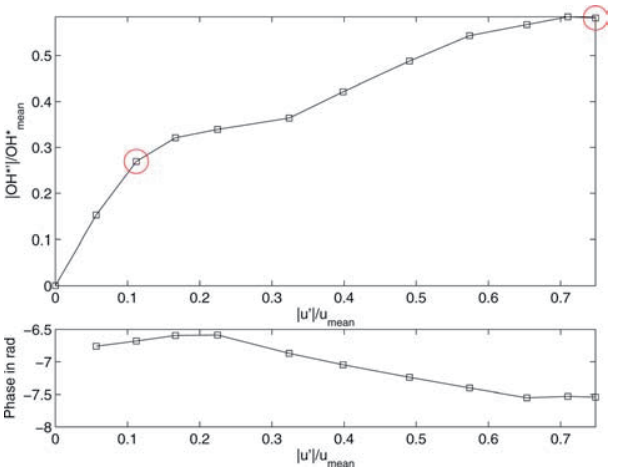

Fig. 14 Amplitude-dependent flame response at 254 Hz

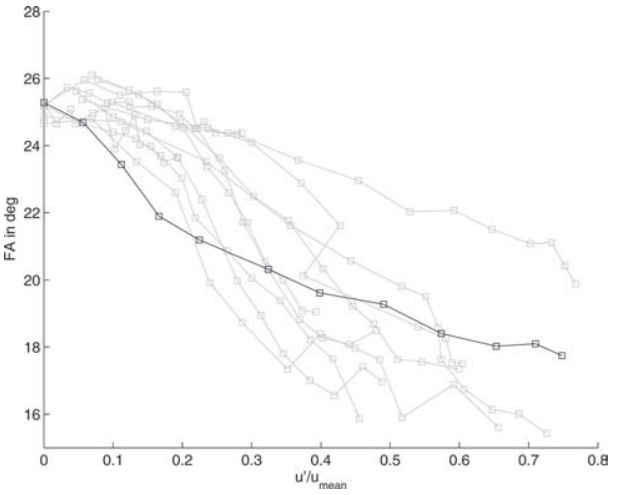

Fig. 15 FA at various forcing amplitudes at 254 Hz (black) and for various other forcing frequencies (gray)

for increasing forcing amplitudes the vortices shed at the combustion chamber inlet gain intensity. Due to an increased entrainment, the growth of the shear layer is increased, which in turn squeezes the inner recirculation zone and leads to the observed narrowing.

Due to the narrowed inner recirculation zone, the flame is continuously anchored in the wake of the center body, near the combustion chamber inlet. For several phases, the flame also increases further downstream (right column of Fig. 13). Figure 16 shows the average over the oscillation cycle of the transverse moment of inertia of the phase-averaged OH* chemiluminescence plotted against the acoustic displacement. The transverse moment of inertia x_{MOI} of the chemiluminescence distribution I is calculated as

$$x_{\mathrm{MOI}} = \frac{\int_A x^2 I(x,y)\mathrm{d}A}{\int_A I(x,y)\mathrm{d}A}$$

This quantity is an indicator of the axial expansion of the flame and grows with higher forcing amplitude for all frequencies investigated. This increases the temporal scatter of the response of the flame to flow perturbations and hence dampens the response.

Oberleithner et al. [17] showed for the present measurement data that the amplification of flow disturbances, due to shear layer instabilities, underlie a saturation at increasing forcing amplitudes,

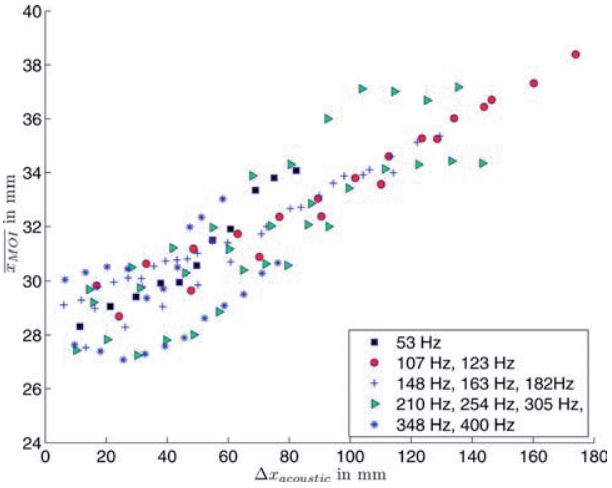

Fig. 16 Average over the oscillation cycle of the transverse moment of inertia of the phase-averaged OH* chemiluminescence distribution plotted against the acoustic displacement. Axial expansion of the flame increases with increasing forcing amplitude.

which correlates with the first saturation in the flame describing function for 254 Hz at $|u'|/\bar{u} \approx 0.2$ (see Fig. 14).

Furthermore, the growth of the shear layer thickness and the decrease of the FA increase the spatial distance between vortices shed at the outer edge of the combustion chamber inlet, convecting along the outer shear layer and the heat release region. Since the shear layer vortices grow only over a finite axial extent, the increased distance reduces the impact on the flame. This may be one reason for the second saturation of the flame describing function at 254 Hz at $|u'|/\bar{u} \approx 0.7$.

Forcing at 400 Hz. For the following test case, the Reynolds number was set to 44,000 and the axial length of the annular section was increased by 30 mm. Figure 17 shows the Abel-deconvoluted images of the flame and the flow field at a forcing frequency of 400 Hz. The normalized forcing amplitudes investigated are $|u'|/\bar{u} = 0.07$ and 0.37, corresponding to the linear and the saturated regime of the flame response, respectively (see Fig. 18). Saturation is present at an oscillation level of $|\mathrm{OH}^*|/\overline{\mathrm{OH}}^* \approx 0.2$. A considerable change in the phase can be observed during the saturation process.

The left half of Fig. 19 shows an OH* image averaged over the entire oscillation, illustrating the average flame size. In the right half, the averaged OH* image has been subtracted from a phase-averaged image at an arbitrary phase, thus corresponding to only the fluctuating part of the chemiluminescence distribution. Two zones are visible in the right half of Fig. 19 that react in phase and are associated with vortices, shed in the same phase at two subsequent oscillation cycles. Contrary to all cases discussed previously, for 400 Hz the convective length scale associated with one oscillation period, i.e., the spatial distance of two subsequent vortices, is smaller than the length of the flame in the OH*-chemiluminescence images. Hence, any perturbation of the heat release rate due to coherent structures in the flow has a local character, i.e., different regions of the flame are counteracting. This mechanism decreases the response at higher frequencies and thus can be identified as being one contribution for the typical low-pass character of premixed flames.

As stated before, velocity oscillations in the azimuthal direction are not considered, as they are small compared to axial velocity fluctuations for high frequencies. A fluctuation of the axial velocity therefore directly causes a fluctuation in the swirl number and thus in the FA. In Fig. 17, for both forcing amplitudes, a meandering movement of the annular jet due to the fluctuation of axial

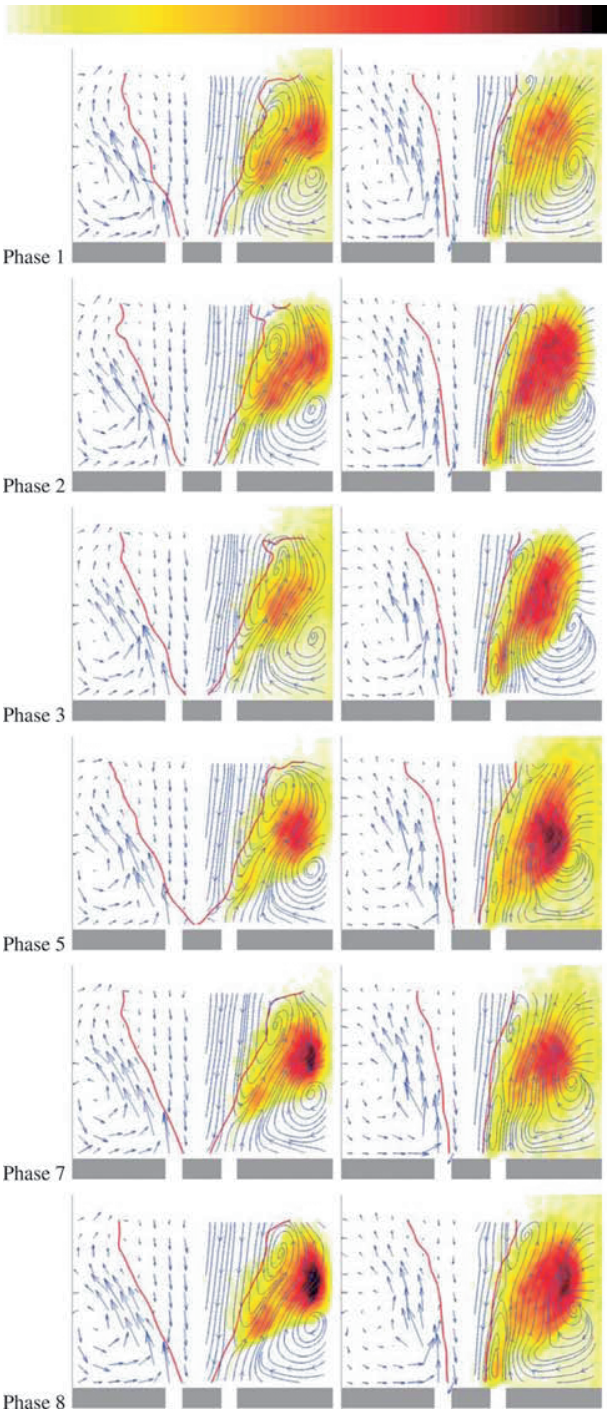

Fig. 17 Two columns corresponding to $|u'|/\bar{u} = 0.07$ (left) and 0.37 (right) at 400 Hz. Each row corresponds to one of eight equidistant phases of the forcing period. Each individual picture shows the OH* image of the flame and the corresponding phase-averaged flow field.

velocity is visible. The maximum of the inlet velocity is reached approximately at phase 5. For the lower forcing amplitude shown, corresponding to the end of the linear regime, a thin flame brush upstream of the main reaction zone starts to develop in the inner shear layer with minor intensity in phase 3 and continuously gains intensity until phase 7, where the maximum of the global heat release rate is reached, and the brush and the main reaction zone merge.

With increasing forcing amplitude, both the meandering of the annular jet and the thin flame brush upstream of the main heat

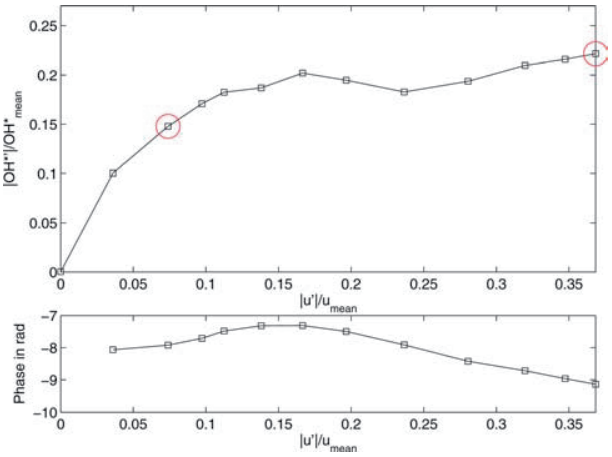

Fig. 18 Amplitude-dependent flame response at 400 Hz

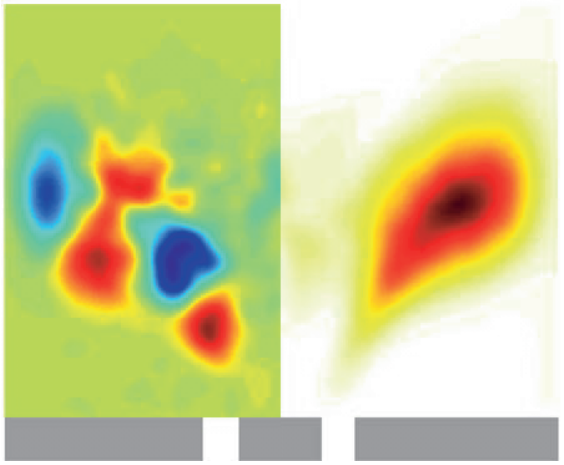

Fig. 19 Left: OH* image averaged over all phases; right: fluctuating part of OH* image at an arbitrary phase illustrating the convective length scale

release region gain intensity. Although the heat release of the latter starts for the highest forcing amplitude around phase 8, where the maximum of the global heat release rate is found, it has a considerable portion of the overall heat release rate in phases 2 and 3, at the minimum of the global heat release rate fluctuation and hence counteracts that.

The mechanisms that were stated to lead to the saturation of the flame describing function at 254 Hz can be clearly identified here as well: vortex shedding at the outer edge of the combustion chamber inlet causes an increased entrainment from the outer recirculation zone and thickens the shear layer. The inner recirculation zone is narrowed and the FA decreased. This leads to an increased distance, and hence decreased interaction, between vortices shed at the outer edge of the combustion chamber inlet and the flame. Furthermore, the axial extent of the flame is increased, which scatters the interaction between the flame and coherent flow structures over a broader phase interval.

Summary

The amplitude-dependent burner transfer functions, relating fluctuations in axial velocity at the swirler inlet to fluctuations in axial and azimuthal velocity at the combustion chamber inlet, were determined with the multimicrophone-method and LDV. For high frequencies, the gain of the azimuthal describing function was found to be an order of magnitude smaller than the gain for the axial describing function. An amplitude-dependent flame response to velocity oscillations was observed over the entire frequency range investigated.

Phase-averaged, Abel-deconvoluted OH* chemiluminescence images and the flow field obtained from PIV measurements were found to be a valuable combination as it enabled the identification of several interaction mechanisms that determine the amplitude dependence of the flame response. The combined knowledge of the time-resolved heat release rate distribution and the flow field of the flame were used to identify various flow-field–heat-release interactions corresponding to characteristic frequency regimes.

53 Hz. Strong swirl number, and hence flow angle, fluctuations were observed to result from axial and azimuthal velocity fluctuations from the swirler. A strong axial oscillation in flame position is induced, which is of the order of the acoustic displacement in the linear regime.

Mid and High Frequency Regime. In the outer shear layer, vortex shedding was observed. Increased entrainment from the outer recirculation zone leads to a more pronounced growth of the outer shear layer. Since the flow is confined, the inner recirculation zone is constricted and significantly narrowed. The FA was found to decrease with increasing forcing amplitude for all frequencies investigated. This leads to a larger distance and hence reduced interaction between vortices shed from the outer edge of the combustion chamber inlet and the reaction zone. Furthermore, an increase of the axial extent of the reaction zone with increasing forcing amplitude was found for all forcing frequencies investigated. This results in an increase of the temporal scatter of the response of the flame to flow field perturbations. These two mechanisms are suggested to be responsible for the observed saturation of the flame response at increasing forcing amplitudes.

High Frequency Regime. The low-pass characteristic of the flame was observed as the convective length scale associated with one oscillation period becomes small compared to the flame length. Different regions of the flame are counteracting each other.

Acknowledgment

Financial support from the Research Association for Combustion Engines (FVV) is gratefully acknowledged.

Nomenclature

f = frequency
F = flame transfer function
G = amplitude of flame transfer function
OH* = intensity of OH* radiation
Q = integral heat release rate
u = axial velocity
v = azimuthal velocity
x_{MOI} = transverse moment of inertia of OH* chemiluminescence distribution
$\Delta x_{\mathrm{acoustic}}$ = acoustic displacement
Δx_{COM} = axial displacement of center of mass of OH* chemiluminescence
ϕ = flame transfer function phase
φ = equivalence ratio
ω = angular oscillation frequency

References

[1] Lieuwen, T. C., and Yang, V., eds., 2005, *Combustion Instabilities in Gas Turbine Engines* (Progress in Astronautics and Aeronautics, Vol. 210), American Institute of Aeronautics and Astronautics, Reston, VA, pp. 445–480.
[2] Dowling, A. P., and Stow, S. R., 2003, "Acoustic Analysis of Gas Turbine Combustors," J. Propul. Power, **19**(5), pp. 751–764.

[3] Paschereit, C. O., Schuermans, B., Bellucci, V., and Flohr, P., 2005, "Implementation of Instability Prediction in Design: ALSTOM Approaches," *Combustion Instabilities in Gas Turbine Engines* (Progress in Astronautics and Aeronautics, Vol. 210), T. C. Lieuwen and V. Yang, eds., American Institute of Aeronautics and Astronautics, Reston, VA, pp. 445–480.
[4] Dowling, A. P., 1997, "Nonlinear Self-Excited Oscillations of a Ducted Flame," J. Fluid Mech., **346**(9), pp. 271–290.
[5] Bellows, B. B., Bobba, M. K., Forte, A., Seitzmann, J. M., and Lieuwen, T., 2007, "Flame Transfer Function Saturation Mechanisms in a Swirl-Stabilized Combustor," Proc. Combust. Inst., **31**(2), pp. 3181–3188.
[6] Balachandran, R., Ayoola, B. O., Kaminski, C. F., Dowling, A. P., and Mastorakos, E., 2005, "Experimental Investigation of the Nonlinear Response of Turbulent Premixed Flames to Imposed Inlet Velocity Oscillations," Combust. Flame, **143**(1–2), pp. 37–55.
[7] Noiray, N., Durox, D., Schuller, T., and Candel, S., 2008, "A Unified Framework for Nonlinear Combustion Instability Analysis Based on the Flame Describing Function," J. Fluid Mech., **615**(11), pp. 139–167.
[8] Schuermans, B., Bellucci, V., Guethe, F., Meili, F., Flohr, P., and Paschereit, C. O., 2004, "A Detailed Analysis of Thermoacoustic Interaction Mechanisms in a Turbulent Premixed Flame," ASME Paper No. GT2004-53831.
[9] Culick, F., Ratner, A., Isella, G., Matveev, K., Palm, S. P., Pun, W., Seywert, C., and Swenson, G., 2001, "Nonuniformities of Mixture Ratio as a Mechanism of Combustion Instabilities in Lean Pre-Mixed Combustors," Jet Propulsion Center, California Institute of Technology, AGTSR Subcontract No. 98-01-SR063.
[10] Schuermans, B., Polifke, W., Paschereit, C. O., and van der Linden, J. H., 2000, "Prediction of Acoustic Pressure Spectra in Combustion Systems Using Swirl Stabilized Gas Turbine Burners," ASME Paper No. 2000-GT-0105.
[11] Lieuwen, T. C., Torres, H., Johnson, C., and Zinn, B. T., 2001, "A Mechanism of Combustion Instability in Lean Premixed Gas Turbine Combustors," ASME J. Eng. Gas Turbines Power, **123**(1), pp. 182–189.
[12] Thumuluru, S. K., and Lieuwen, T., 2009, "Characterisation of Acoustically Forced Swirl Flame Dynamics," Proc. Combust. Inst., **32**(2), pp. 2893–2900.
[13] Schimek, S., Moeck, J. P., and Paschereit, C. O., 2011, "An Experimental Investigation of the Nonlinear Response of an Atmospheric Swirl-Stabilized Premixed Flame," ASME J. Eng. Gas Turbines Power, **133**(10), p. 101502.
[14] Palies, P., Schuller, T., Durox, D., and Candel, S., 2011, "Modeling of Premixed Swirling Flames Transfer Functions," Proc. Combust. Inst., **33**(2), pp. 2967–2974.
[15] Poinsot, T. J., Trouvé, A. C., Veynante, D. P., Candel, S. M., and Esposito, E. J., 1987, "Vortex-Driven Acoustically Coupled Combustion Instabilities," J. Fluid Mech., **177**(4), pp. 265–292.
[16] Armitage, C. A., Balachandran, R., Mastorakos, E., and Cant, R. S., 2006, "Investigation of the Nonlinear Response of Turbulent Premixed Flames to Imposed Inlet Velocity Oscillations," Combust. Flame, **146**(3), pp. 419–436.
[17] Oberleithner, K., Schimek, S., and Paschereit, C. O., 2012, "On the Impact of Shear Flow Instabilities on Global Heat Release Rate Fluctuations: Linear Stability Analysis of an Isothermal and a Reacting Swirling Jet," ASME Paper No. GT2012-69774.
[18] Palies, P., Durox, D., Schuller, T., and Candel, S., 2010, "The Combined Dynamics of Swirler and Turbulent Premixed Swirling Flames," Combust. Flame, **157**(9), pp. 1698–1717.
[19] Leuckel, W., 1967, "Swirl Intensities, Swirl Types and Energy Losses of Different Swirl Generating Devices," International Flame Research Foundation, Ijmuiden, The Netherlands, Technical Report No. G02/a/16.
[20] Schneider, C., 2004, "Über die Charakterisierung von Turbulenzstrukturen in verdrallten Strömungen," Ph.D. thesis, Technische Universität Darmstadt, Darmstadt, Germany.
[21] Paschereit, C. O., Schuermans, B., Polifke, W., and Mattson, O., 2002, "Measurement of Transfer Matrices and Source Terms of Premixed Flames," ASME J. Eng. Gas Turbines Power, **124**(2), pp. 239–247.
[22] Güthe, F., and Schuermans, B., 2007, "Phase-Locking in Post-Processing for Pulsating Flames," Meas. Sci. Technol., **18**(9), pp. 3036–3042.
[23] Jaffe, S., Larjo, J., and Henberg, R., 1991, "Abel Inversion Using the Fast Fourier Transform," 10th International Symposium on Plasma Chemistry, Bochum, Germany, Aug. 4–9.

Combustion and Flame 162 (2015) 86–99

Contents lists available at ScienceDirect

Combustion and Flame

journal homepage: www.elsevier.com/locate/combustflame

Shear flow instabilities in swirl-stabilized combustors and their impact on the amplitude dependent flame response: A linear stability analysis

Kilian Oberleithner *, Sebastian Schimek, Christian Oliver Paschereit

Institut für Strömungsmechanik und Technische Akustik, Hermann-Föttinger-Institut, Technische Universität Berlin, Müller-Breslau-Str. 8, 10623 Berlin, Germany

ARTICLE INFO

Article history:
Received 26 September 2013
Received in revised form 20 January 2014
Accepted 15 July 2014
Available online 20 August 2014

Keywords:
Swirl flame
Hydrodynamic instability
Flame describing function
Linear stability analysis

ABSTRACT

The hydrodynamic instabilities in the flow field of a swirl-stabilized combustor are investigated theoretically. These instabilities give rise to large-scale flow structures that interact with the flame front causing unsteady heat release rate fluctuations. The streamwise growth of these coherent structures depends on the receptivity of the shear layer, which can be predicted numerically by means of linear stability analysis. This analysis is applied to the reacting flow field of a perfectly premixed swirl-stabilized combustor that is subjected to strong axial forcing mimicking thermoacoustic oscillations. The linear stability analysis reveals a clear correlation between the shear layer receptivity and the measured amplitude dependent flame transfer function. The stability analysis based on the natural flow predicts the distinctive frequency dependent flame response to low amplitude forcing. At these conditions, the flow reveals strong spatial amplification near the nozzle, causing the inlet perturbations to be significantly amplified before they reach the flame. At higher forcing amplitudes, the flow instabilities saturate, which manifests in a saturation of the flame response. The saturation of the shear layers predicted from the linear stability analysis is compared to phase-locked measurements of the forced flow field revealing good qualitative agreement. The analysis of the mean flow stability offers a powerful analytical tool to investigate the impact of shear flow instabilities on the flame describing function.

1. Introduction

This work focuses on the role of shear flow instabilities in the coupling between the acoustic field and the flame in modern lean premixed combustors. These combustion systems are highly susceptible to thermoacoustic instabilities that are driven by a constructive interference of pressure and heat release rate fluctuations [1–3]. The associated limit-cycle oscillations have a detrimental effect on the combustion process and on the engine life time [4]. The flow field in the combustor closes the feedback loop converting acoustic perturbations emanated from the flame into flow fluctuations that, in turn, propagate into the flame and induce heat release rate fluctuations.

The linear stability of a combustion system is determined by the flame's response to low amplitude acoustic perturbations. This is typically quantified by the flame transfer function (FTF) that relates inflow perturbations to the global heat release rate fluctuations. It is valid for the low amplitude (linear) regime, where the heat release rate fluctuations increase linearly with increasing perturbation amplitude. At unstable conditions, the oscillation amplitudes increase and nonlinearities in the flame response become effective. This is expressed by the amplitude dependent transfer function also called the flame describing function (FDF) [5,6]. The nonlinearities captured by the FDF determine the limit-cycle amplitude of the instability.

Up to date, there is no rigorous method available that allows for predicting the FDF for a given combustion system revealing no other option than costly experimental assessment. This calls for a better understanding of the physics buried in the FTF and the FDF in order to develop new models that require less empirical input to predict thermoacoustic instabilities.

The difficulties in predicting the FDF stem from the multiple mechanisms that determine the flame's response to acoustic perturbations. In technically premixed flames, equivalence ratio fluctuations can cause significant heat release rate fluctuations. At perfectly premixed conditions, the fluctuations in the flow field are the main driver of the unsteady heat release. Moreover, the flame-front itself features inherent nonlinear dynamics that interfere with the flow dynamics thereby affecting the FDF [7].

Flow–flame interactions and their impact on the heat release rate fluctuations have been extensively studied within the last

* Corresponding author.
E-mail address: kilian.oberleithner@pi.tu-berlin.de (K. Oberleithner).

http://dx.doi.org/10.1016/j.combustflame.2014.07.012
0010-2180/

decade [8–12]. Two main mechanisms have been identified, the vortex–flame interactions and the swirl number fluctuations. The first is the consequence of shear layer instabilities that cause the formation of large-scale (coherent) flow structures that propagate into the flame front. The vortex–flame interactions alter the instantaneous heat release rate fluctuations in several ways, such as flame roll-up [13], mixing of burned and unburned gas and subsequent flame reignition [14]. The intensity of the vortex–flame interaction and its impact on the FTF depends on the underlying flow instability. Helical (skew-symmetric) coherent structures prevalent in natural swirling jets, although affecting the flame locally [14], do not contribute to the global heat release rate fluctuations [15]. In contrast, the axisymmetric Kelvin–Helmholtz-type instability that couples with plane acoustic waves, significantly affects the global heat release rate fluctuations. Thereby, the gain in the FTF depends on the growth of the vortical structures, their lifetime before impinging the flame, and thus, on the flame shape [11,13,16,17]. Swirl number fluctuations are generated by the interference of vorticity waves generated in the swirler and plane acoustic waves. This may lead to oscillations of the opening angle of the annular swirling jet and, consequently, of the flame [18]. The oscillations of the flame angle may interfere with the roll-up of the flame tip (vortex–flame interactions) thereby affecting the FTF [17].

All the previous work mentioned here focuses on the dynamics of the flame and how they are affected by the fluctuating flow field. In this study we focus on the generation of these flow fluctuations rather then on how they actually interact with the flame. Our focus lies on the underlying hydrodynamic instabilities that lead to the formation of the coherent flow structures before they interact with the flame. We adopt an analytic approach to predict the flow response to the incoming acoustic perturbations.

The adopted approach is based on the linearized Navier–Stokes equations in conjunction with a normal mode perturbation ansatz, leading to the well-known Orr–Sommerfeld eigenvalue problem [19,20]. Equipped with an eddy viscosity model, this method provides an analytic framework for the formation of coherent structures in turbulent shear flows of various kinds. Fundamental research on elementary flow configurations such as the mixing layer or the axisymmetric jet revealed that coherent flow structures are driven by an inherent flow instability and their characteristics (frequency, wavenumber, and amplitude) are well modeled by linear eigenmodes of the Orr–Sommerfeld operator [21–24].

Within the framework of linear hydrodynamic stability analysis there are different methods applicable to different types of instabilities. A global stability analysis, utilizing a two- or three-dimensional perturbation ansatz, predicts weather the entire flow field is unstable to a single flow-inherent oscillatory mode [25,26]. Examples for global instabilities are the precessing vortex core of a strongly swirling jet [27–29] or the *von Kármán vortex street* encountered in the cylinder wake [30,31]. Internal resonance in the flow field triggers these global instabilities that then manifest in stable limit-cycle oscillations. Globally stable flows can still be convectively unstable. These flows act as amplifiers allowing a wide range of perturbation modes to be amplified in downstream direction [24,32]. The overall growth of these instabilities depends on the spatial growthrates of the flow field that is traversed by the perturbation. These growth rates are conveniently derived from a local spatial stability analysis utilizing a one-dimensional perturbation ansatz. Examples for convectively unstable flows are the mixing layer or the cold axisymmetric jet [21,23].

Although, shear flow instabilities have been extensively studied within the last four decades, the established theoretical concepts have only recently entered the focus of the combustion dynamics community. O'Connor and Lieuwen [12] emphasize the importance of flow instabilities as the link between acoustic waves and flame oscillations. Within the same group, the destabilizing effect of density inhomogeneities on a bluff-body-stabilized flame was investigated employing an local linear stability approach [33]. This methodology was used recently within our group to reveal the impact of combustion on the formation of a precessing vortex core [29,34].

The flow considered in this work is globally stable and a local spatial stability analysis is adopted, providing the spatial growth rates and the overall amplification of the inlet perturbations for a given combustor flow field. We apply the analysis to a perfectly-premixed swirl-stabilized flame that is forced axially mimicking thermoacoustic oscillations. The FDF is obtained for a wide range of frequencies and amplitudes and correlated with the results from the linear stability analysis. Connections are drawn between the amplification occurring in the shear layers and the global heat release rate fluctuations.

The goal of this work is to demonstrate this analytic approach on an realistic combustor flow. The correlations between the FDF and the results from the stability analysis must remain qualitative as the vortex–flame interactions explained above are not resolved by this approach. In order to *quantitatively* predict the heat release rate fluctuations, the flame dynamic must be derived from a flame-front tracking equation (e.g. the *G*-equation [35,36]) utilizing the flow field derived from the stability analysis. This (initiative) study is understood as a first step towards an analytical model for a FDF based on hydrodynamic linear stability analysis.

The present manuscript is organized in the following way: The reader is first introduced to the concept of linear stability analysis applied to a turbulent flow in Section 2. The combustion test rig, the measurement techniques, and the considered operating condition are outlined in Section 3. The flame response to inlet perturbations quantified by the FDF is discussed in Section 4. Based on the experimental observation, a working hypothesis is formulated in Section 5, which relates the observed flame response to the shear flow instability. The results of the linear stability analysis of the natural and forced combustor flow are presented in Section 6. The theoretical results are correlated with the experimental observations in Section 7 and the working hypothesis is validated. The study is concluded in Section 8.

2. Theoretical principal and approach

Local linear stability analysis is employed to model the large-scale flow structures encountered in the combustor subjected to acoustic forcing. For the sake of simplicity, the combustor flow is assumed to be isothermal. Generally, a non-uniform density/temperature field in the combustor affects the growth rates of the instabilities [37,38]. This is crucial for self-excited instabilities like the precessing vortex core, where the growth rates in flow regions driving the internal resonance must be accurately predicted. As demonstrated by Oberleithner et al. [29], significant changes of the density field, induced by a reattachment of the flame, cause a complete suppression of the precessing vortex core. However, for convectively unstable flows as investigated here, inaccuracies in the predicted growth rates are not expected to qualitatively alter the results as these instabilities are externally driven and remain unstable over a wide range of parameters. Moreover, in the present investigation, the flame shape changes only weakly with increasing forcing amplitude, and hence, the stability analysis of the different forcing cases should be, at the least, qualitatively correct. The main theoretical approach is in line with the analysis applied to the isothermal unconfined swirling jet reported in Ref. [28] and is, therefore, only briefly described here.

2.1. Formulation of the local linear stability eigenvalue problem

Cylindrical coordinates are used in this work, with x originating at the nozzle exit and directed along the jet axis and with $r = 0$ representing the jet centerline and θ the azimuthal angle.

In its classical form, linear hydrodynamic stability analysis describes the growth of an infinitesimal velocity and pressure perturbation, $\mathbf{v}'(\mathbf{x},t) = (v'_x, v'_r, v'_\theta)$ and p', respectively, on a laminar steady base flow $\mathbf{V}(\mathbf{x}) = (V_x, V_r, V_\theta)$. The formation of this small perturbation is described by the Navier–Stokes equations and the continuity equation linearized around the base flow, which, for an incompressible axisymmetric flow, can be written as

$$\frac{\partial \mathbf{v}'}{\partial t} + \mathbf{v}' \cdot \nabla \mathbf{V} + \mathbf{V} \cdot \nabla \mathbf{v}' = -\nabla p' + \frac{1}{\mathrm{Re}} \nabla^2 \mathbf{v}' \tag{1a}$$

$$\nabla \cdot \mathbf{v}' = 0. \tag{1b}$$

Within the framework of *local* stability analysis, the flow field is sliced into radial velocity profiles and the flow is treated as *locally parallel*, meaning that the analysis is applied to a fictitious parallel flow at each streamwise location. Hence, the flow can be treated as homogeneous in streamwise and azimuthal direction and in time, and the perturbation can be decomposed in the following way

$$[\mathbf{v}'(\mathbf{x},t), p'(\mathbf{x},t)] = \Re\{[\hat{\mathbf{v}}(r), \hat{p}(r)] \mathrm{e}^{i(\alpha x + m\theta - \omega t)}\}, \tag{2}$$

with $\alpha = \alpha_r + i\alpha_i$ being the complex streamwise wavenumber, $\omega = \omega_r + i\omega_i$ the complex frequency, m the real azimuthal wavenumber, and $[\hat{\mathbf{v}}(r), \hat{p}(r)]$ the disturbance eigenfunctions, where $\Re$ refers to the real part.

By introducing ansatz (2) into the equations of motion (1), the four partial differential equations convert into four ordinary differential equations. With the boundary conditions at the combustor walls [39]

$$\hat{v}_x = \hat{v}_r = \hat{v}_\theta = 0 \quad \text{and} \quad \mathrm{d}\hat{p}/\mathrm{d}r = 0 \tag{3}$$

and in the limit along the centerline ($r = 0$)

$$\hat{v}_x = \hat{v}_r = \hat{v}_\theta = \hat{p} = 0 \quad \text{if} \quad |m| > 1 \tag{4a}$$

$$\left.\begin{aligned} &\hat{v}_x = \hat{p} = 0 \\ &\hat{v}_r + m\hat{v}_\theta = 0 \\ &2\mathrm{d}\hat{v}_r/\mathrm{d}r + m\mathrm{d}\hat{v}_\theta/\mathrm{d}r = 0 \end{aligned}\right\} \quad \text{if} \quad |m| = 1 \tag{4b}$$

$$\left.\begin{aligned} &\hat{v}_r(0) = \hat{v}_\theta(0) = 0 \\ &\hat{v}_x \quad \text{and} \quad \hat{p} \quad \text{finite} \end{aligned}\right\} \quad \text{if} \quad m = 0, \tag{4c}$$

the system (1) can be written as an eigenvalue problem with either ω or α being the eigenvalue and $[\hat{\mathbf{v}}, \hat{p}]^T$ the eigenfunctions.

2.2. Analysis of streamwise evolving flows

The above introduced eigenvalue problem can be solved for a complex ω and a given real α, for a complex α and a given real ω, or for a complex α and a complex ω. In this work, we adopt the second approach, which is most applicable to open shear flows that act as noise amplifiers [32]. This so-called spatial analysis describes the streamwise growth and decay of flow perturbations initiated at a certain axial location, e.g. $x = 0$. The corresponding velocity field is then given by

$$\mathbf{v}'(\mathbf{x},t) = \Re\left\{A_0(x)\hat{\mathbf{v}}(x,r) \exp\left[i\left(\int_0^x \alpha(\xi)d\xi + m\theta - \omega_r t\right)\right]\right\}, \tag{5}$$

with $A_0(x)$ being a slowly varying amplitude scaling that accounts for the streamwise variation of the eigenfunctions. For weakly non-parallel flows, this amplitude scaling can be assessed from an ordinary differential equation employing the eigenfunction and its adjoint [40]. By taking the (complex) term $A_0(x)\hat{\mathbf{v}}(x,r)$ into consideration, the growth rate and phase velocity become dependent on x, r, and on the velocity component, which is in line with experimental observations [41]. However, for the sake of simplicity, we omit the non-parallel correction and focus on the exponent of Eq. (5), assigning the spatial growth rate to $-\alpha_i$ and the streamwise phase velocity to $c_{\mathrm{ph}} = \omega_r/\alpha_r$. As discussed later, this leads to an underprediction of the actual growth rates and phase velocities, however, leaving the frequencies unaffected. Throughout this work, the azimuthal wave number is set to $m = 0$ as the forcing is purely axisymmetric, representing longitudinal acoustic waves. A recently conducted stability analysis of an unconfined swirling jet could show that the axisymmetric Kelvin–Helmholtz instability is not affected by the azimuthal velocity component [42], and therefore, the stability eigenvalue problem is solved for mean flow profiles having the form $\mathbf{V}(r) = (V_x(r), 0, 0)^T$. The insignificance of the azimuthal component was further validated for a number of streamwise stations where azimuthal velocity profiles were available from LDV measurements.

2.3. Linear stability analysis of turbulent flows

To apply linear stability concepts to turbulent mean flows, it is assumed that the scale of the coherent structures is much larger than the scale of the random turbulence. This separation of scales is quantified by the triple decomposition [43]. The time and space dependent flow $\mathbf{v}(\mathbf{x},t)$ is decomposed into a time-averaged part $\overline{\mathbf{v}}(\mathbf{x})$, a periodic (coherent) part $\mathbf{v}^c(\mathbf{x},t)$, and a randomly fluctuating (stochastic) part $\mathbf{v}^s(\mathbf{x},t)$, yielding

$$\mathbf{v}(\mathbf{x},t) = \overline{\mathbf{v}}(\mathbf{x}) + \mathbf{v}^c(\mathbf{x},t) + \mathbf{v}^s(\mathbf{x},t).$$

Analogous to the laminar base flow analysis, it is assumed that the coherent part that is periodic in time and space is represented by an eigenmode of the mean flow. Expressed more formally, the mean of the turbulent flow $\overline{\mathbf{v}}$ is being identified as the base flow $\mathbf{V}$ in the system of Eq. (1), and the coherent fluctuation $\mathbf{v}^c$ represents the perturbation $\mathbf{v}'$.

As shown by numerous previous studies, the analysis of the turbulent mean flow is capable to model the coherent structures that arise from inherent flow instabilities [23,28,41,44]. In contrast to the laminar base flow analysis, the mean flow analysis is capable to not only predict the linear growth but also the nonlinear saturation of the flow structures that reside naturally in the flow. The ability of the linear analysis to reflect the nonlinear saturated state was demonstrated rigorously on the finite amplitude vortex shedding in the cylinder wake [31,45,46] and, more recently, on the precession of the vortex core in swirling jets [28,29]. Principally, the linear analysis of an oscillating flow is rendered nonlinear due to the nonlinearities forming the mean flow. Hence, the mean flow analysis is rather an analytic than a predictive tool revealing information about the inherent oscillations that form the actual mean flow.

Although the direct interaction between the coherent structures, the mean flow, and the turbulent fluctuations is not modeled explicitly in the present approach, it is acknowledged that fine-scale turbulence provides additional mixing and behaves like an added eddy viscosity. This fictitious viscosity, ν_t, adds to the kinematic viscosity ν, significantly reducing the Reynolds number $\mathrm{Re} = V_0 D/(\nu_t + \nu)$ used in Eq. (1), where V_0 is the plug-flow velocity and D the combustor inlet diameter. Following the well known Boussinesq approximation, the eddy viscosity is expressed by

$$\nu_t = -\overline{v_x^s v_r^s} \Big/ \left[\frac{\partial \overline{v}_x}{\partial r} + \frac{\partial \overline{v}_r}{\partial x}\right].$$

It is derived from the PIV snapshots following the same procedure as in the recently conducted stability analysis of a moderately

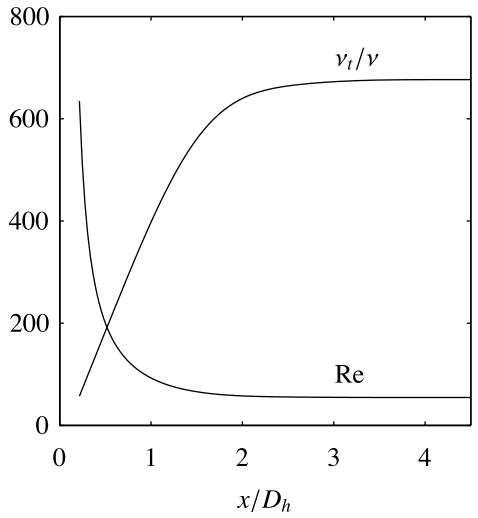

Fig. 1. Streamwise eddy viscosity and Reynolds number used for the stability analysis.

swirling jet [42]. The eddy viscosity is weighted by an intermittency factor that is derived from the PIV snapshots and then averaged in radial direction. Figure 1 shows the eddy viscosity and the corresponding Reynolds number for the unforced combustor flow. The previous increases continuously near the nozzle lip indicating the streamwise enhancement of fine-scale turbulent fluctuations.

2.4. Numerical implementation

The eigenvalue problem of the spatial linear stability analysis is efficiently solved using the Chebyshev spectral collocation methods [39]. A detailed description of the numerical approach is given in [28]. In the present study, the numerical scheme is further simplified by implementing the MATLAB^{TM}Arnoldi-iteration-based routine EIGS, which solves the eigenvalue problem and returns only one eigenvalue that is closest to a given estimate. The eigenvalue problem is first solved for one specific combination of the parameters $[\omega_r, \overline{\mathbf{v}}(x,r), \mathrm{Re}(x)]$ using the standard MATLAB routine EIG, which returns all eigenvalues, including the spurious ones. The physically meaningful solutions are then identified, *a posteriori*, by using two independent criteria [28]. Starting from this solution, the eigenvalue problem is solved for a new set of parameters $[\omega_r, \overline{\mathbf{v}}(x,r), \mathrm{Re}(x)]$ with the EIGS routine. The required estimate is derived from cubic extrapolation of the previously obtained solutions while going in small increments through the ω_r-x-parameter space. All results are cross-checked pointwise by using the standard EIG routine. The computations are conducted using 200 Chebyshev points. A two-parameter transformation proposed by Malik et al. [47] is used to map the Chebyshev collocation points onto the physical domain of the problem, in accordance to the method used in Ref. [28].

3. Experimental setup and procedure

The atmospheric combustor test rig used for the present investigation is shown schematically in Fig. 2. The upstream section of the burner consists of a swirl generator of the movable block type [48] (Fig. 3). Eight fixed blocks are mounted on one disk, eight movable blocks on another. Between the blocks, pairwise radial and tangential slots are formed (see the two blue-filled arrows on[1] the right-hand-side of Fig. 3). The fuel–air mixture enters radially into the swirler. By turning the disks towards each other, the size of the radial and tangential slots can be varied and the tangential momentum of the fluid can be adjusted. In this study the swirler was set to a swirl number of $S = 0.7$. The swirler is followed by an annular duct with an outer diameter of 55 mm and a center body with a diameter of 27.5 mm. This yields an hydrodynamic diameter of $D_h = 27.5$ mm. The area discontinuity to the combustion chamber with a diameter of 200 mm establishes vortex breakdown that leads to a recirculation zone and a stabilization of the flame in the resulting shear layers.

The combustor was run in a perfectly premixed mode, with natural gas injected far upstream of the combustor near the loudspeakers with an equivalence ratio of $\phi = 0.7$ at a facility Reynolds number of $\mathrm{Re}_{D_h} = 37,000$. The 300 mm long combustion chamber is made from silica glass in order to provide optical access for chemiluminescence and laser measurements (i.e., integral OH* emissions recorded with a photomultiplier, OH*-chemiluminescence images acquired with an ICCD camera, PIV and LDV measurements). The water cooled exhaust tube is 700 mm long and was equipped with an orifice at the downstream end in order to avoid self-excited thermoacoustic instabilities. The main feature of the test rig, concerning the realization of high forcing amplitudes for FDF measurements, is the combination of four 18-in. woofers (B&C 18PS76, with a maximum electrical power of 600 W per speaker) with a variable upstream impedance of the combustor. To realize the latter, the length of the tube between the speakers and the burner inlet can be varied with a computer controlled traversing system. This mechanism allows the forcing of the woofers to be used in resonance over the desired frequency range.

The OH*-chemiluminescence was measured in two ways. A photomultiplier with a 307 nm band-pass filter was used to detect the time-resolved global OH*-chemiluminescence in order to allow for an estimation of the heat release rate fluctuations. Simultaneously, an intensified CCD camera, also equipped with a 307 nm band pass filter, was used to gain information on the instantaneous spatial distribution of the heat release rate with a low temporal resolution (≈5 Hz) compared to the oscillation frequencies of the flame. For every case presented, 500 pictures were acquired. A trigger pulse from the camera system was recorded and was used in post processing to phase-average the images with respect to the excitation signal [49]. The phase-averaged images correspond to the projection of an approximately axisymmetric intensity distribution. An Abel deconvolution scheme [50] was applied to the phase-averaged images to recover the radial intensity distribution from the projection.

The velocity fluctuation in the annular jet at the combustion chamber inlet was measured with a 2-component LDV system. It allows for time-resolved measurements of two velocity components, in the present case axial and tangential, at one point in the center of the radial extent of the annular jet, approximately 7 mm downstream of the combustion chamber inlet.

For different lengths of the upstream tube, a sine sweep between 50 and 500 Hz was used as a forcing signal. In this way, resonance frequencies were identified. Subsequently, at these frequencies a sinusoidal excitation was applied for ≈120 s with measurements of inlet velocity fluctuations (LDV) global heat release fluctuations (photo multiplier) and spatial heat release distribution (ICCD camera). The procedure was repeated for various amplitudes. From these data the FDF and average OH*-chemiluminescence images were calculated.

PIV measurements were carried out in the reacting flow field for characteristic forcing conditions (see below). The flow was seeded with aluminum oxide particles. An Nd:YAG laser (see Fig. 2) was used to generate a light sheet (≈1 mm thick) that was aligned with the jet axis in order to obtain the radial and axial velocity component. The strong out-of-plane velocity component

[1] For interpretation of color in Fig. 3, the reader is referred to the web version of this article.

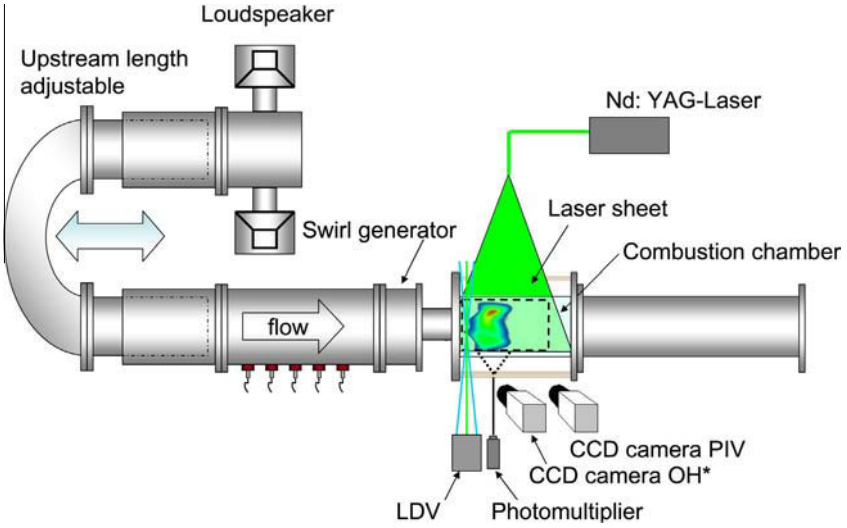

Fig. 2. Test rig overview with measurement devices.

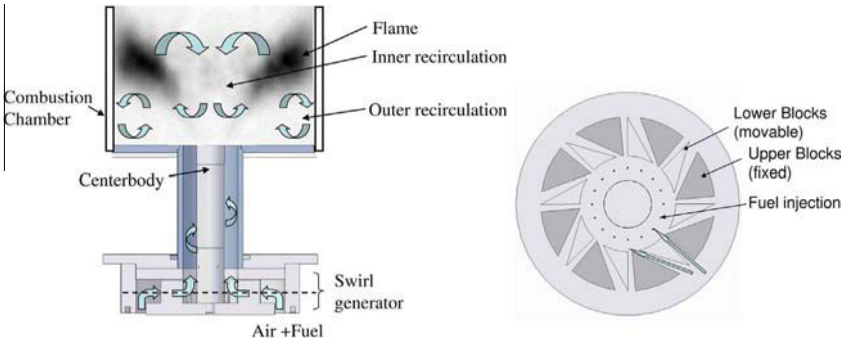

Fig. 3. left: Sketch of combustor – gray shaded region indicates heat release region; right: sketch of swirl generator (crossectional view).

associated with swirling flows required a rather short pulse separation of $\approx 6\,\mu s$ in order to minimize lost particle pairs. For the cross-correlation of the acquired particle image pairs, a multigrid evaluation strategy was used (final interrogation size of 32×32 pixels at 50% overlap) including window deformation, Whittaker peak fitting, and B-spline reconstruction. For this PIV algorithm the measurement error is approximately 0.1 pixels [51], which corresponds to an error for the instantaneous velocity components of approximately 5% for the present arrangement. At distinct points of the FDF, 300 PIV snapshots were taken for the stability analysis and to investigate coherent structures. PIV snapshots were taken at a frame rate of approximately 3 Hz, and hence, the acquired flow-field snapshots are considered as uncorrelated. During PIV acquisition, the trigger signal for the laser was recorded together with the sinusoidal forcing signal. In post-processing, an instantaneous phase angle was derived from the latter and assigned to each individual PIV snapshots, which allows for an *a posteriori* phase-averaging of the flow field. A similar approach was recently applied to extract the coherent structures of a self-excited swirling jet, where the phase angle of each PIV snapshot was derive from a proper orthogonal decomposition [28,52].

4. Experimental observations of the flame response

4.1. Flame describing function (FDF)

We consider the reacting flow inside the combustor that is subjected to axial forcing. The flame's response to the axial forcing is expressed by the FDF defined as

$$F(f;|u'|) = \frac{Q'/\overline{Q}}{u'/\overline{u}},$$

where Q' and u' are the Fourier transform of the fluctuations in heat release rate and combustion chamber inlet velocity, respectively, f is the oscillation (forcing) frequency, and $|u'|$ denotes the fundamental velocity fluctuation amplitude. As the heat release rate cannot be measured directly, a common assumption is that the FDF can be represented as the ratio of normalized fluctuations in OH^*-chemiluminescence and combustor inlet velocity, yielding

$$F(f;|u'|) = \frac{OH^*/\overline{OH^*}}{u'/\overline{u}}.$$

The combustor inlet velocities are derived from the time-resolved LDV measurements.

The FDF is displayed in Fig. 4a. As the heat release rate fluctuations are normalized by the forcing amplitude, non-collapsing graphs imply a nonlinear flame response. Figure 4b shows the phase delay between the inlet perturbations and the global heat release rate fluctuations. The slope of these graphs refers to the time delay between the inlet perturbations and global heat release rate fluctuations.

At low amplitude forcing ($u'/\overline{u} = 0.05$), the FDF reveals a pronounced frequency dependence of the flame response. At $f = 254$ Hz, the normalized heat release rate oscillations are nearly thrice as strong as the normalized inlet perturbations. The phase delay shown in Fig. 4b decays approximately linearly with increasing frequency revealing an approximate time delay between the inlet and the flame center of 4.4 ms. The FDF at $u'/\overline{u} = 0.05$

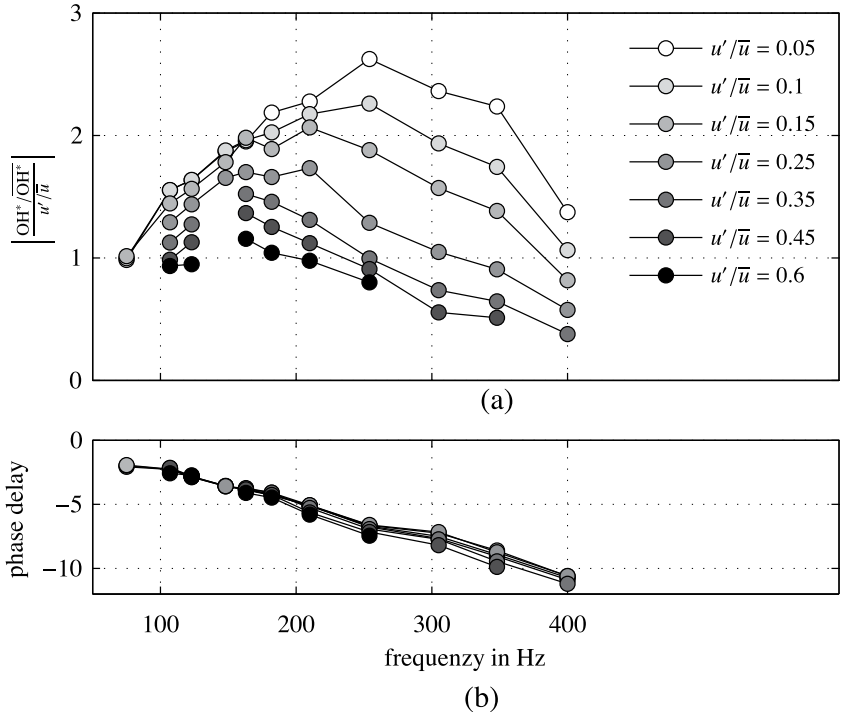

Fig. 4. (a) Amplitude of the flame describing function (FDF) of the perfectly premixed swirl-stabilized flame. (b) Phase delay between the inlet perturbation and the global heat release rate fluctuations.

represents the lowest forcing case and is considered as an approximation of the (linear) FTF of the unforced system.

An increase of the forcing amplitude causes a drastic change of the global flame response. The FDF flattens significantly revealing a weaker dependence of the heat release fluctuations on the forcing frequency (see e.g. $u'/\overline{u} = 0.25$ in Fig. 4a). At sufficiently high amplitudes ($u'/\overline{u} = 0.6$), the FDF shows a nearly constant gain for a wide frequency regime with a slight reduction for higher frequencies. The saturation of the flame response is most emphasized around the peak frequency of the linear FTF indicating that the mechanism that causes this peak becomes successively less effective with higher forcing amplitudes.

This saturation process is investigated in more detail by forcing the flame at a wide range of amplitudes at the constant frequency of 254 Hz. Figure 5 shows the global heat release rate fluctuations as a function of forcing amplitude. Significant gain is encountered at weak forcing, reflecting the strong sensitivity at this particular forcing frequency. By increasing the forcing amplitude, a first saturation sets in and the heat release rate fluctuations plateau at an intermediate level of approximately 0.35% of the mean heat release rate fluctuations, before they continue to increase at a lower slope and converge ultimately to 50%. The plateau indicates that two distinct processes are involved in the saturation of the flame response with the first being active for low to moderate forcing. Similar

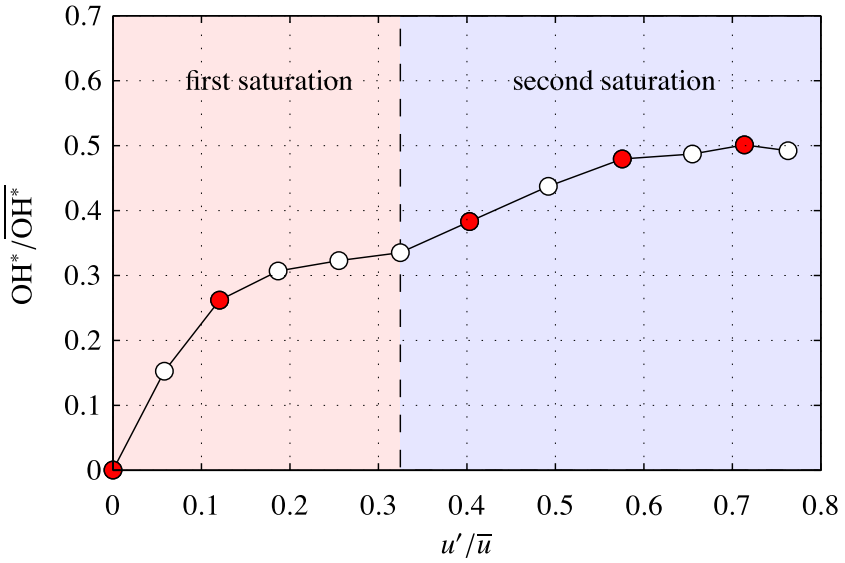

Fig. 5. Response of the global heat release rate fluctuation OH^* to amplitude sweeps at 254 Hz. Two distinct saturation regimes are encountered. Stability analysis is performed for the measurements marked by red-filled circles. (For interpretation of the references to color in this figure legend, the reader is referred to the web version of this article.)

double-saturation transfer functions have been observed in other configurations, suggesting that this observation indicates a more general mechanism [10,11]. Moreover, the inflection point of the measured flame response indicates multiple stability limits.

4.2. Flame dynamics

OH* imaging and PIV was conducted of the flame forced at 254 Hz. Figure 6 shows contours of phase-averaged Abel-deconvoluted OH* images for three different forcing amplitudes. The lowest amplitude corresponds to the linear FTF, the moderate amplitude to the first saturation regime, and the highest amplitude to the second saturation regime (confirm with Fig. 5). The OH* distribution is depicted at eight different phase angles showing how the flame shape is modified during one forcing cycle. The 0° phase angle refers to the maximum of the inlet velocity fluctuations, while the 45° refers to the maximum of the global OH* fluctuations. This is consistent with the FTF's time delay of 4.4 ms, which

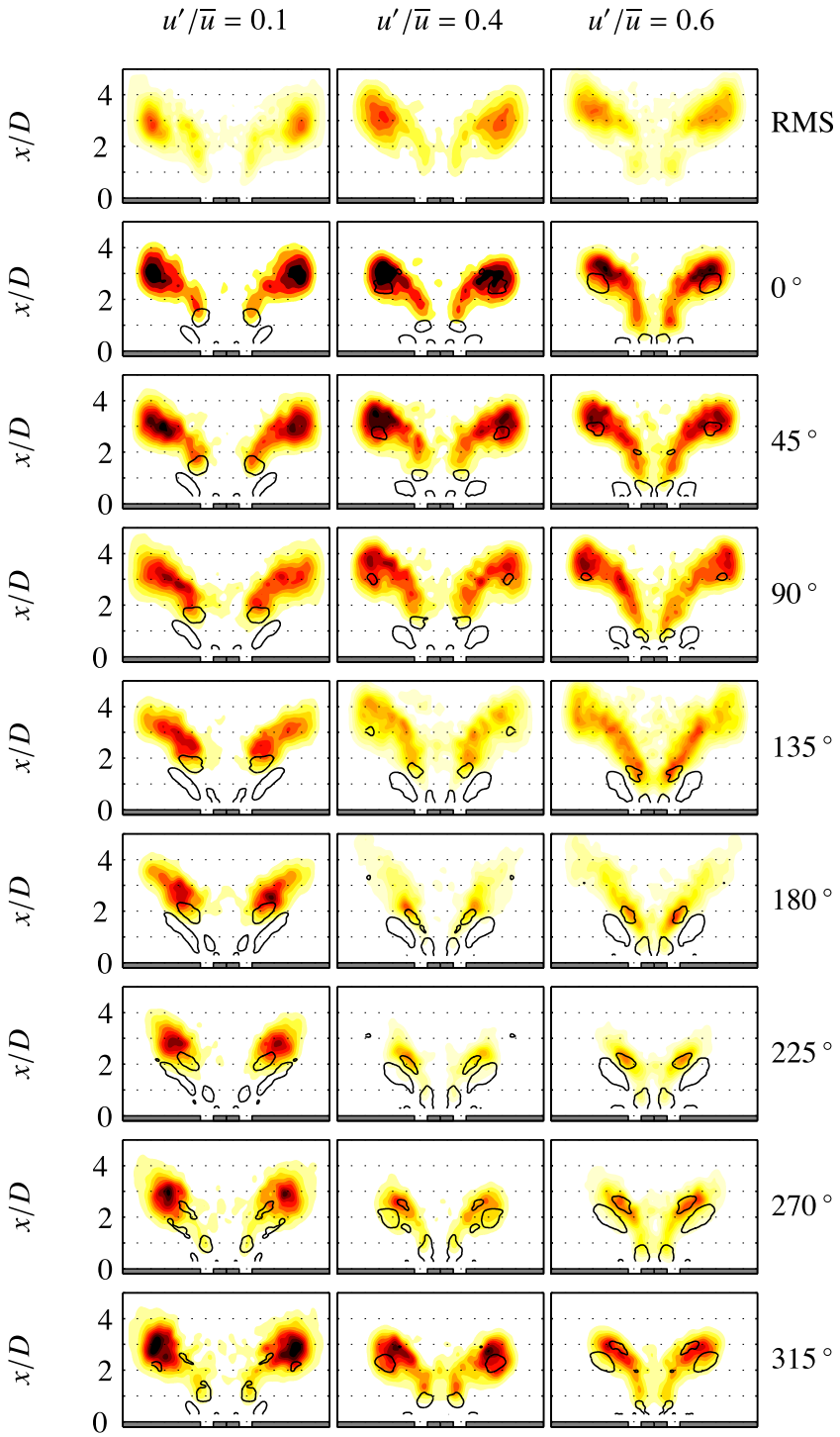

Fig. 6. Color-coded contours of the phase-averaged OH* images of the flame forced at 254 Hz. The contour lines represent an isocontour of the q-criterion ($q = 0.5$) derived from phase-averaged PIV snapshots. It indicates the dominant vortical structures and their trajectory over one forcing cycle. The first row shows the root mean square of the OH* fluctuations indicating regions of highest heat release rate fluctuations.

corresponds approximately to $1\frac{1}{8}$ forcing periods. The first row in Fig. 6 shows the root mean square (RMS) of the OH* fluctuations indicating the intensity of the heat release rate fluctuations.

In order to identify the coherent flow structures, the q-criterion, with $q = 0.25\left(\Omega^2 - S^2\right)$, is computed from the phase-averaged flow field, where Ω and S refer to the magnitude of the vorticity and rate-of-strain tensor, respectively [53]. The isocontour $q = 0.5$ is superimposed onto the phase-averaged OH* images indicating the development of the coherent flow structures during one forcing cycle.

In the following, the major observations relevant for the present study are briefly summarized. A detailed description of flame dynamics at this operating conditions are given in Ref. [11]. For all forcing amplitudes, the OH* images do not show a pronounced oscillation of the flame opening angle. This indicates that swirl fluctuations are not relevant for this configuration. Consistently, LDV measurements at the combustor inlet show a vanishing azimuthal velocity fluctuations for frequencies larger than 200 Hz (see FTF measurements in Ref. [11]). Apparently, with higher frequencies, the vorticity waves generated in the swirler diffuse before they reach the combustor inlet.

Regarding the q-criterion in the linear case ($u'/\overline{u} = 0.1$), a vortex ring is generated at the inner edge of the burner mouth (see e.g. 0°). It convects downstream along the inner shear layer. After $1\frac{1}{8}$ periods (4.4 ms) this vortex has propagated to a downstream location of $x/D = 1.4$, which is still far away from the region of high OH* fluctuation intensity (RMS). This structure does not seem to play an important role for the characteristic of the FTF. A second, counter-rotating vortex ring is generated at the outer edge of the burner mouth (see e.g. 270°). It propagates along the outer shear layer at a somewhat higher convection velocity. This structure is relatively weak at this forcing amplitude and becomes invisible within one forcing cycle (see e.g. 315°).

By increasing the forcing amplitude, the generation of the outer vortex ring is strongly enhanced. The q-criterion clearly shows a strong vortex generated at the outer edge of the burner mouth (see e.g. 0°). Within the delay time of 4.4 ms, this structure propagates along the outer shear layer to a downstream location of $x/D = 2.7$, which is close to the region of maxim RMS(OH*) located at $x/D = 3.2$. The phase-locked OH* images clearly show how the outer vortex induces a roll-up of the flame tip.

Hence, the heat release rate fluctuations encountered presently are driven by the interaction of the outer vortex with the flame front. Similar flow–flame interactions have been observed in an axially forced laminar flame [13]. There, the flame surface was rolled up by the vortices generated in the axisymmetric shear layer upstream the flame. However, the present case is more complex since the inner and outer shear layer give rise to a vortex pair, where the inner vortex is stronger for low forcing, while the outer becomes more energetic with higher forcing.

5. Working hypothesis

The experimental observations give rise to the following questions: What determines the frequency dependent gain of the linear FTF? What are the mechanisms driving the first and second saturation regime? These questions are tackled with hydrodynamic linear stability analysis, using the following working hypothesis:

1. *The linear stability of the mean flow reflects the receptivity at natural and forced conditions.*
   It is assumed that the linear stability analysis reveals the growth rates of the instabilities that are inherent to the actual mean flow. It should provide the growth rates for all forcing cases, and hence, it should allow monitoring the saturation of the shear layers at increasing forcing amplitude. The principal scenario is sketched in Fig. 7. The gray box symbolizes the steady state that sets in for each forcing amplitude reflecting the interplay of the flow instabilities amplifying the incoming perturbation and the mean flow that is altered by the resulting coherent structures. A linear stability analysis applied to the mean flow reflects this steady state, with the eigenmodes being representative of the forced coherent flow structures.
2. *Large-scale coherent structures cause heat release fluctuations.*
   It is assumed that the global heat release rate fluctuations correlate directly with the flow oscillation in the region of the mean flame. This is a strong simplification and it is not expected to hold in a quantitative manner. The nonlinear transfer of the coherent motion to global heat release rate fluctuations, which stem from nonlinearities of the flame itself are neglected [7]. However, it is reasonable to assume that stronger vortical structures in the flame region cause stronger heat release rate fluctuations [54].
3. *The gain of the FTF is determined by shear layer instabilities.*
   The velocity perturbations at the combustor inlet are amplified in the shear layers due to Kelvin–Helmholtz-type hydrodynamic instabilities. This leads to the formation of large-scale coherent flow structures that interact with the flame inducing heat release rate fluctuations. The spatial growth rates of coherent structures are generally frequency dependent, and we postulate that this is the dominant cause for the frequency dependence of the flame response to low amplitude forcing. We neglect swirler-induced azimuthal velocity perturbations and their interference with the coherent structures [17,18], which may affect the gain of the FTF.
4. *Saturation of flame response is linked to saturation of shear layer instability.*
   Forcing the flow at higher amplitudes creates stronger coherent structures that modify the mean flow. This goes in hand with a change of the shear layer receptivity, which should be reflected by lower growth rates and earlier saturation of the forced coherent structures. This saturation process, which is most pronounced in the frequency range of high natural receptivity, is linked to the saturation of the flame response, again neglecting any nonlinearities inherent to the flame dynamics.

6. Results from linear stability analysis

To validate the working hypothesis, we apply linear stability analysis to the mean flow field of the perfectly premixed swirl-stabilized flame. The operating conditions are chosen such that the combustor is thermoacoustically stable. Moreover, the natural and forced flow field is globally stable and does not feature any self-excited flow oscillations such as a precessing vortex core [29]. Linear stability analysis is applied to the mean flow at

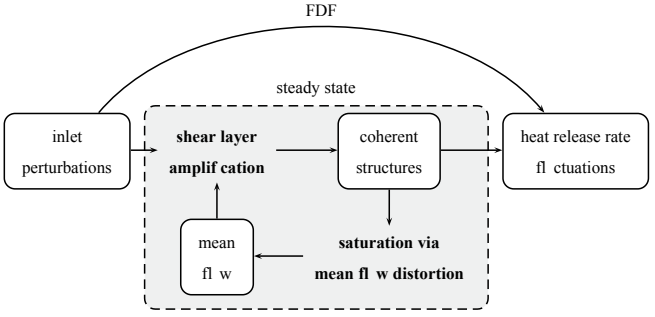

Fig. 7. Schematic showing how the inlet perturbations are related to the heat release rate fluctuations. Linear stability analysis of the mean flow reflects the equilibrium between the forced coherent structures and the mean flow.

different forcing amplitudes in order to monitor the changes in the shear layer receptivity.

6.1. Receptivity of the natural flow (infinitesimal amplitude forcing)

We first investigate the instabilities in the natural (unforced) flow. This will serve as the baseline configuration to which the forced cases are compared to. The flow under consideration is an axisymmetric swirling jet that undergoes vortex breakdown. Figure 8a shows streamlines along the coaxial plane derived from the PIV measurements. They indicate a large inner recirculation zone associated with vortex breakdown that exceeds the entire measurement domain and a smaller outer recirculation zone between the annular jet and the combustor walls. The solid circles refer to the maximum of the axial velocity profiles at each x location and mark the boundary between the inner and the outer shear layer. The contours shown in Fig. 8a represent the time-averaged OH^*-chemiluminescence intensity with the intention to visualize the mean location of the flame. Without forcing, the flame is nearly detached from the combustor inlet with its root located in the inner shear layer and its maximum located in the outer shear layer.

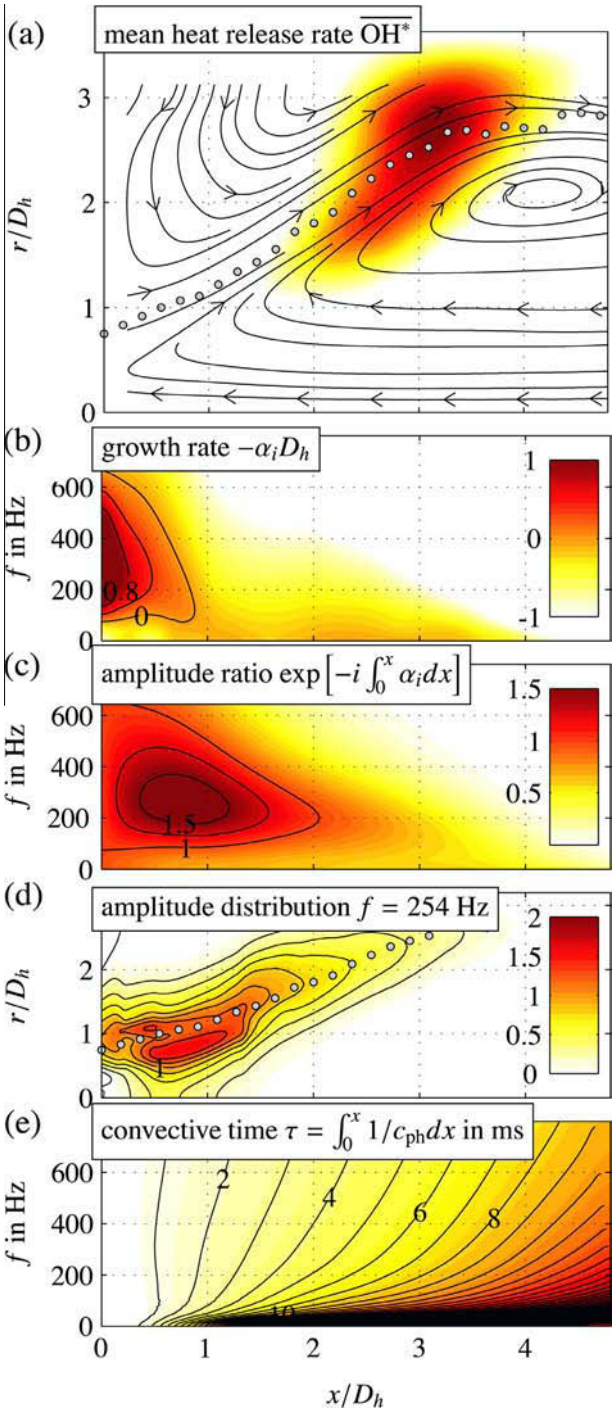

Fig. 8. Baseline configuration (no forcing): (a) Mean flow streamlines with contours of the Abel-deconvoluted OH^* fields indicating the mean heat release rate fluctuations (arbitrary units); results of the stability analysis showing (b) spatial growth rates $-\alpha_i$, (c) amplitude ratio $\exp\left[-i\int_0^x \alpha_i dx\right]$, (d) oscillation amplitude at $f = 254$ Hz, and (e) convective time $\tau = \int_0^x 1/c_{ph} dx$ in ms; solid circles (a, d) mark the annular jet center R_{max}.

Results of the spatial stability analysis for the axisymmetric mode are displayed in Fig. 8b–e. The contours of spatial growth rate $-\alpha_i$ characterize the sensitivity of the flow to axisymmetric disturbances ($m = 0$) as a function of frequency. The zero contour line separates the stable ($-\alpha_i < 0$) from the unstable ($-\alpha_i > 0$) regime. The mean flow is highly unstable at the nozzle exit where the shear layers are relatively thin. With downstream distance, the shear layers spread and the growth rates decay, with the mean flow becoming stable downstream of $x/D_h = 1$.

The amplitude ratio shown in Fig. 8c provides an approximate measure of the amplitude to which an input disturbance with unit amplitude initiated at $x = 0$ is amplified with downstream distance. Overall maximum amplification is reached at $x/D_h \approx 0.8$ for a disturbance frequency of 253 Hz. Note that this frequency compares remarkably well with the peak frequency of the FDF at low forcing amplitudes (see white-filled symbols in Fig. 4), which provides a first indication that the frequency dependence of the heat release rate fluctuations is related to the receptivity of the shear layer.

Figure 8d displays the coherent amplitude distribution $|\mathbf{v}^c|$ approximated from Eq. (5) for a disturbance frequency of $\omega_r/(2\pi) = 254$ Hz. The overall maximum of the perturbation field is encountered in the inner shear layer at approximately one diameter downstream of the combustor inlet. Further downstream, the amplitude distribution aligns with the annular jet, similar to the mean flame location.

The streamwise phase velocity of the instability wave, defined as $c_{ph} = \omega_r/\alpha_r$, allows for estimating the convective time $\tau(x) = \int_0^x 1/c_{ph} dx$. It corresponds to the duration of a wave at a given frequency to travel from the nozzle to a location x. Shear flows are typically dispersive and waves at different frequencies travel at different phase velocities. This causes the convective time to vary with f. The analysis reveals that waves become nearly non-dispersive for higher frequencies, which is a typical feature of shear flows [23].

6.2. Receptivity of the forced flow (finite amplitudes forcing)

In order to quantify the saturation of the flow receptivity, the analysis is applied to the flow forced at different amplitudes. The analysis is conducted for the flow configurations marked by red-filled circles in Fig. 5. The results for the natural flow, discussed in the previous section, are representative for the flame response to very low amplitudes. The analysis of the flow forced at $u'/\overline{u} = 0.1$ is shown in Fig. 9, representing the flow receptivity in the first saturation regime. The results for $u'/\overline{u} = 0.4$, shown in Fig. 10, refer to the second saturation regime. The results for the forcing amplitudes $u'/\overline{u} = 0.6$ and $u'/\overline{u} = 0.8$ are very similar to $u'/\overline{u} = 0.4$ and are therefore not shown.

Forcing the flow at moderate amplitudes ($u'/\overline{u} = 0.1$) does not cause a significant distortion of the mean flow and the mean flame location (compare Fig. 9a with the base line configuration shown in Fig. 8a). The flame root is slightly shifted upstream and the mean

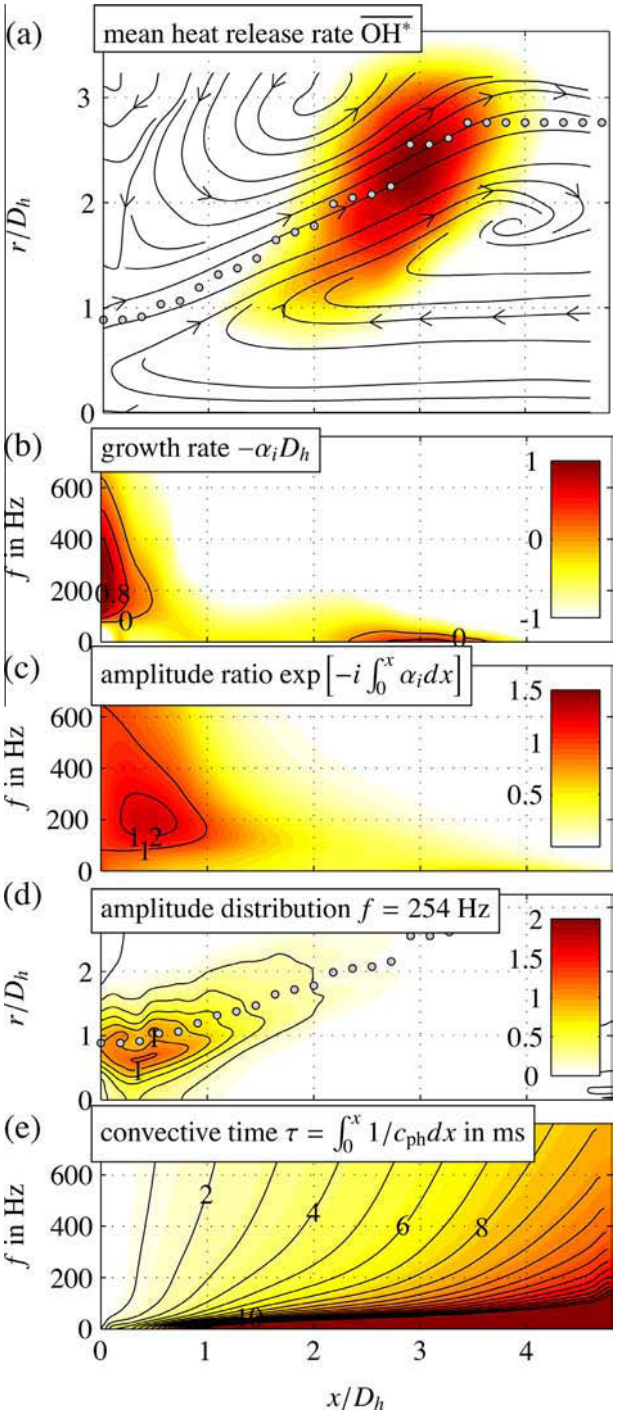

Fig. 9. Jet forced at $u'/\overline{u} = 0.1$ and 254 Hz: (a) Mean flow streamlines with contours of the Abel-deconvoluted OH* fields indicating the mean heat release rate fluctuations (arbitrary units); results of the stability analysis showing (b) spatial growth rates $-\alpha_i$, (c) amplitude ratio $\exp\left[-i\int_0^x \alpha_i dx\right]$, (d) oscillation amplitude at $f = 254$ Hz, and (e) convective time $\tau = \int_0^x 1/c_{ph} dx$ in ms; solid circles (a,d) mark the annular jet center R_{max}.

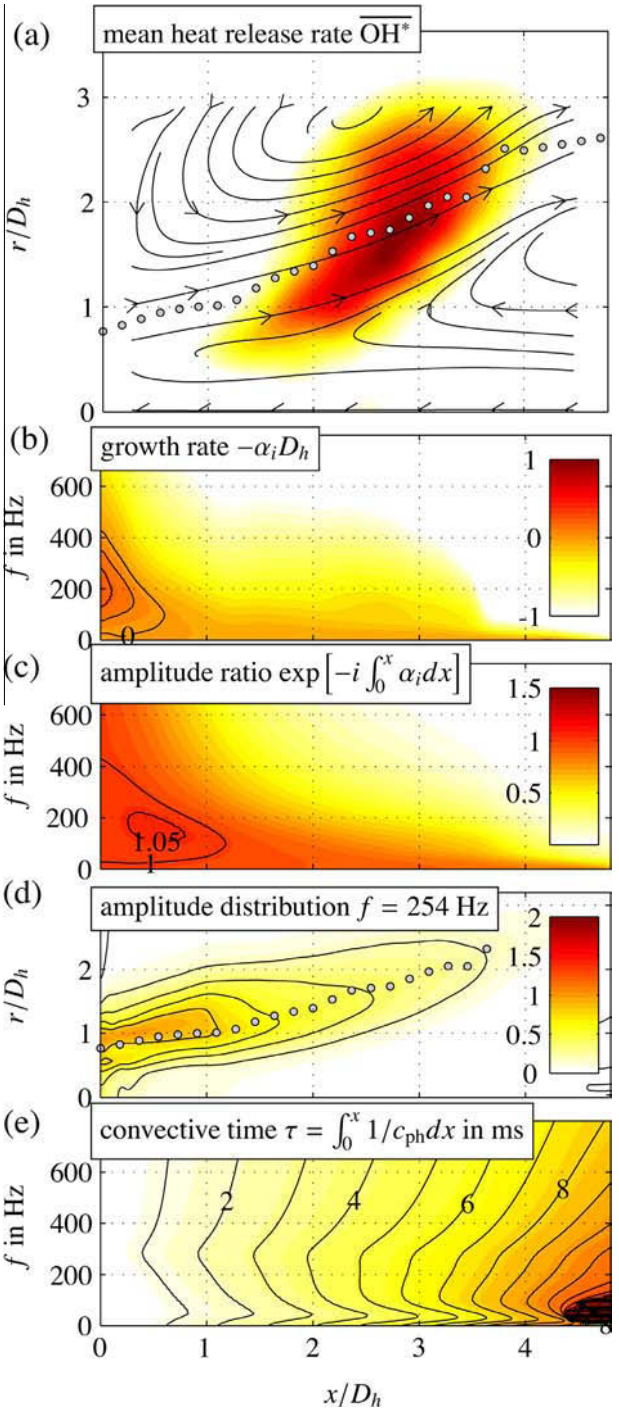

Fig. 10. Jet forced at $u'/\overline{u} = 0.4$ and 254 Hz: (a) Mean flow streamlines with contours of the Abel-deconvoluted OH* fields indicating the mean heat release rate fluctuations (arbitrary units); results of the stability analysis showing (b) spatial growth rates $-\alpha_i$, (c) amplitude ratio $\exp\left[-i\int_0^x \alpha_i dx\right]$, (d) oscillation amplitude at $f = 254$ Hz, and (e) convective time $\tau = \int_0^x 1/c_{ph} dx$ in ms; solid circles (a,d) mark the annular jet center R_{max}.

heat release rate fluctuations are somewhat enhanced in the inner shear layer. However, the linear stability of the forced mean flow shows some significant changes in the resulting growth rates (Fig. 9b). Moderate forcing shifts the overall maximum amplification to lower frequencies and saturation occurs further upstream resulting in a reduced amplitude ratio (Fig. 9c). The lower amplification rates and the lower unstable frequency band indicates that the forcing has already significantly reduced the receptivity in the shear layers. The amplitude distribution of the forced mode remains qualitatively similar to the natural case revealing stronger amplification in the inner shear layer than in the outer shear layer. Similarly, the time delay depicted in Fig. 9e is hardly affected by the forcing.

A further increase of the forcing amplitude to $u'/\overline{u} = 0.4$ induces a significant change of the mean flow (Fig. 10a). The jet opening angle is strongly decreased resulting in a much larger outer and

a smaller inner recirculation zone. Moreover, the mean flame location is shifted inwards and the flame root is displaced further upstream. The growth rates derived from the stability analysis are significantly reduced yielding a maximum amplitude ratio that is hardly above one (Fig. 10b and c). At this forcing condition, the shear layer is basically neutrally stable and the inlet perturbations do not undergo any spatial amplification. Moreover, it is worth mentioning that the forcing alters the mean flow as such, that all frequencies become stable. In other words, the heavily forced flow has lost its ability to promote spatially growing modes.

The amplitude distribution of the strongly forced jet peaks in the outer shear layer (Fig. 10d), in contrast to the weakly forced case, where the amplitude peaks in the inner shear layer (Fig. 9d). The outward shift of the amplitude distribution with higher forcing amplitudes agrees well with the experimental observations. At low forcing amplitudes, coherent structures grow predominantly in the inner shear layer, while for stronger forcing, the experimental data indicates a strong vortex in the outer shear layer (compare with q-criterion shown in Fig. 6). The strong vortical structures in the outer shear layer enhance the entrainment of ambient fluid and cause the constriction of the jet column and the narrowing of the recirculation zone. Further downstream, the coherent amplitude peaks at the maximum mean axial velocity (R_{max}) in between the inner and the outer shear layer reflecting the oscillation of the entire annular jet in the flame region, similar to the natural and weakly forced jet. The time delay depicted in Fig. 10e is also altered by the forcing, yielding faster transfer times. This can be explained by the constriction of the jet resulting in higher axial convection velocities and to the shift of the amplitude distribution to regions of higher streamwise velocities. In the next section, the predicted amplitude distribution is directly compared to the phase-averaged flow measurements, supporting these argumentations. Moreover, the constriction of the jet column at strong forcing is consistent with experimental observations conducted in strongly forced swirling isothermal jets [55].

7. Conjunction and validation

In this section the theoretical predictions presented in Section 6 are compared to the experimental observations described in Section 4. This allows for a *a posteriori* justification of the working hypothesis formulated in Section 5. To recall, the main objective of this work is to relate the FTF and the FDF to the receptivity of the shear layers to inlet perturbations. The latter is expressed by the spatial growth rate of the axisymmetric mode derived from the linear stability analysis.

7.1. Amplification in the linear FDF regime

Figure 11 represents a condensate of the theoretical results described in Section 6. It depicts the maximum amplitude ratio that is encountered for a given frequency. The graphs shown in Fig. 11 represent the amplitude dependent transfer function of the shear flow, relating the inflow perturbations to the response in the flow field. In analogy to the FDF and the FTF, one can define a flow transfer function and a flow describing function, representing the natural and forced flow response, respectively. Starting with the natural flow (white-filled circles), the highest amplitude ratio is encountered at a frequency of 253 Hz, showing that the flow field responds strongest to this particular forcing frequency. Perturbations at frequencies below 100 Hz and above 600 Hz are poorly amplified. A comparison of this shear flow transfer function with the FTF depicted by the white-filled circles in Fig. 4a reveals clear correlations. The flame response to low amplitude forcing shows basically the same frequency dependence as the shear layer

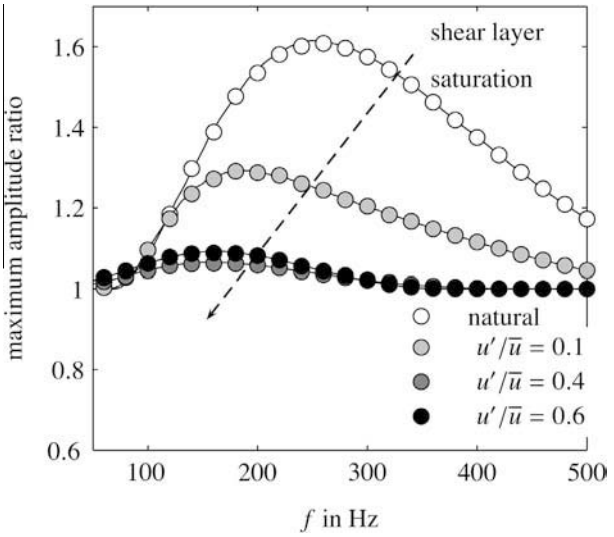

Fig. 11. Amplitude dependent transfer function of the hydrodynamic flow field showing the maximum amplitude ratio of the axisymmetric mode $m = 0$ versus actuation frequency derived from linear stability analysis. The analysis is based on the natural mean flow and on the flow forced at 254 Hz at various amplitudes $u'/\bar{u}$. The shear layer saturates with increasing forcing amplitude indicated by a decrease of the maximum amplitude ratio.

with maximum gain at $f = 254$ Hz and a similar frequency band. The good agreement between the flow and the flame transfer function provides strong indications that the characteristic of the FTF is determined by the receptivity of the shear layers.

The convection velocities of the structures observed from the phase-averaged flow field (Fig. 6) can be related to the convective time τ derived from the stability analysis. For the weakly forced case, the structures in the inner shear layer travel in 4.4 ms to $x/D_h = 1.4$, while the outer vortex travels somewhat further. This correlates quite well with the theoretically derived phase velocity. An instability wave forced at 254 Hz is predicted to propagate in 4.5 ms to $x/D_h = 1.7$ (see Fig. 9e). For high forcing amplitudes, the experiments indicate an increase of the convection velocities due to the jet constriction. This is likewise reflected by the phase velocity obtained from the stability analysis. Within 4.4 ms, the forced instability now travels to a downstream position of $x/D = 2.3$ (see Fig. 10e). This correlates reasonably well with the travel distance of the outer vortex of $x/D = 2.7$ (see Fig. 6). Note that the phase velocity c_{ph}, from which the time delay is calculated, is derived from a quasi-parallel flow analysis, and it represents only a radially averaged value. In order to calculate the phase velocity for the inner and the outer structure separately, one would have to take the streamwise change of the local eigenfunctions into consideration [40,41].

7.2. Nonlinear saturation

At amplitudes exceeding the linear regime, the change of the flow transfer function (Fig. 11) and the FTF (Fig. 4) follows the same trend. Both, the flow field and the flame, encounter significant reduction of gain with increasing amplitude. At $u'/\bar{u} = 0.4$, the shear layer has nearly saturated, which is reflected by an amplitude ratio of one. The saturation of the shear layer receptivity is likely to be the reason for the plateauing of the flame response occurring at the same amplitudes as shown in Fig. 5. Moreover, the peak of the FDF is shifted to lower frequencies with increasing amplitudes, showing maximum gain at around 160 Hz for $u'/\bar{u} > 0.35$. The same trend is reflected in the flow transfer function with a maximum amplitude ratio at around 160 Hz for

$u'/\overline{u} > 0.4$. This agreement is somewhat unexpected, as the predictions are based on the mean flow forced at 254 Hz and must not necessarily hold for other forcing frequencies. This suggests that for high amplitude forcing the mean flow corrections are similar within a certain frequency band. A validation of this conclusion would require mean flow measurements at various forcing frequencies, which has not been done within this study.

The comparison of the FDF with the flow describing function reveals that the nonlinear saturation of the global flame response is connected to the nonlinear saturation of the forced flow instabilities. This is further elucidated by extracting the streamwise growth of the forced coherent structures from the experimental data. Therefore, the coherent flow field $\mathbf{v}^c(\mathbf{x},t)$ is obtained from phase-averaged measurements using $\mathbf{v}^c(\mathbf{x},t) = \mathbf{v}^p(\mathbf{x},t) - \mathbf{V}(\mathbf{x})$, with $\mathbf{v}^p(\mathbf{x},t)$ being the phase-averaged velocity and $\mathbf{V}(\mathbf{x})$ the time-averaged velocity. A measure of the coherent amplitude at a given axial position is then obtained by integrating the coherent velocity magnitude $|\mathbf{v}^c|$ in radial direction. The amplitude ratio is derived by normalizing the coherent amplitude with the inlet perturbation that is, by definition, the mean flow amplitude at the nozzle multiplied by $u'/\overline{u}$, yielding

$$\text{amplitude ratio} := \frac{\left(\int_0^\infty |\mathbf{v}^c|^2 r\,\mathrm{d}r\right)^{0.5}}{u'/\bar{u}\left(\int_0^\infty |\mathbf{V}_0|^2 r\,\mathrm{d}r\right)^{0.5}}, \tag{6}$$

with $\mathbf{V}_0(r)$ representing the mean velocity profiles at the nozzle lip. Figure 12 shows the amplitude ratio of the coherent structures forced at 254 Hz at the same amplitudes as considered for the stability analysis. The perturbations forced at $u'/\overline{u} = 0.1$ undergo significant streamwise growth near the nozzle, saturate at $x/D_h \approx 1$, and decay. With increasing forcing amplitudes this growth is significantly reduced until hardly any amplification is encountered for $u'/\overline{u} = 0.6$. This reproduces the trend predicted by the stability analysis, however, the growth rates encountered in the experiment are much higher. The reason for this strong underestimation of the overall growth of perturbation is due to several reasons that are discussed at the end of this section. Nonetheless, the analysis is qualitatively in line with the experimental findings showing a significant reduction of the shear layer receptivity with increasing forcing amplitude. It is therefore concluded that the first saturation of the global flame response shown in Fig. 5 is caused by the strong diminution of the gain of the forced coherent structures.

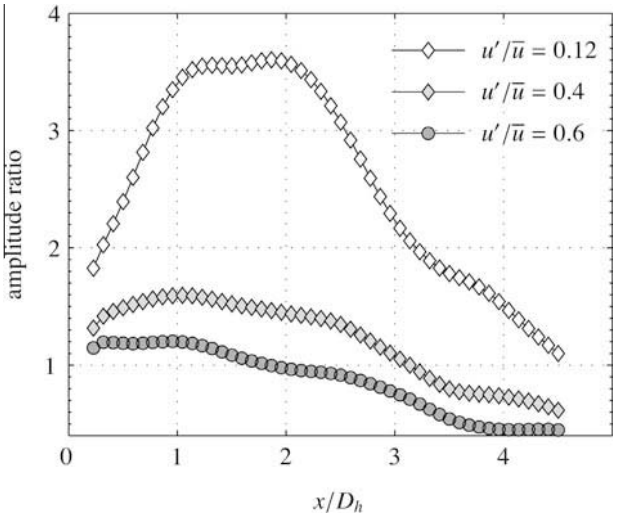

Fig. 12. Amplitude ratio of the forced shear layer derived from phase-locked PIV measurements. At low amplitude forcing of $u'/\overline{u} = 0.1$, strong streamwise amplification is encountered upstream of $x/D_h < 1.2$. At high amplitude forcing of $u'/\overline{u} > 0.4$, the shear layer receptivity is low and only weak streamwise amplification is encountered.

7.3. Comparison of the perturbation fields

The validity of the linear stability approach is further assessed by comparing the coherent velocity field obtained from the phase-locked measurements with the amplitude distribution derived from the stability analysis. Radial profiles of the streamwise and radial velocity component are displayed in Fig. 13 for two axial locations, respectively. The first profile ($x/D_h = 0.5$) corresponds approximately to the axial location where the coherent structure reaches maximum amplitude, while the second ($x/D_h = 1.5$) corresponds approximately to the root location of the flame (compare with Fig. 10a). The radial profiles of the corresponding mean axial velocity component – the main input for the stability analysis – is shown in the bottom row of Fig. 13. The agreement of the predicted coherent amplitude distribution with the measured phase-locked data is remarkably good, taking into consideration the strong simplifications that have been made for the stability analysis. Strikingly, the amplitude distribution is well modeled far beyond the streamwise point of neutral amplification, indicating that the analysis not only captures the growth but also part of the decay of the coherent structures. The modulus of the radial coherent velocity component $|v_r^c|$ peaks in the outer shear layer, indicating the strong entrainment at this high forcing amplitude. The modulus of the axial coherent velocity component $|v_r^c|$ shows strong similarities to the one found in two-dimensional

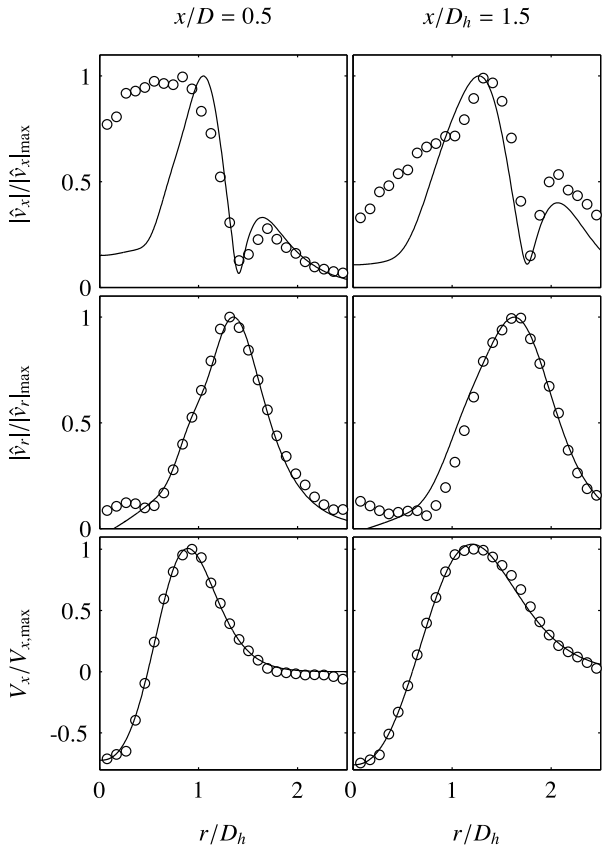

Fig. 13. Normalized amplitude distribution of axial and radial coherent velocity component for the reacting flow forced at $u'/\overline{u} = 0.4$ and 254 Hz derived at two axial locations. Lines refer to theoretical results and circles to phase-locked PIV measurements. Bottom row displays the corresponding mean axial velocity profile where circles refer to measurements and lines to the fit that was used in the stability analysis.

mixing layers [23], reflecting the roll-up of eddy-like structures. The strong underestimation of the coherent axial velocity near the jet center is presumably due to the neglect of density inhomogeneities. The inner recirculation zone of this particular flow configuration is filled with hot burned gases giving rise to higher velocities. This indicates the error source leading to the underestimation of the streamwise phase velocity, as the streamwise propagation velocity of a instability wave depends crucially on its radial amplitude distribution with respect to the mean flow profile [42].

7.4. Comments on the prediction accuracy

The comparison of the experimental findings with the theoretical prediction reveal a good quantitative match of the frequency response and amplitude distribution. The computed growth rates, although correctly predicting the nonlinear saturation, are strongly underestimated and only match the experimental findings qualitatively.

The inaccurate prediction of the growth rates is caused by the following reasons, ranked by their significance:

- *Inconsistent definition of streamwise growth rates and phase velocities:* The spatial growth rates derived from the quasi-parallel stability analysis cannot be consistently compared to measurements. The exponent $-\alpha_i$ of Eq. (5) corresponds to the growth rate of a parallel flow and it does not account for the actual shape of the eigenfunctions and their changes with x and r. This causes a significant underestimation of the actual growth rate particularly for a jet with outward directed shear layers as encountered here. The outward movement of the instability waves results in an increase of the crosswise integrated amplitude, which is not reflected by α_i. A rigorous comparison between experiment and prediction would require to reconstruct the entire perturbation field using a weakly non-parallel correction scheme [40]. However, the good prediction of the shape of the perturbation field shows that the analysis is principally valid for a wide streamwise extend and captures the major flow features.
- *Turbulence model:* The eddy viscosity is extracted from measured turbulent shear stress averaged across the outer shear layer. This quantity is a rough estimation of the actual turbulence and is not rigorously valid for swirling jets. Moreover, turbulent stresses obtained from PIV are subjected to noise, particularly for reacting flow measurements, and the eddy viscosity is likely to be overestimated. This results in higher turbulent damping which typically reduces the growth rates.
- *Non-uniform density effects:* Density gradients can significantly alter the growth rates of instabilities. Typical examples are the onset of global instability in low density (hot) jets [56]. The poor prediction of the axial velocity distribution in the inner shear layer indicates the insufficiency of the present approach for this flow region. This is consistent with a recently conducted stability analysis of a self-excited reacting flow field taking the density stratification into account [29]. The authors could show that a significant qualitative change of the flame shape (e.g. transition from a detached to attached flame) has a drastic effect on the stability of the flow. In the present study, the flame shape remains qualitatively similar, particularly at weak and moderate forcing, and hence, the density distribution is not assumed to alter the trend derived from the isothermal analysis. However, for very strong forcing, where the flame is displaced upstream and into the inner shear layer the density field becomes significant. One may speculate whether the second flame saturation encountered at high forcing is related to a density effect.

8. Summary and concluding remarks

This work focuses on the formation of coherent flow structures in a reacting combustor flow and its impact on the global heat release rate fluctuations. A perfectly premixed swirl-stabilized flame is forced axially mimicking the dynamics associated with thermoacoustic instability. Phase-averaged flow field and OH^* Chemiluminescence measurements show that heat release fluctuations are generated through the roll-up of the flame tip due to large-scale coherent flow structures imping the flame front. The aim of this work is to demonstrate an analytic scheme that allows for predicting the flow's response to acoustic forcing with the far goal of developing an analytic model for thermoacoustic instabilities.

In classical fashion, the flame's response to the forcing is first characterized by a flame describing function (FDF) essentially treating the flow field and the flame in a black box manner. We then depart from this treatment and focus particularly on the flow dynamics by using hydrodynamic linear stability analysis. Based solely on the mean flow, the analysis provides detailed information about the formation of the coherent flow structures excited by the inflow perturbations. In analogy to the FDF, the analytic approach presented here provides a flow describing function, which characterizes the flow's response to the inflow perturbations.

It is shown that the receptivity of the shear flow is highest for the unforced case with a significant dependence of the gain on the perturbation frequency. This dependence is also found in the FTF revealing that the maximum gain in the flame response is associated with maximum growth of the shear layer instability. With stronger forcing, the receptivity of the shear layer decreases and so does the gain in the corresponding FDF. At sufficiently strong forcing, the shear layer is saturated and the inflow perturbations are transported to the flame front without any amplification. The diminishing receptivity of the shear layer is reflected by an intermediate saturation of the heat release rate fluctuations.

The presently observed saturation of the shear layer receptivity with increasing forcing amplitude is consistent with the findings of Mankbadi & Liu [57], who investigated forced turbulent round jets using an energy integral description. The authors explain the saturation process "in terms of a modification of the mean flow by the increasingly high energy levels of the large-scale structures in such a manner that it chokes off its own energy supply from the mean flow". At the combustion operating condition investigated here, the heat release rate oscillations undergo two distinctive regions of saturation. As suggested here, the first saturation regime is caused by a saturation of the shear layer receptivity. The second saturation occurring at very high amplitudes is presumably attributed to flow–flame interactions that have not been addressed in this study. A similar double-saturated flame response was observed in other configurations [10,11], suggesting that the present findings are of general importance. Even more significant, we could recently show that under certain operating conditions, the saturation of the flame response is entirely a result of the saturation of the shear layer receptivity [58].

To conclude, the theoretical framework adopted here is promising for the analysis of combustor flows. Based on the time-averaged flow, this method allows for predicting the large-scale coherent flow structures at thermoacoustically stable conditions and at the limit-cycle. As demonstrated here, the method is applicable to complex high-Reynolds-number flows with multiple shear layers. In the present work, the heat release rate fluctuations were predominantly caused by a strong vortex in the outer shear layer interacting with the flame. It remains to be investigated how this approach is applicable to other flame–flow interactions.

Acknowledgments

The authors kindly acknowledge the financial support of the German Research Foundation (DFG) and the Research Association for Combustion Engines (FVV). This work was supported by a fellowship within the Postdoc-Program of the German Academic Exchange Service (DAAD). We appreciate valuable stimulating discussions with Jonas Moeck.

References

[1] B.J.W.S. Rayleigh, The Theory of Sound, vol. 2, Macmillan, 1896.
[2] S. Candel, Proc. Combust. Inst. 29 (2002) 1–28.
[3] Y. Huang, V. Yang, Prog. Energy Combust. Sci. 35 (2009) 293–364.
[4] T.C. Lieuwen, V. Yang (Eds.), Combustion Instabilities in Gas Turbine Engines, Progress in Astronautics and Aeronautics, vol. 210, AIAA, Inc., 2005.
[5] A.P. Dowling, J. Fluid Mech. 346 (1997) 271–290.
[6] N. Noiray, D. Durox, T. Schuller, S. Candel, J. Fluid Mech. 615 (2008) 139–167.
[7] Preetham, H. Santosh, T. Lieuwen, J. Propul. Power 24 (2008) 1390–1402.
[8] T.J. Poinsot, A.C. Trouvé, D.P. Veynante, S.M. Candel, E.J. Esposito, J. Fluid Mech. 177 (1987) 265–292.
[9] R. Balachandran, B.O. Ayoola, C.F. Kaminski, A.P. Dowling, E. Mastorakos, Combust. Flame 143 (2005) 37–55.
[10] S.K. Thumuluru, T. Lieuwen, Proc. Combust. Inst. 32 (2009) 2893–2900.
[11] S. Schimek, J.P. Moeck, C.O. Paschereit, in: 47th AIAA/ASME/SAE/ASEE Joint Propulsion Conference and Exhibit, San Diego, California, July 31–August 3, AIAA Paper No. 2011-5702.
[12] J. O'Connor, T. Lieuwen, J. Eng. Gas Turb. Power 134 (2011) 011501.
[13] D. Durox, T. Schuller, S. Candel, Proc. Combust. Inst. 30 (2005) 1717–1724.
[14] M. Stöhr, I. Boxx, C.D. Carter, W. Meier, Combust. Flame 159 (2012) 2636–2649.
[15] J.P. Moeck, J.-F. Bourgouin, D. Durox, T. Schuller, S. Candel, Combust. Flame 159 (2012) 2650–2668.
[16] D. Durox, T. Schuller, N. Noiray, S. Candel, Proc. Combust. Inst. 32 (2009) 1391–1398.
[17] P. Palies, T. Schuller, D. Durox, L.Y.M. Gicquel, S. Candel, Phys. Fluids 23 (2011).
[18] P. Palies, D. Durox, T. Schuller, S. Candel, Combust. Flame 157 (2010) 1698–1717.
[19] P. Schmid, D. Henningson, Stability and Transition in Shear Flows, Springer Verlag, 2001.
[20] P.G. Drazin, W.H. Reid, Hydrodynamic Stability, Cambridge Mathematical Library, 2004.
[21] A. Michalke, J. Fluid Mech. 23 (1965) 521–544.
[22] P. Freymuth, J. Fluid Mech. 25 (1966) 683–704.
[23] J. Cohen, I. Wygnanski, J. Fluid Mech. 176 (1987) 191–219.
[24] C.-M. Ho, P. Huerre, Annu. Rev. Fluid Mech. 16 (1984) 365–424.
[25] J.-M. Chomaz, Annu. Rev. Fluid Mech. 37 (2005) 357–392.
[26] V. Theofilis, Annu. Rev. Fluid Mech. 43 (2011) 319–352.
[27] F. Gallaire, M. Ruith, E. Meiburg, J.-M. Chomaz, P. Huerre, J. Fluid Mech. 549 (2006) 71–80.
[28] K. Oberleithner, M. Sieber, C.N. Nayeri, C.O. Paschereit, C. Petz, H.-C. Hege, B.R. Noack, I. Wygnanski, J. Fluid Mech. 679 (2011) 383–414.
[29] K. Oberleithner, S. Terhaar, L. Rukes, C.O. Paschereit, J. Eng. Gas Turb. Power 135 (12) (2013) 121506. 9p.
[30] X. Yang, A. Zebib, Phys. Fluids 1 (1989) 689–696.
[31] D. Barkley, Europhys. Lett. 75 (2006) 750–756.
[32] P. Huerre, P.A. Monkewitz, Annu. Rev. Fluid Mech. 22 (1990) 473–537.
[33] B. Emerson, J. O'Connor, M. Juniper, T. Lieuwen, J. Fluid Mech. 706 (2012) 219–250.
[34] S. Terhaar, K. Oberleithner, C.O. Paschereit, Proc. Combust. Inst. 2 (2014) 1–10, http://dx.doi.org/10.1016/j.proci.2014.07.035 (in press) ISSN: 1540-7489.
[35] T. Schuller, S. Ducruix, D. Durox, S. Candel, Proc. Combust. Inst. 29 (2002) 107–113.
[36] T. Lieuwen, J. Propul. Power 19 (2003) 765–781.
[37] P.A. Monkewitz, K.D. Sohn, AIAA J. 26 (1988) 911–916.
[38] P.A. Monkewitz, D.W. Bechert, B. Barsikow, B. Lehmann, J. Fluid Mech. 213 (1990) 611–639.
[39] M.R. Khorrami, M.R. Malik, R.L. Ash, J. Comput. Phys. 81 (1989) 206–229.
[40] D.G. Crighton, M. Gaster, J. Fluid Mech. 77 (1976) 397–413.
[41] M. Gaster, E. Kit, I. Wygnanski, J. Fluid Mech. 150 (1985) 23–39.
[42] K. Oberleithner, C.O. Paschereit, I. Wygnanski, J. Fluid Mech. 741 (2014) 156–199.
[43] A.K.M.F. Hussain, W.C. Reynolds, J. Fluid Mech. 41 (1970) 241–258.
[44] K. Gudmundsson, T. Colonius, J. Fluid Mech. 689 (2011) 97–128.
[45] B. Pier, J. Fluid Mech. 458 (2002) 407–417.
[46] B.R. Noack, K. Afanasiev, M. Morzyński, G. Tadmor, F. Thiele, J. Fluid Mech. 497 (2003) 335–363.
[47] M.R. Malik, T.A. Zang, M.Y. Hussaini, J. Comput. Phys. 61 (1985) 64–88.
[48] W. Leuckel, Swirl Intensities, Swirl Types and Energy Losses of Different Swirl Generating Devices, Technical Report, Doc. No. G02/a/16, International Flame Research Foundation, Ijmuiden, The Netherlands, 1967.
[49] F. Güthe, B. Schuermans, Meas. Sci. Technol. 18 (2007) 3036–3042.
[50] S. Jaffe, J. Larjo, R. Henberg, in: 10th International Symposium on Plasma Chemistry, Bochum.
[51] M. Raffel, C. Willert, S. Wereley, J. Kompenhans, Particle Image Velocimetry, in: A Practical Guide, second ed., Springer Press, 2007.
[52] M. Stöhr, R. Sadanandan, W. Meier, Exp. Fluids 51 (2011) 1153–1167. 10.1007/s00348-011-1134-y..
[53] J. Jeong, F. Hussain, J. Fluid Mech. 285 (1995) 69–94.
[54] C. Armitage, R. Balachandran, E. Mastorakos, R. Cant, Combust. Flame 146 (2006) 419–436.
[55] K. Oberleithner, M. Sieber, C.N. Nayeri, C.O. Paschereit, J. Phys: Conf. Ser. 318 (2011) 032050.
[56] P.A. Monkewitz, Phys. Fluids 31 (1988) 999–1006.
[57] R. Mankbadi, J.T.C. Liu, Philos. Trans. A Math. Phys. Eng. Sci. 298 (1981) 541–602.
[58] S. Terhaar, B. Ćosić, C.O. Paschereit, K. Oberleithner, J. Eng. Gas Turb. Power 136 (2014).

Chapter 5

Results

As stated before, the publications given in chapter 4 are in the following referred to as:

- 𝔄: Schimek, S., Moeck, J. P., and Paschereit, C. O., 2011. An Experimental Investigation of the Nonlinear Response of an Atmospheric Swirl-Stabilized Premixed Flame. *Journal of Engineering for Gas Turbines and Power* , 133(10), p. 101502. DOI:10.1115/1.4002946

- 𝔅: Schimek, S., Cosic, B., Moeck, J. P., Terhaar, S., and Paschereit, C. O., 2014. Amplitude-dependent flow field and flame response to axial and tangential velocity fluctuations. *Journal of Engineering for Gas Turbines and Power*, 137(8), Dec., p. 081501. DOI:10.1115/1.4029368

- ℭ: Oberleithner, K., Schimek, S., and Paschereit, C. O., 2015. Shear flow instabilities in swirl-stabilized combustors and their impact on the amplitude dependent flame response: A linear stability analysis. *Combustion and Flame*, 162(1), Jan., pp. 8699. DOI:10.1016/j.combustflame.2014.07.012

5.1 Acoustic characterization of flames

The straightforward approach for a comprehensive acoustic characterization of a flame is to measure the acoustic transfer matrix of the flame. Practically, this is done by measuring the burner transfer matrix without the flame and the combined flame and burner transfer matrix, and then extracting the acoustic flame transfer matrix from both transfer matrices. In order to determine all unknowns of a transfer matrix, the planar acoustic field both upstream and downstream of the combustor must be measured for two linearly independent forcing conditions - the so-called two load method [61]. Acoustic source terms of the flame are neglected in this context, since their amplitude is rather small compared to the forcing amplitudes used within the scope of the presented investigations.

The test rig used features a high forcing amplitude source upstream of the burner. Forcing from upstream, the linear independency for two load conditions can be realized by exchanging the acoustic downstream boundary condition, for example, by mounting an orifice at the end of the exhaust tube. But even neglecting the problem that an orifice can have significant influence on the flow field in the combustor and may change the characteristic of the flame, practically this hardly can be realized for amplitude dependent measurements, since the same forcing amplitude at the flame must be present for the two forcing conditions. From the practical point of view, this method was a priori assumed to be not feasible and imprecise and the focus was set on capturing the response of the flame in terms of OH^* chemiluminescence fluctuations, which are for the present, perfectly premixed application a good surrogate for heat release fluctuations.

The relation between the normalized OH^* chemiluminescence fluctuations and the normalized velocity fluctuations at the combustion chamber inlet yields the flame transfer function or the amplitude dependent flame transfer function, known as the flame describing function. The flame transfer matrix or the flame describing matrix can be derived applying the Rankine-Hugoniot relations (equation 2.20). Applying the network modeling techniques described in chapter 2, limit cycle amplitudes can be predicted for certain acoustic boundary conditions with this approach [46].

In the following, the main results of the three publications given in the previous chapter are summarized and discussed. Two measurement campaigns with slightly different operational setups and different measurement techniques have been carried out, leading to the data and results discussed.

The first campaign aimed at the general identification of changes in the flame shape that are associated with nonlinearities in the flame transfer function. The results of this campaign were published in $\mathfrak{A}$. The goal of the second campaign was the investigation of changes in the flow field occurring during the saturation of the flame response. The results of this measurement campaign are presented in two publications, the first one, $\mathfrak{B}$, dealing primarily with the results and discussion of the measurements, the second, $\mathfrak{C}$, with a comparison of the results with a hydrodynamic stability analysis of the flow field.

5.2 First measurement campaign

After the development and setup of the new test rig used for the present investigations, the capability of forcing with the desired high amplitudes had been successfully proven [27]. It had been shown that velocity fluctuations on the order of magnitude of the mean flow can be reached nearly over the entire frequency regime between 50 Hz and 500 Hz.

The acoustic transfer function of the combustor without the flame was found to be rather independent from the forcing amplitude (not explicitly published).

For the first measurement campaign, a setup was chosen with four microphones upstream of the combustor, a photomultiplier capturing the time resolved total OH^* chemiluminescence

of the flame, and an intensified CCD camera capturing the instantaneous spatial OH* chemiluminescence distribution.

For various frequencies, the amplitude-dependent flame response was measured. Since the acoustic transfer function of the burner without the flame was known to be rather independent from the forcing amplitude, the nonlinear phenomena observed in these measurements were attributed to the flame describing function.

Rather phenomenological amplitude-dependent effects of the flame shape and the overall OH* chemiluminescence intensity during the oscillation at different frequencies were investigated. For this purpose, the OH* chemiluminescence images obtained were phase-averaged and Abel deconvoluted. The results were published in [A].

5.2.1 Flame transfer function and flame describing function

The amplitude of the measured flame transfer function features a maximum at a forcing frequency of 128 Hz and a monotonous decay for higher and lower frequencies ([A] fig. 6). For frequencies higher than 260 Hz and lower than 60 Hz, the amplitude rises slightly again. The decay of the phase corresponds to a time delay of 5.9 ms, which corresponds very well to the frequency of the self excited instability frequency of 173 Hz that was obtained by changing the acoustic downstream reflection coefficient by removing the orifice at the end of the exhaust tube ([A] fig. 15).

Palies et al. [62] state that saturations in the gain of the flame describing function occur most notably, i.e. at lower forcing levels, for frequency regimes which feature a relatively high gain in the linear flame response. This finding was confirmed by the measurement results obtained. For example, at a forcing frequency of 50 Hz, where the amplitude of the flame response in the linear regime is relatively low around 0.4, a significant saturation in the gain of the flame describing function is observed at a normalized forcing amplitude of $\frac{u'}{u_{mean}} \approx$ 1.5 ([A] fig. 16 bottom). At a forcing frequency of 128 Hz, however, where the maximum gain of the flame transfer function was observed at approximately 1.5, the saturation in the amplitude of the flame describing function occurs at relatively low normalized forcing amplitudes of $\frac{u'}{u_{mean}} \approx 0.2$ ([A] fig. 7).

Dowling [4] argued in 1997 that the main saturation process is related to the heat release of the flame. Since the heat release cannot become negative in a flame, for heat release fluctuations $\frac{Q'}{Q_{mean}} > 1$ necessarily a non sinusoidal distortion of the flame response has to be present. For the self-excited thermoacoustic instability, where the instantaneous heat release reached more than 3.5 times the average value ([A] fig. 15), this behavior could be observed. Furthermore, the non-sinusoidal distortion has been found not only to be present at very high forcing amplitudes, but to increase gradually from the smallest excitation levels applied in the linear flame response regime up to the highest forcing amplitudes. [A] fig. 9 shows the phase-averaged spatially integrated OH* chemiluminescence image intensities for various forcing amplitudes at 128 Hz over one oscillation. Even for relatively small forcing amplitudes, the distortion of the sinusoidal forcing is evident. Moreover, a significant rise of harmonics to the mono-frequent forcing can be found in the flame response, starting at

very low forcing amplitudes and increasing gradually, while the response of the flame at the forcing frequency is linear up to $\frac{u'}{u_{mean}}$=0.18 ($\mathfrak{A}$ fig. 7).

5.2.2 Average flame shape and position for changing forcing amplitudes

Although the detailed flame dynamics observed differ for different frequency regimes, some general trends over the entire frequency regime investigated were found. Especially for the mean properties of the flame occurring for increasing forcing amplitudes systematic changes were observed.

One of the most significant observation was that the flame shape averaged over one oscillation period changes with increasing forcing amplitude. In order to quantify this finding, the center of mass (COM) of the mean OH^* chemiluminescence images were calculated for different forcing frequencies and forcing amplitudes. It was observed that the COM is shifted downstream for increasing forcing amplitudes at several forcing frequencies ($\mathfrak{A}$ fig. 11). Please note that the strongest displacements correspond to the frequencies with the highest amplitudes in the flame transfer function and the strongest saturations in the flame describing function. Consequently, the convective time delay associated with the time disturbances generated in the combustor or at the combustion chamber inlet need to travel from their origin to the flame front is enhanced. Consequently, a slight decrease of the phase can be observed for the respective frequencies in the flame describing function ($\mathfrak{A}$ fig. 7, 12). The shift of the COM and the corresponding change in the phase of the flame response partially occurs even at relatively low forcing amplitudes where the amplitude of the flame response is still linear and increases gradually with increasing forcing amplitudes ($\mathfrak{A}$ fig. 12).

A change in the phase of the flame describing function may alter the thermoacoustic stability of a system, since the phase between pressure and heat release fluctuations changes and, hence, whether the Rayleigh criterion is met. Practically, for the establishment of a limit cycle not necessarily a nonlinearity in the gain of the flame describing function has to be present. An amplitude dependency of the phase may, on the one hand, decrease the growth rate of the system and establish a limit cycle oscillation. On the other hand, it may increase the growth rate and a system which is linearly stable may become unstable as soon as it is triggered and a certain fluctuation amplitude is reached (subcritical instability).

Please note that throughout all measurements carried out, it has been observed that if a significant change in the phase of the flame describing function is present, it is a decay of the phase for increasing forcing amplitudes, i.e., an increase of the characteristic convective time delays of the flame.

Furthermore, $\mathfrak{A}$ fig. 11 shows that for several forcing frequencies, a shift of the COM towards the central combustor axis is present. Due to a lower swirl number used in the second measurement campaign, the effect is pronounced much stronger in the respective measurement data and therefore is discussed later.

5.2.3 Flame front dynamics

The detailed flame front dynamics during an oscillation are given by the phase-averaged Abel-deconvoluted OH* chemiluminescence images. For a forcing frequency of 128 Hz, a meandering shape of the flame branches during a part of the oscillation (0° - 90°) can be observed for smaller forcing amplitudes (𝔄 fig. 8). The reasons for this behavior of the flame branches is discussed later in detail. For forcing amplitudes of $\frac{u'}{u_{mean}}$=0.46 and higher, the meandering cannot be observed, since the OH* chemiluminescence intensity nearly vanishes during the respective phases.

For a forcing frequency of 292 Hz, the OH* chemiluminescence images show a significant roll-up of the flame branches in the outer recirculation zone for forcing amplitudes of $\frac{u'}{u_{mean}}$=0.69 and higher (𝔄 fig. 13). In the measurements of Balachandran et al. [9], it was observed that roll-up events of the flame branches coincide with nonlinearities of the flame response. This finding is not confirmed by the present measurement data, since the flame response at 292 Hz is rather linear up to $\frac{u'}{u_{mean}}$=0.69 and features only weak nonlinearities for the higher forcing amplitudes investigated (𝔄 fig. 12).

5.3 Second measurement campaign

The observed systematic change of the flame structure averaged over one oscillation period raised the question of whether a systematic change of the average flow field is also associated for increasing forcing amplitudes. In order to eliminate the influence of equivalence ratio fluctuations, in the second campaign the combustor was operated in a perfectly premixed mode with fuel injection far upstream of the combustor. For perfectly premixed conditions, the flame response is mainly attributed to interactions of the flow field and the flame, hence, changes in the flow are of primary interest.

Although the describing function of the burner was found to be only marginal amplitude-dependent, the flame describing function could not be separated from the burner-flame describing function with the measurement techniques used above.

In order to answer these questions another measurement setup was chosen. Additional to the measurement techniques applied before, a PIV system was installed in order to measure the instantaneous flow field in the combustor that was in the post processing phase-averaged and a two component LDA system was used to measure highly time resolved the axial and azimuthal velocity components in the annular jet close to the combustion chamber inlet. Furthermore some geometrical changes of the setup and slightly different operating conditions were chosen for practical reasons, hence, the measurement data of the two measurement campaigns can not be directly compared.

5.3.1 Burner describing function and mode conversion effect

A perturbation in the flow velocity impinging the swirl generator from upstream results in the generation of two different types of perturbations downstream of the swirler. The first is

an axial velocity fluctuation, which is an acoustic wave and is transported downstream with the speed of sound. The second is an azimuthal velocity fluctuation, which is a perturbation of the flow field and is transported with the mean flow velocity in axial direction. For combustors where the swirl generator is not directly located at the combustion chamber inlet, but is separated by an annular passage from the combustion chamber inlet as in the present setup, a difference in the transport velocities result in a phase lag between the axial and azimuthal velocity fluctuation entering the combustion chamber and, hence, in a fluctuation of the swirl number at the combustion chamber inlet and a fluctuation of the flame angle.

Komarek et al. [63] investigated the influence of this so-called mode conversion effect on the linear flame response. They varied the axial distance between the swirler and the combustion chamber inlet and studied the effect of the resulting change of the phase between axial and tangential velocity fluctuation on the flame transfer function. Palies et al. [15, 44, 64] extended this idea for modeling and measurements of the flame describing function on a setup with a relatively low Reynolds numbers (3900 - 6000) and Strouhal numbers approximately half an order of magnitude lower than in the present setup.

In the second measurement campaign, leading to the data analyzed in $\mathfrak{B}$ and $\mathfrak{C}$, the mode conversion effect and the resulting swirl number fluctuations were studied. The burner describing function was determined from the velocity fluctuation upstream of the burner, gained from the microphone data upstream of the burner and the LDA data measured in the annular jet close to the combustion chamber inlet. The amplitude dependency of the burner describing function was found to be rather moderate and only occurs at a few frequencies ($\mathfrak{B}$ fig. 5, 6).

The gain of the axial-axial burner describing function, relating axial velocity fluctuations at the combustion chamber inlet to the axial velocity fluctuation upstream of the swirler shows a nearly monotonous decay starting at 53 Hz at $\frac{u'}{u_{mean}}0.47$ until 250 Hz at $\frac{u'}{u_{mean}}0.1$ and remaining constant for higher frequencies. The phase is relatively constant over the entire frequency regime investigated at values between 0.3 and 0.85.

The gain of the axial-azimuthal burner describing function, relating azimuthal velocity fluctuations at the combustion chamber inlet to the axial velocity fluctuation upstream of the swirler has a slightly higher gain at 53 Hz of $\frac{u'}{u_{mean}}0.56$ and features an even stronger decay with increasing frequencies until 210 Hz where it is approximately one order of magnitude lower than the gain of the axial-axial burner describing function. Hence, fluctuations in the azimuthal direction are neglected in the following for frequencies above 210 Hz. The phase of the axial-azimuthal burner describing function decreases continuously corresponding to a time lag of $\approx$ 4.4 ms, related to the convective time of the mean flow from the swirler to the combustion chamber inlet as discussed above. At 53 Hz, the time lag led to a high fluctuation in the swirl number and an associated fluctuation of the flame angle, whereas at 123 Hz, axial and azimuthal velocity fluctuations were approximately in phase and a strong fluctuation of the flame angle was not present.

An approach similar to the methodologies of Komarek et al. [63] was conducted. At 53 Hz, a phase lag of nearly π was observed, i.e., axial and azimuthal velocity fluctuations counteracting and resulting in maximum swirl number fluctuations. The annular section between

the swirl generator bottom and the combustion chamber inlet was extended to a total length of $\approx 350\,\mathrm{mm}$ in order to realize a phase of nearly 2π, leading to in-phase fluctuations of the two velocity components and, thus, suppressing swirl number fluctuations. It was found that the increased length of the annulus results in a nearly complete damping of the azimuthal velocity fluctuations at the combustion chamber inlet due to viscous damping in the duct. The resulting swirl number fluctuations at 53 Hz were decreased compared to those of the initial setup, but were still significant. Hence, the respective data are not further discussed here.

It can be concluded that for the present setup with a significant distance between the swirl generator and the combustion chamber inlet at technically relevant operating conditions, i.e., at high Reynolds numbers, the mode conversion effect is only significant for low to moderate frequencies. Azimuthal fluctuations are damped at high frequencies due to viscous damping and swirl number fluctuations may result from axial velocity fluctuations at relatively constant azimuthal velocities. If the axial distance between the swirler and the combustion chamber inlet is increased, the viscous damping of the azimuthal velocity fluctuations becomes stronger and the frequency regime where mode conversion is of interest moves to lower frequencies.

5.3.2 Flame describing function, flame and flow field dynamics

Compared to the measurements of the first measurement campaign, the operating conditions were slightly changed. In order to ease the use of the enhanced measurement techniques, the diameter of the combustion chamber was increased from 105 mm to 200 mm and the preheating of the combustion air was switched off. Furthermore, the power and the equivalence ratio were slightly increased in order to achieve a better flame stabilization without the preheating. As described above, the combustor was operated in perfectly premixed operation mode. The flame describing functions measured in both campaigns, however, feature similar characteristics. The strongest expression of the saturation in the gain of the flame describing function is in the frequency regime, where the gain has the highest values (𝔅 fig. 7), confirming the findings of Palies et al. [62]. Especially for frequencies above 200 Hz, an increase of the absolute value of the phase with increasing forcing amplitude is again visible, which has been shown to result from a downstream movement of the fluctuating part of the flame.

At 53 Hz, as described above, mode conversion leads to a strong fluctuation of the swirl number, which results in a fluctuation of the flame angle. Figure 10 in 𝔅 shows that for small forcing amplitudes, the axial displacement of the center of mass of the OH^* chemiluminescence image is even higher at 53 Hz than the acoustic displacement in the axial direction, due to the velocity fluctuation. This clearly indicates that the swirl number fluctuation leads to an axial displacement of the flame area. For increasing forcing amplitudes, the axial displacement of the center of mass of the OH^* chemiluminescence image relative to the acoustic displacement decreases. This behavior is probably related to the general increase of the axial moment of inertia of the phase-averaged OH^* chemiluminescence images averaged over one oscillation, which indicates, that the fluctuating instantaneous flame becomes longer in the axial direction with increasing forcing amplitude. Neither the gain

nor the phase of the flame describing function indicate significant nonlinearities at that frequency.

The present example shows that the linear regime of the flame response may reach far beyond a normalized forcing amplitude of a few percent. Although normalized forcing amplitudes of $\frac{u'}{u_{mean}} \approx 0.5$ were achieved and an enormous displacement of the flame branches, especially in the outer recirculation zone is observed, no significant saturation in the flame describing function is present.

The axial displacement of the center of mass of the OH^* chemiluminescence images relative to the acoustic displacement tends to decrease with increasing forcing frequency. This trend should not be over interpreted, since the calculation of the center of mass takes the entire image into account. Especially for very high frequencies, the axial length of the image is very large compared to the convective length along the annular jet associated with one oscillation period, which means that every image captures the flame behavior of more than one oscillation period ($\mathfrak{B}$ fig. 19). Counteracting areas that contribute to subsequent oscillation periods suppress the movement of the global center of mass.

The observed general increase of the length of the flame in the axial direction during the oscillation with increasing forcing amplitudes ($\mathfrak{B}$ fig. 16) is especially of interest for high forcing frequencies. For high forcing frequencies, the convective length scale associated with one oscillation period becomes small compared to the flame length. This phenomenon is expected to promote the counteraction of different flame regions identified by Palies et al. [15] and leads to the well known low-pass characteristic of flames. The increase of the axial extension of the flame with increasing forcing amplitudes may enhance the low-pass character of the flame and lead to a saturation in the flame response. The saturations in the gain of the flame describing functions at 254 Hz ($\mathfrak{B}$ fig. 14) and 400 Hz ($\mathfrak{B}$ fig. 18) may, in part, be caused by this effect, beside hydrodynamic effects as will be discussed later.

The systematic changes in the average flame shape for increasing forcing amplitudes observed in the first measurement campaign were confirmed in this second campaign. A systematic downstream movement of the fluctuating part of the flame at increased forcing levels was observed as well (not shown). Furthermore, a systematic decrease of the average flame angle with increasing forcing amplitudes was identified over the entire frequency regime investigated ($\mathfrak{B}$ fig. 15). The effect is not only caused by the downstream shift of the center of mass of the flame, but also by a movement of the flame towards the combustor axis.

This trend is also confirmed by the flow field captured with PIV. At all investigated frequencies, it is obvious that with increasing forcing amplitude, the inner recirculation zone, indicated by the red line in $\mathfrak{B}$ fig. 8, 11, 13 and 17, becomes narrower with increasing forcing amplitudes. It is assumed that this trend is caused by entrainment, especially of the outer shear layer due to vortices shed at the outer edge of the annular combustion chamber inlet. The entrainment leads to an increased radial thickness of the shear layers of the annular jet. Since the flow is confined by the outer walls of the combustion chamber, the inner recirculation zone is squeezed. The systematic change in the flame shape for increasing forcing amplitudes was confirmed by Ćosić [49]. It is assumed that the reduction

of the volume of the inner recirculation zone is the reason for the observed downstream shift of the fluctuating part of the flame at increasing forcing amplitudes.

For the lower forcing amplitudes in 𝔅 fig. 8, 11, 13 and 17, the line of zero axial velocity, indicating the inner recirculation zone, features strong bumps, which result from coherent vortices shed at the outer edge of the annular combustion chamber inlet. During one oscillation period, it can be observed that these vortices convect along the outer shear layer accompanied by the according bump of the inner recirculation zone. With increasing forcing amplitude, the outer shear layer becomes thicker, as mentioned above. Except for the forcing at 53 Hz, it can be observed that the bumps of the inner shear layer mostly vanish. Due to the increased thickness of the jet and the associated shear layers, the influence of vortices shed at the outer edge of the annular combustion chamber inlet on the inner recirculation zone is suppressed.

At the higher forcing amplitude at 53 Hz, the bumps at the inner recirculation zone are still obvious, although the diameter of the inner recirculation zone is significantly decreased. As discussed before, due to mode conversion at this frequency, the entire annular jet meanders in the radial direction, causing the deformation of the inner recirculation zone.

The most important finding in the flow field and flame dynamics in the combustion chamber in publication 𝔅 is the systematic change of the mean flow field. Over the entire frequency regime investigated, it was observed that the inner recirculation zone narrows with increasing forcing amplitude and the flame opening angle of the V-shaped flame decreases. Coherent structures shed at the combustion chamber inlet due to the forcing increase the entrainment of the annular jet and lead to an increased thickening of the shear layers. Due to the confinement of the flow, the inner recirculation zone is constricted. The decreased volume of the inner recirculation zone is assumed to cause the downstream movement of the fluctuating regions of the flame and the associated increase of the absolute value of the phase of the flame describing function, especially at moderate and high forcing frequencies.

5.3.3 Hydrodynamic local linear stability analysis

The identified changes of the mean flow field and especially the shear layers raised the question, of whether these have an influence on perturbations, i.e., vortices that are shed on the combustion chamber inlet and convect with the flow downstream, interacting with the flame front.

Vortices impinging the flame front are known to alter the heat release in several ways. Several studies focus on the detailed interaction between vortices and the flame front. A key mechanism is the roll-up mechanism of the flame [9, 41, 65–67]. Especially the outer flame branch of V-flames is often observed to roll-up due to vortices that convect along the outer shear layer and impinge the flame front. The strong deformation of the flame front locally increases the flame surface and the heat release and is regarded to be one driving mechanism of the flame response to coherent structures. Furthermore, coherent structures locally increase the turbulence level and the associated mixing of unburnt and burnt gases, which may lead to a local ignition of the flame [68]. In addition, the increased turbulence

level that is associated with coherent structures locally increases the flame speed when impinging the flame front and may lead to an upstream propagation of the flame.

The hydrodynamic stability analysis is based on the eigenvalue problem of the Orr-Sommerfeld equation in conjunction with an eddy viscosity model. The Orr-Sommerfeld equation can be derived from a normal mode perturbation ansatz for the linearized Navier-Stokes equations. This hydrodynamic stability approach has been studied extensively in the last decades. O'Connor and Lieuwen [24] emphasized the effect of hydrodynamic instabilities of the flow field and the associated amplification of coherent structures on the flame response.

Flow structures may feature different types of instabilities. They may be globally unstable, which means that a self-sustaining coherent structure is present in the flow. In swirl stabilized combustion systems, the presence of precessing vortex cores is an often observed phenomenon. Since precessing vortex cores are skew symmetric, their direct effect on the thermoacoustic behavior of combustion systems can be neglected, as they do not feature oscillations in the global heat release [26]. Also, in non-swirling flows global instabilities as the well known van Kármán vortex street in wakes can be observed [22].

In the scope of thermoacoustic analysis of combustion systems, convective instabilities are of high interest. Although a flow is globally stable, it may feature flow regions, especially the shear layers, that are susceptible to certain perturbation modes. Perturbations, e.g., coherent vortices that are convected along these regions, are amplified. The amplification depends on the spatial growth rate. An integration of the local spatial growth rate in the streamwise direction allows for the determination of the overall amplification of perturbations of a certain mode. The local spatial growth rates can be derived from the hydrodynamic stability approach. The aim in the scope of this study is to analyze the amplification of coherent structures shed from the combustion chamber inlet during their convection to the flame front. Since the detailed vortex-flame interaction is not taken into account in this analysis, the approach gives only qualitative results for the influence of the amplified perturbations on the flame describing function.

5.3.3.1 Application to experimental data

For the analysis, the mean flow in the combustor is sliced into radial profiles. At each axial position x the mean flow is treated as an incompressible quasi-parallel flow, neglecting azimuthal and radial mean velocity components. Each radial profile of the axial velocity in conjunction with Equation 2.24 and 2.25 leads to an eigenvalue problem that is solved iteratively for real angular frequencies ω_r, leading to the complex eigenvalue α, which is the complex axial wave number and the corresponding eigenfunctions H, F, G and P, representing the axial, radial and azimuthal velocities as well as the pressure. As stated before, for the present analysis of the flame response, only the axisymmetric mode is taken into account, leading to the real azimuthal wave number $m = 0$. The growth rate for a certain perturbation with a real angular frequency ω_r at an axial position x can be derived from the negative imaginary part of the axial wave number α_i and the associated streamwise phase velocity from the real part of the axial wave number as $c_{ph} = \omega_r/\alpha_r$.

Adopting this method to the different axial slices of the flow field, the frequency dependent growth rate for perturbations generated at a particular position in the flow field, i.e., at the combustion chamber inlet, can be integrated in the axial direction to the flame position. Thus, it can be determined how strong perturbations emitted at the combustion chamber inlet are amplified during their convection along the shear layers to the flame.

The hydrodynamic stability analysis is applied to the unforced natural flow in the combustor as well as to the mean flow field at acoustically forced conditions. The mean flow field is assumed to be a steady solution of the Navier-Stokes equation with nonlinear coherent Reynolds stresses. Changes in the stability can be obtained from the mean flow field analysis with the adopted approach as long as the coherent structures mainly interact with the mean flow field. Interactions with other coherent modes or the occurrence of harmonics are not captured by the model. However, it has been recently shown that this approach leads to accurate results in similar reacting and non-reacting flow configurations [23, 69].

Thus, the amplification rates for the different mean flow fields at various forcing conditions are determined. Since for the analysis, the mean flow field at the particular forcing condition must be known, this tool can currently only be used analytically in post processing rather than in a predictive way. As described above, the exact interaction of coherent structures with the flame front is not taken into account. It is assumed that the heat release response of the flame to a particular perturbation correlates in a monotonous manner with the amplitude of the perturbation.

For the hydrodynamic stability analysis, the PIV measurement data at a forcing frequency of 254 Hz were analyzed. For lower frequencies, as shown above, the occurrence of flame angle fluctuations due to mode conversion might have complicated the analysis. For frequencies above 200 Hz, azimuthal velocity fluctuations have been shown to be negligible. The applied axisymmetric forcing generates fluctuations that are mostly related to the Kelvin-Helmholtz instabilities in the shear layers.

At 254 Hz, the flame response shows two different saturation regimes, separated by an inflexion point. It is assumed that the two regimes are caused by different superposed mechanisms in the flame response. Similar characteristics of the flame response have been also observed by Thumuluru et al. [13]. Generally, inflexion points may lead to complex flame stability behavior. Neglecting nonlinearities in the damping of a combustion system, an inflexion point is a necessary prerequisite for the occurrence of subcritical thermoacoustic instabilities [51]. Furthermore, they can lead to more than one stable limit cycle amplitude.

5.3.3.2 Main uncertainties of the linear hydrodynamic stability analysis

The spatial growth rates are predicted depending on the axial location in the flow field. They do not account for the radial distribution, which is reflected by the eigenfunctions of the stability analysis. For an increase in the accuracy, the amplification of coherent structures along their flow path must be calculated.

The eddy viscosity used for the analysis is assumed to be constant in radial direction. It is calculated from the turbulent shear stress averaged across the outer shear layer. Radial

variations are neglected. Furthermore, noise in the PIV data, especially in the vicinity of the flame tend to overpredict turbulent stresses, which probably leads to a general overestimation of the turbulent damping.

The flow in the combustor is assumed to be isothermal. Density variations and their effect on the stability of the flow field are neglected. Especially in the inner shear layer, where the flame reaches far upstream for increased forcing amplitudes, this induces a significant error. Although Oberleithner et al. [69] showed that changes in the density field of a combustor may alter the global stability of a combustor flow, it is assumed that the receptivity of the shear layers and the amplification of perturbations is rather qualitatively constant over a wide range of parameters and the results are not qualitatively changed.

Radial velocity components in the mean flow field are neglected in the current analysis. For an improved accuracy of the analysis, a weakly non-parallel correction scheme similar to the ansatz of Crighton and Gaster [70] could be taken into account.

Generally, it can be said that spatial growth rates are underpredicted by the current approach, whereas turbulent damping is overpredicted. However, the analysis carried out is rather of a qualitative character in order to understand the general mechanisms during saturation at increasing forcing amplitudes.

5.3.3.3 Results of the linear hydrodynamic stability analysis

In this section, the major results of the linear hydrodynamic stability analysis [1] are summarized. $\mathfrak{C}$ fig. 8 shows the results of the stability analysis of the unforced mean flow field. The focus lies on the plots b-d of the figure. In plot b, the growth rate -αD_h, which reflects the sensitivity of the shear layers, is plotted over the axial length x/D_h of the combustor for frequencies up to 800 Hz. Regions with -αD_h >0 are convectively unstable and perturbations are amplified, whereas for -αD_h <0, perturbations are dampened. Especially close to the combustion chamber inlet, the flow is highly unstable for a wide frequency-band, which is related to the relatively thin shear layers. With increasing distance from the combustion chamber inlet, the thickness of the shear layer increases and the amplification rate of perturbations decays.

Plot c shows the development of the amplitude ratio of amplified perturbations with increasing downstream distance. The maximum of the amplification ratio is reached at $x/D_h \approx 0.8$ at a frequency of 253 Hz and agrees very well with the maximum frequency of the flame transfer function. The decay of perturbations due to the mean flow field is only partially captured by the ansatz applied. Hence, in the following, the decay of the oscillations will be neglected and the maximum amplification ratio for each frequency will be analyzed, i.e., the amplification ratio at the axial position where the growth rate becomes zero. Analogously to the definition of the acoustic flame transfer function and the flame describing function, a flow transfer function and the flow describing function may be defined. The first is the maximum amplification ratio of oscillations of variable frequencies at unforced conditions and the second, delivering the maximum amplification rate of oscillations of

[1] The linear hydrodynamic stability analysis has been carried out by Dr.-Ing. Kilian Oberleithner

variable frequencies calculated from the mean flow field of various forcing amplitudes at a forcing frequency of 254 Hz.

In $\mathfrak{C}$ figure 9 and 10 b and c, the growth rate and the amplitude ratio for the normalized forcing amplitudes of $\frac{u'}{u_{mean}}$= 0.1 and $\frac{u'}{u_{mean}}$=0.4 are given analogue to the plots for the unforced flow field. The growth rate is generally found to decrease with increasing forcing amplitude. Furthermore, the maximum of the amplification ratio moves towards lower frequencies with increasing forcing amplitudes.

The main result of the hydrodynamic stability analysis can be found in $\mathfrak{C}$ figure 11, which shows the flow describing function. The white doted line shows the maximum amplification ratio of the flow for the unforced case. A comparison with the linear flame transfer function, (white dots in $\mathfrak{C}$ fig. 4) shows remarkable qualitative agreement. Both curves feature a maximum at ≈254 Hz and a similar decay versus higher and lower frequencies. Furthermore, a comparison of the flame describing function and the flow describing function exhibit a similar saturation with increasing forcing amplitudes. The curves flatten and the maximum of the curves moves towards lower frequencies. For the highest forcing amplitudes plotted, the flow describing function is approximately constant at one, revealing that the shear layer looses its amplifying character due to the change of the mean flow field. Note that for the flow describing function, the change of the maximum amplification ratio is derived from the mean flow field forced at 254 Hz. The change of the shear layer receptivity of the mean flow field at this distinct forcing frequency seems to reflect the characteristics at several forcing frequencies that were applied for the measurements of the flame describing function. In order to answer the question of whether the change of the mean flow field for forcing at a broad frequency regime is similar, further flow field measurements would need to be carried out. Oberleithner and Paschereit [71] recently found that at least the development of growth rates at increasing forcing amplitudes is similar over a wide frequency range, as will be discussed later.

The first saturation of the flame response at a forcing frequency of 254 Hz ($\mathfrak{C}$ fig. 5) occurs at the same forcing amplitudes as the saturation of the flow describing function. The qualitative similarity of the flow describing function and the flame describing function suggest a direct physical link. It can be concluded that the amplitude-dependent flame response and several associated saturations are directly driven by the saturation of the shear layer receptivity and the corresponding decrease of the amplification ratio of the associated coherent structures.

Plot d in $\mathfrak{C}$ figures 8-10 shows the spatial amplitude distribution of the amplification ratio. In the unforced case, the maximum of the amplification is located at the inner shear layer. With increasing forcing amplitude, the maximum moves towards the outer shear layer. It can be concluded that in the unforced case, the amplification of perturbations in the inner shear layer is stronger than in the outer. This trend is inverted with increasing forcing amplitude.

$\mathfrak{C}$ figure 12 shows the normalized amplification ratio of coherent structures at several axial positions calculated from the phase-averaged PIV measurements for several forcing amplitudes at a forcing frequency of 254 Hz. A comparison with the predicted amplification ratios

from the hydrodynamic stability analysis (ℭ fig. 9-10 c) shows a good qualitative agreement. For $\frac{u'}{u_{mean}}$=0.1, a strong amplification close to the combustion chamber inlet can be observed that reduces significantly with increasing forcing amplitudes. As stated above, the absolute value of the amplification ratio is significantly underestimated in the model. However, the qualitative agreement of the general trends are captured by the hydrodynamic stability analysis.

From the eigenfunctions of the hydrodynamic stability analysis the radial distribution of the normalized axial and radial coherent velocity are derived and are compared to the coherent modes from the phase-averaged PIV data at two axial positions (ℭ fig. 13). A remarkable agreement of the coherent radial velocity and a very good agreement for the coherent axial velocity with the exception of the vicinity of the center of the combustion chamber was identified. The strong deviations of the coherent axial velocity close to the combustor axis are probably caused by neglecting the density inhomogeneities in the hydrodynamic stability analysis.

5.3.4 Flame dynamics

In ℭ figure 6, the phase-averaged Abel deconvoluted OH* chemiluminescence images are shown for three different forcing amplitudes, $\frac{u'}{u_{mean}}$=0.1, associated with the linear flame response region, $\frac{u'}{u_{mean}}$=0.4, slightly above the first saturation of the flame response, and $\frac{u'}{u_{mean}}$=0.6, close to the second saturation region of the flame response. From the PIV data, the q-criterion q=$0.25(\Omega^2 - S^2)$ is computed, with Ω being the vorticity tensor and S, the rate-of-strain tensor [72]. Vortices are indicated in the plots by the isocontour line q=0.5. The coordinates in the plots are normalized with the hydraulic diameter of the combustor D.

In the first row, the RMS of the OH* chemiluminescence fluctuations are plotted, indicating the local distribution of heat release fluctuation. For the lowest forcing amplitude, the region of the strongest fluctuations is located at an axial position of x/D ≈2.7 and a radial position of |y|/D≈0.75. For the two higher forcing amplitudes the region of maximal heat release fluctuation is shifted slightly towards the center line of the combustion chamber at |y|/D≈0.6, which corresponds to the observed narrowing of the inner recirculation zone and the general decrease of the flame angle observed for increasing forcing amplitudes. Furthermore, the axial position of the center of the heat release fluctuations is shifted downstream to x/D ≈3 and x/D ≈3.2 for $\frac{u'}{u_{mean}}$=0.4 and $\frac{u'}{u_{mean}}$=0.6, respectively. This agrees with the finding that the average flame position indicated by the center of mass of the OH* chemiluminescence images moves downstream with increasing forcing amplitudes as described above.

At 0° (second row), the inlet velocity is at its maximum and after 4.4 ms, which corresponds to approximately $1\frac{1}{8}$ oscillation periods, the OH* chemiluminescence reaches its maximum. While the inlet velocity increases (225° - 315°), a vortex pair indicated by the q-criterion isocontour line begins to form at the annular combustion chamber inlet, i.e., a vortex at the outer edge and a counter rotating vortex at the inner edge, which subsequently convect along the inner and outer shears layer downstream.

Regarding the outer vortex, it can be observed that for all forcing conditions, the separation of the vortex structure from the bottom plate of the combustor takes place at 45° - 90° and the convection velocity is approximately equal. The vortex is located at approximately $x/D \approx 2.2$ at 315° close to the flame. For the two higher forcing amplitudes after $1\frac{1}{8}$ periods (45°), when the maximum of the heat release is reached, the vortex is at an axial position of $x/D \approx 2.7$, which is close to the maximum of the OH* chemiluminescence fluctuations. It can be observed that the vortex leads to a roll-up of the flame branches. Similar roll-up of flames due to vortices have been also observed by Durox et al. [66].

In contrast, the shedding of the inner vortex and the convection velocity depends on the forcing amplitude. For $\frac{u'}{u_{mean}}$=0.1, the separation starts at 180°, for $\frac{u'}{u_{mean}}$=0.4 at 315°, and at $\frac{u'}{u_{mean}}$=0.6 at 90°. Although for the highest forcing amplitude, the separation is delayed for 0.75 periods, at 270° the inner vortex has approximately the same position for all forcing amplitudes, which is due to an increased convective velocity of the inner vortex at increasing forcing amplitudes. For the highest forcing amplitude $\frac{u'}{u_{mean}}$=0.6, between 180° and 270°, the position of the inner vortex coincides with and probably causes the region of maximum OH* chemiluminescence. Note that this local increase of OH* chemiluminescence takes place during the minimum of the global OH* chemiluminescence and, hence, dampens the flame response to the forcing. Furthermore, it is assumed that the extended adherence of the inner vortex to the centerbody and an associated increased generation of turbulence in this region at high forcing amplitudes is responsible for the upstream extension of the inner flame branch prior to the shedding of the vortex. The extension of the average flame in axial direction enhances the low-pass character of the flame. Both mechanisms might be an explanation for the second saturation observed in the flame response.

It is assumed that the main mechanism leading to the heat release response due to the flow field oscillation is attributed to the outer vortex flame interaction, whereas the inner vortex flame interaction has a rather counteracting, i.e., damping influence.

5.3.5 Conclusions

It has been shown that the linear hydrodynamic stability analysis of the mean flow field of the unforced and forced flow is able to capture the main mechanisms in the flow, in terms of the amplification of coherent structures. The predicted eigenfunctions were found to agree very well with the normalized coherent velocity fluctuations from the phase-averaged PIV data of the forced flame. The axial distribution of coherent kinetic energy distribution in the axial direction could be shown to be qualitatively predicted from the amplification ratios derived from the spatial growth rates of the analysis. Despite several simplifications in the applied ansatz, it can be concluded that the method is capable of predicting qualitatively the amplification of coherent structures in the flow.

The flow transfer function, which is representative for the amplification of coherent structures in the shear layer has been found to agree qualitatively very well to the linear flame transfer function. Furthermore, the flow describing function for increasing forcing amplitudes at a forcing frequency of 254 Hz features the same characteristics as the flame describing function. Although this was not assumed, this behavior is reasonable if it can

be assumed that the change of the mean flow field with increasing forcing amplitudes is similar for a broad range of forcing frequencies.

The basic mechanism of the saturation of the flow describing function is depicted in ℭ fig. 7. Coherent structures generated at the combustion chamber inlet are amplified due to the receptivity and the amplifying character of the shear layers. The enhanced entrainment, which is generated by the coherent structures alters the shape of the shear layer and the mean flow field. The thickness of the shear layer increases with increasing amplitude of the coherent structures, i.e., with increasing forcing amplitude. This distortion of the mean flow field leads to a decrease of the receptivity of the shear layers.

The results of this study propose that the characteristics of the flame describing function and several associated saturations of the flame response are significantly driven by the flow describing function and its saturation. Nevertheless, for the entire representation of the flame describing function, further mechanisms, e.g., equivalence ratio fluctuations, mode conversion, detailed vortex flame interaction, etc. must be taken into account.

Furthermore, it was identified that vortices at the inner shear layer and outer shear layer do not necessarily interact constructively. In this particular case, the outer vortex was found to be the main driver for the flame response, whereas the inner vortex and the associated upstream movement of the flame branch in the inner shear layer counteracts the global heat release fluctuation and has a damping influence on the flame response.

5.4 Subsequent related research

Krediet et al. [73, 74] numerically investigated a very similar configuration to that presented here. They simulated the unforced and forced reacting flow field in the combustor with a reacting large eddy simulation, based on an in house code of Siemens. They compared the obtained data to experimental results and calculated the flame describing function. They found a good agreement between experimental data and numerical results. Flow field and flame position in the unforced case could be reproduced in the simulation very good. Saturation processes for several frequencies were predicted in good agreement with the experimental findings. The prediction of the phase of the flame describing function rather failed.

At 115 Hz they observed a strong fluctuation in the flame area due to mode conversion. They identified that during one oscillation, the strain rate in the flow field of the combustor undergoes large fluctuations. Especially during the decrease of the global heat release, the strain locally reaches large values, which they assume to be the reason for a local flame quenching.

In a further publication, Krediet et al. [75] investigated the effect of mode conversion on the flame describing function. They found a nearly linear correlation of the amplitude of tangential velocity fluctuations close to the combustion chamber inlet and fluctuations of the integrated flame surface density, which is assumed to be a direct indicator for heat release fluctuations.

Based on results of their large eddy simulation and the experimental data, the group carried out limit cycle predictions and compared them to growth rates obtained from linear analysis [7]. They found a good correlation between the linear growth rates and the predicted and measured limit cycle amplitudes. Since especially nonlinear computations and experimental investigations are quite expensive, they emphasize the importance of linear analysis in early design phases for screening systems with regard to their thermoacoustic behavior.

The work on the contribution of coherent structures amplified by the hydrodynamic instability of the flow field on the flame describing function has been successfully continued subsequent to the publication of $\mathfrak{C}$ in our work group and beyond. The finding that the flow transfer function reflects the characteristic of the linear flame response over a broad frequency range has been confirmed for several different configurations [46, 76–78]. Furthermore, it has been found that with increasing forcing amplitudes, the amplification rate of coherent structures in the shear layers diminishes, which leads to a saturation of the growth of perturbations similar to the saturations of the flame describing function [46, 76–78].

Recently, Oberleithner and Paschereit [71] modeled the flame transfer function and the flame describing function with a two time lag approach similar to Komarek and Polifke [45] on a combustor developed for hydrogen combustion. The first time lag is attributed to swirl fluctuations due to mode conversion. The second time lag is modeled with a linear hydrodynamic stability analysis approach similar to the ansatz in $\mathfrak{C}$. In comparison to other studies dealing with time lag models [19, 45], the parameters in the second term, i.e., convective time delay and standard deviation attributed to the hydrodynamic effects, are not fitted, but fully derived from the stability analysis. The results match the amplitude and the phase of the measured flame transfer function and the flame describing function very well.

Furthermore, it could be shown that the observed changes of the mean flow field at high forcing amplitudes over a broad frequency range are similar with regard to spacial growth rates [71]. This implies that the hydrodynamic stability for high forcing amplitudes over a broad frequency range can be modeled, if the forcing amplitude-dependent mean flow field at one particular forcing frequency is known. This has quite some practical relevance. Especially for high pressure applications, it is very difficult to realize sufficient forcing amplitudes for flame describing function measurements over a broad frequency range. The realization of high forcing amplitudes at one frequency, e.g., at a resonance frequency of the combustion system or with an actuator designed for a particular forcing frequency is much easier.

Terhaar et al. [76] confirmed that neglecting the azimuthal velocity component has only marginal influence on the results of the linear hydrodynamic stability analysis. They investigated the influence of the swirl number on the hydrodynamic stability and the flame response. A low swirl number leads to a high amplification rate of perturbations for small forcing amplitudes with a strong saturation for increased forcing, whereas for higher swirl numbers, the flow describing function features a smaller gain at low forcing amplitudes and a much less pronounced saturation for increasing forcing amplitudes. The same characteristics were observed in the associated flame describing functions.

Furthermore, they compared the changes of the mean flow field at increasing forcing amplitudes with a forced mean flow field at isothermal, non-reacting conditions and found that the later was much less changed due to the applied forcing. Hence, the change of the average flow field might be caused by the interaction of coherent structures with the strong density gradients associated with the combustion. However, saturations observed in the non-reacting flow describing function were similar to those of the reacting flow field.

Recently, Ćosić et al. [46] showed that the prediction of limit cycle oscillation amplitudes from the flame describing function with amplitude-dependent network models is also possible for an industrial relevant combustor at a high Reynolds number and technically premixed conditions. Furthermore, they investigated the sensitivity of the flame describing function on several operating parameters. Since in industrial applications, boundary conditions like mass flows are not as constant as in laboratory applications, the sensitivity of the flame describing function is crucial for a sustaining gas turbine operation. Especially fluctuations in the air mass flow lead to significant changes in the flame describing function, which must be taken into account when estimating the thermoacoustic stability of a combustion system under relevant conditions.

In another study, Ćosić et al. [77] investigated the interplay of equivalence ratio fluctuations and the amplification of coherent structures in the flow on the flame describing function. They decomposed the flame describing function in two parts, one related to equivalence ratio fluctuations and one related to coherent structures and investigated both while varying the degree of fuel unmixedness. They found that the interaction is rather a one way effect. The amplifying characteristics of the hydrodynamic flow field and the shear layers remain rather unchanged when the combustion operation is gradually changed from a technically premixed to perfectly premixed mode. In contrast, they found that equivalence ratio fluctuations were significantly attenuated by the coherent structures and the associated increased mixing, which led to a saturation even at relatively small forcing amplitudes in the equivalence ratio related part of the flame describing function. Furthermore, they emphasized that variations in the mean flame position may change the phase lags of the two mechanisms and alter the interference of the two mechanisms having substantial influence on the flame describing function.

5.4.1 Summary

The flame describing function for an industrial sized swirl-stabilized, perfectly premixed, atmospheric combustor at high Reynolds numbers has been measured and the flow field and flame dynamics were analyzed by OH^* chemiluminescence, LDA, PIV and microphone measurements.

Especially for low frequencies, the mode conversion effect was observed to lead to strong fluctuations in flame angle. An axial displacement larger than the acoustic displacement due to acoustic forcing and associated deformations of the flame front was observed without causing nonlinearities in the flame describing function.

A systematic increase of the thickness of the shear layers of the annular jet due to entrainment with increasing forcing amplitudes was observed at all frequencies. Since the flame

is confined by the combustion chamber walls, the diameter of the inner recirculation zone was found to be squeezed gradually. A downstream movement of the fluctuating region of the reaction zone and an increase of the axial expansion of the flame due to the decreased volume of the inner recirculation zone was observed, leading to an increase of the convective time delays of the flame. Amplitude-dependent changes of the phase of the flame describing function are of high importance, since they may alter the stability of the combustion system. Furthermore the increased axial expansion of the flame was found to enhance the low pass character of the flame, which may lead to the establishment of limit cycles, especially at high frequencies.

A hydrodynamic stability analysis was applied to the unforced and forced mean flow field in the combustor. Although the approach has significant simplifications, the results obtained reproduce several characteristics of the flow. The measured distribution of coherent kinetic energy in the forced system agrees very well with the predictions of the analysis. The flow describing function representing the amplification of coherent structures in the shear layers was found to qualitatively agree very well with the flame describing function. Thus, it is assumed that the change of the amplification of coherent structures in the shear layers due to the change of the mean flow field is a key mechanism in understanding and predicting flame describing functions. The driving mechanism can be summarized as follows: Coherent structures generated upstream of the flame are amplified by the shear layers of the annular jet. With increasing forcing amplitude, associated entrainment thickens the shear layers, leading to a decreased instability of the shear layers and a saturation of the amplification of coherent structures. A number of recent studies confirmed the assumption that the flow describing function has a direct link to the flame describing function over a broad range of frequencies and confirmed the potential of the adopted approach.

However, for a comprehensive understanding and modeling of the flame describing function, there are several further mechanisms, e.g., equivalence ratio fluctuations, mode conversion, detailed vortex flame interaction or flame lift-off that have a strong influence and must be taken into account.

Bibliography

[1] T. C. Lieuwen and V. Yang, editors. *Combustion Instabilities in Gas Turbine Engines*. Progress in Astronautics and Aeronautics vol. 210. AIAA, Inc., Reston, VA, 2005.

[2] A. P. Dowling and S. R. Stow. Acoustic Analysis of Gas Turbine Combustors. *Journal of Propulsion and Power*, 19(5):751–764, 2003.

[3] C. O. Paschereit, B. Schuermans, V. Bellucci, and P. Flohr. Implementation of Instability Prediction in Design: ALSTOM Approaches. In T. Lieuwen and V. Yang, editors, *Combustion Instabilities in Gas Turbine Engines*, volume 210 of *Progress in Astronautics and Aeronautics*, pages 445–480. AIAA, Inc., Reston, 2005.

[4] A. P. Dowling. Nonlinear self-excited oscillations of a ducted flame. *Journal of Fluid Mechanics*, 346:271–290, 1997.

[5] N. Noiray, D. Durox, T. Schuller, and S. Candel. A unified framework for nonlinear combustion instability analysis based on the flame describing function. *Journal of Fluid Mechanics*, 615:139–167, 2008.

[6] P. Palies, D. Durox, T. Schuller, and S. Candel. Nonlinear combustion instability analysis based on the flame describing function applied to turbulent premixed swirling flames. *Combustion and Flame*, 158(10):1980–1991, 2011. ISSN 00102180. doi: 10.1016/j.combustflame.2011.02.012. URL http://dx.doi.org/10.1016/j.combustflame.2011.02.012.

[7] W. Krebs, H. Krediet, S. Hermeth, T. E. P. Poinsot, S. Schimek, and C. O. Paschereit. Comparison of Nonlinear to Linear Thermoacoustic Stability Analysis of a Gas Turbine Combustion System. *Journal of Engineering for Gas Turbines and Power*, 135(8): 081503 (8 Pages), 2013. ISSN 0742-4795 (online), 1528-8919 (print). doi: 10.1115/1.4023887.

[8] B. B. Bellows, M. K. Bobba, A. Forte, J. M. Seitzmann, and T. Lieuwen. Flame transfer function saturation mechanisms in a swirl-stabilized combustor. *Proceedings of the Combustion Institute*, 31:3181–3188, 2007.

[9] R. Balachandran, B. O. Ayoola, C. F. Kaminski, A. P. Dowling, and E. Mastorakos. Experimental investigation of the nonlinear response of turbulent premixed flames to imposed inlet velocity oscillations. *Combustion and Flame*, 143(1–2):37–55, 2005.

[10] F. Culick. *DYNAMICS OF COMBUSTION SYSTEMS : FUNDAMENTALS , ACOUSTICS , AND CONTROL*. Number September. California Institute of Technology, 2001.

[11] B. Schuermans, W. Polifke, C. O. Paschereit, and J. H. van der Linden. Prediction of Acoustic Pressure Spectra in Combustion Systems Using Swirl Stabilized Gas Turbine Burners. In *Proceedings of ASME Turbo Expo 2000 - 2000-GT-0105*, 2000.

[12] T. C. Lieuwen, H. Torres, C. Johnson, and B. T. Zinn. A Mechanism of Combustion Instability in Lean Premixed Gas Turbine Combustors. *Journal of Engineering for Gas Turbines and Power*, 123(1):182–189, 2001.

[13] K. Thumuluru S. and T. Lieuwen. Characterisation of acoustically forced swirl flame dynamics. *Proceedings of the Combustion Insitute*, 32:2893–2900, 2009.

[14] P. Palies, T. Schuller, D. Durox, and S. Candel. Modeling of premixed swirling flames transfer functions. *Proceedings of the Combustion Institute*, 33:2967–2974, 2011.

[15] P. Palies, D. Durox, T. Schuller, and S. Candel. The combined dynamics of swirler and turbulent premixed swirling flames. *Combustion and Flame*, 157(9):1698–1717, 2010. ISSN 0010-2180. doi: DOI:10.1016/j.combustflame.2010.02.011.

[16] T. J. Poinsot, A. C. Trouvé, D. P. Veynante, S. M. Candel, and E. J. Esposito. Vortex-driven acoustically coupled combustion instabilities. *Journal of Fluid Mechanics*, 177: 265–292, 1987.

[17] C. A. Armitage, R. Balachandran, E. Mastorakos, and R. S. Cant. Investigation of the nonlinear response of turbulent premixed flames to imposed inlet velocity oscillations. *Combustion and Flame*, 146:419–436, 2006.

[18] A. A. Peracchio and W. M. Proscia. Nonlinear Heat-Release/Acoustic Model for Thermoacoustic Instability in Lean Premixed Combustors. *Journal of Engineering for Gas Turbines and Power*, 121(3):415, 1999.

[19] B. Schuermans, V. Bellucci, F. Guethe, F. Meili, P. Flohr, and C. O. Paschereit. A Detailed Analysis of Thermoacoustic Interaction Mechanisms in a Turbulent Premixed Flame. In *Proceedings of ASME Turbo Expo 2004 - GT2004-53831*, 2004.

[20] A. Michalke. On spatially growing disturbances in an inviscid shear layer. *Journal of Fluid Mechanics*, 23(03):521, mar 2006. ISSN 0022-1120. doi: 10.1017/S0022112065001520. URL http://journals.cambridge.org/abstract_S0022112065001520.

[21] J. Cohen and I. Wygnanski. The evolution of instabilities in the axisymmetric jet. Part 1. The linear growth of disturbances near the nozzle. *Journal of Fluid Mechanics*, 176(-1):191, apr 2006. ISSN 0022-1120. doi: 10.1017/S0022112087000624. URL http://journals.cambridge.org/abstract_S0022112087000624.

[22] D. Barkley. Linear analysis of the cylinder wake mean flow. *Europhysics Letters (EPL)*, 75(5):750–756, sep 2006. ISSN 0295-5075. doi: 10.1209/epl/i2006-10168-7. URL http://iopscience.iop.org/article/10.1209/epl/i2006-10168-7.

[23] K. Oberleithner, M. Sieber, C. N. Nayeri, C. O. Paschereit, C. Petz, H.-C. Hege, B. R. Noack, and I. Wygnanski. Three-dimensional coherent structures in a swirling jet undergoing vortex breakdown: stability analysis and empirical mode construction. *Journal of Fluid Mechanics*, 679:383–414, may 2011. ISSN 0022-1120. doi: 10.1017/jfm.2011.141. URL http://journals.cambridge.org/abstract_S0022112011001418.

[24] J. O'Connor and T. Lieuwen. Further Characterization of the Disturbance Field in a Transversely Excited Swirl-Stabilized Flame. *Journal of Engineering for Gas Turbines and Power*, 134(1):011501, jan 2012. ISSN 07424795. doi: 10.1115/1.4004186. URL https://gasturbinespower.asmedigitalcollection.asme.org/article.aspx?articleID=1429666.

[25] P. Paredes, S. Terhaar, K. Oberleithner, V. Theofilis, and C. Oliver Paschereit. Global and Local Hydrodynamic Stability Analysis as a Tool for Combustor Dynamics Modeling. *Journal of Engineering for Gas Turbines and Power*, 138(2):021504, sep 2015. ISSN 0742-4795. doi: 10.1115/1.4031183. URL http://gasturbinespower.asmedigitalcollection.asme.org/article.aspx?articleid=2423628.

[26] J. P. Moeck, J.-F. Bourgouin, D. Durox, T. Schuller, and S. Candel. Nonlinear interaction between a precessing vortex core and acoustic oscillations in a turbulent swirling flame. *Combustion and Flame*, 159(8):2650–2668, aug 2012. ISSN 00102180. doi: 10.1016/j.combustflame.2012.04.002. URL http://www.sciencedirect.com/science/article/pii/S0010218012001216.

[27] S. Schimek, J. P. Moeck, and C. O. Paschereit. Design of a combustion test rig with high amplitude forcing capabilities for nonlinear flame transfer function measurements. In *Proceedings of the 16th International Congress on Sound and Vibration*, 2009.

[28] J. P. Moeck. *Analysis, Modeling, and Control of Thermoacoustic Instabilities*. PhD thesis, Technische Universität Berlin, 2010.

[29] B. Schuermans. *Modeling and Control of Thermoacoustic Instabilities*. PhD thesis, École Polytechnique Fédéral de Lausanne, 2003.

[30] F. E. C. Culick. *Unsteady Motions in Combustion Chambers for Propulsion Systems*. NATO/RTO, 2006.

[31] S. W. Rienstra and A. Hirschberg. *An Introduction to Acoustics*. Eindhoven University of Technology, 2006. URL http://www.win.tue.nl/$\sim$sjoerdr/papers/boek.pdf.

[32] T. Lieuwen. *Combustion instabilities in gas turbine engines: operational experience, fundamental mechanisms and modeling*. AIAA Inc., Reston, VA, Progress in Astronautics and Aeronautics, 210, pp. 445-480, 2005.

[33] M. R. Bothien. *Impedance Tuning: A Method for Active Control of the Acoustic Boundary Conditions of Combustion Test Rigs*. PhD thesis, Technische Universität Berlin, 2008.

[34] H. Levine and J. Schwinger. On the Radiation of Sound from an Unflanged Circular Pipe. *Physical Review*, 73(4):383–406, 1948.

[35] F. Silva, P. Guillemaina, J. Kergomarda, B. Mallaronia, and A. N. Norrisb. Approximation formulae for the acoustic radiation impedance of a cylindrical pipe. *Journal of Sound and Vibration*, 322:255–263, 2009.

[36] W. E. Zorumski. Generalized radiation impedances and reflection coefficients of circular and annular ducts. *Journal of the Acoustical Society of America*, 54:1667–1673, 1973.

[37] A. M. G. Gentemann, A. Fischer, S. Evesque, and W. Polifke. Acoustic Transfer Matrix Reconstruction and Analysis for Ducts with Sudden Change of Area. In *9th AIAA/CEAS Aeroacoustics Conference and Exhibit, 2003, South Carolina.*

[38] A. Fischer. *Hybride, thermoakustische Charakterisierung von Drallbrennern.* PhD thesis, Lehrstuhl für Thermodynamik, TU München, 2004.

[39] J. J. Keller. Thermoacoustic Oscillations in Combustion Chambers of Gas Turbines. *AIAA Journal*, 33(12):2280–2287, 1995.

[40] A. Huber and W. Polifke. Impact of Fuel Supply Impedance on Combustion Stability of Gas Turbines. In *Volume 3: Combustion, Fuels and Emissions, Parts A and B*, pages 887–899. ASME, jan 2008. ISBN 978-0-7918-4313-0. doi: 10.1115/GT2008-51193. URL http://proceedings.asmedigitalcollection.asme.org/proceeding.aspx?articleid=1624044.

[41] Y. Huang and V. Yang. Dynamics and stability of lean-premixed swirl-stabilized combustion. *Progress in Energy and Combustion Science*, 35(4):293–364, 2009. ISSN 03601285. doi: 10.1016/j.pecs.2009.01.002. URL http://dx.doi.org/10.1016/j.pecs.2009.01.002.

[42] S. R. Stow and A. P. Dowling. LOW-ORDER MODELLING OF THERMOACOUSTIC LIMIT CYCLES. *Proceedings of ASME TURBO EXPO 2004 Power for Land, Sea, and Air June 1417, 2004, Vienna, Austria - GT2004-54245*, 2004.

[43] S. M. Candel and T. J. Poinsot. Flame Stretch and the Balance Equation for the Flame Area. *Combustion Science and Technology*, 70(1-3):1–15, 1990. ISSN 0010-2202. doi: 10.1080/00102209008951608.

[44] P. Palies, D. Durox, T. Schuller, and S. Candel. Swirling Flame Dynamics and Describing Function. In *48th AIAA Aerospace Sciences Meeting Including the New Horizons Forum and Aerospace Exposition*, Reston, Virigina, jan 2010. American Institute of Aeronautics and Astronautics. ISBN 978-1-60086-959-4. doi: 10.2514/6.2010-431. URL http://arc.aiaa.org/doi/10.2514/6.2010-431.

[45] T. Komarek and W. Polifke. Impact of Swirl Fluctuations on the Flame Response of a Perfectly Premixed Swirl Burner. *Journal of Engineering for Gas Turbines and Power*, 132(6):061503, 2010. ISSN 07424795. doi: 10.1115/1.4000127.

[46] B. Ćosić, J. P. Moeck, and C. O. Paschereit. Nonlinear Instability Analysis for Partially Premixed Swirl Flames. *Combustion Science and Technology*, 186(6):713–736, may 2014. ISSN 0010-2202. doi: 10.1080/00102202.2013.876420. URL http://www.tandfonline.com/doi/abs/10.1080/00102202.2013.876420.

[47] Strutt, J. W. (3rd∼Baron∼Rayleigh). The Explanation of Certain Acoustical Phenomena. *Nature*, 18:319–321, 1878. doi: 10.1038/018319a0.

[48] U. Ingard. On the Theory and Design of Acoustic Resonators. *The Journal of the Acoustical Society of America*, 25(6), 1953.

[49] B. Cosic. *Nonlinear Thermoacoustic Stability Analysis of Gas Turbine Combustion Chambers*. PhD thesis, Technische Universität Berlin, 2014.

[50] T. C. Lieuwen. Experimental Investigation of Limit-Cycle Oscillations in an Unstable Gas Turbine Combustor. *Journal of Propulsion and Power*, 18(1):61–67, 2002.

[51] J. P. Moeck, M. R. Bothien, S. Schimek, A. Lacarelle, and C. O. Paschereit. Subcritical Thermoacoustic Instabilities in a Premixed Combustor. *14th AIAA/CEAS Aeroacoustics Conference (29th AIAA Aeroacoustics Conference)*, (May):1–18, 2008. doi: 10.2514/6.2008-2946.

[52] K. Balasubramanian and R. I. Sujith. Non-normality and nonlinearity in combustion–acoustic interaction in diffusion flames. *Journal of Fluid Mechanics*, 594:29–57, 2008.

[53] M. P. Juniper. Triggering in the horizontal Rijke tube: non-normality, transient growth and bypass transition. *Journal of Fluid Mechanics*, 667:272–308, 2011. ISSN 1469-7645. doi: 10.1017/S0022112010004453. URL http://journals.cambridge.org/article_S0022112010004453.

[54] K. Oberleithner. *On Turbulent Swirling Jets: Vortex Breakdown, Coherent Structures, and their Control*. PhD thesis, Technischen Universität Berlin, 2012. URL http://opus.kobv.de/tuberlin/volltexte/2012/3593/.

[55] A. K. M. F. Hussain and W. C. Reynolds. The mechanics of an organized wave in turbulent shear flow. Part 2. Experimental results. *Journal of Fluid Mechanics*, 54 (02):241, jul 1972. ISSN 0022-1120. doi: 10.1017/S0022112072000667. URL http://www.journals.cambridge.org/abstract_S0022112072000667.

[56] M. Raffel, C. E. Willert, steven Wereley, and J. Kompenhans. *Particle Image Velocimetry: A Practical Guide*. 2013. ISBN 3662036371. URL https://books.google.com/books?hl=de&lr=&id=v3r1CAAAQBAJ&pgis=1.

[57] C. Tropea, A. L. Yarin, and J. F. Foss. *Springer Handbook of Experimental Fluid Mechanics, Band 1*. 2007. ISBN 3540251413. URL https://books.google.com/books?hl=de&lr=&id=y0xDUAdQAlkC&pgis=1.

[58] F. Güthe and B. Schuermans. Phase-locking in post-processing for pulsating flames. *Measurement Science and Technology*, 18(9):3036–3042, 2007.

[59] Z.-G. Yuan. The filtered Abel transform and its application in combustion diagnostics. *NASA/CR–2003-212121*, 1995.

[60] S. M. Jaffe, J. Larjo, and R. Henberg. Abel inversion using the fast Fourier transform. In *Proceedings of the 10th International Symposium on Plasma Chemistry (ISPC'10), Bochum, Germany, August*, pages 4–9, 1991.

[61] M. L. Munjal and A. G. Doige. Theory of a two source-location method for direct experimental evaluation of the four-pole parameters of an aeroacoustic element. *Journal of Sound and Vibration*, 141:323–333, 1990.

[62] P. Palies, D. Durox, T. Schuller, P. Morenton, and S. Candel. Dynamics of premixed confined swirling flames. *Comptes Rendus Mecanique*, 337:395–405, 2009.

[63] T. Komarek and W. Polifke. Impact of Swirl Fluctuations on the Flame Response of a Perfectly Premixed Swirl Burner. *Journal of Engineering for Gas Turbines and Power*, 132(6):061503, 2010. ISSN 07424795. doi: 10.1115/1.4000127.

[64] P. Palies, T. Schuller, D. Durox, and S. Candel. Modeling of premixed swirling flames transfer functions. *Proceedings of the Combustion Institute*, 33(2):2967–2974, 2011. ISSN 15407489. doi: 10.1016/j.proci.2010.06.059. URL http://dx.doi.org/10.1016/j.proci.2010.06.059.

[65] C. Külsheimer and H. Büchner. Combustion dynamics of turbulent swirling flames. *Combustion and Flame*, 131(1-2):70–84, oct 2002. ISSN 00102180. doi: 10.1016/S0010-2180(02)00394-2. URL http://www.sciencedirect.com/science/article/pii/S0010218002003942.

[66] D. Durox, T. Schuller, and S. Candel. Combustion dynamics of inverted conical flames. *Proceedings of the Combustion Institute*, 30(2):1717–1724, jan 2005. ISSN 15407489. doi: 10.1016/j.proci.2004.08.067. URL http://www.sciencedirect.com/science/article/pii/S0082078404001298.

[67] B. B. Bellows, M. K. Bobba, J. M. Seitzmann, and T. Lieuwen. Nonlinear Flame Transfer Function Characteristics in a Swirl-Stabilized Combustor. *Journal of Engineering for Gas Turbines and Power*, 129:954–961, 2007.

[68] M. Stöhr, I. Boxx, C. D. Carter, and W. Meier. Experimental study of vortex-flame interaction in a gas turbine model combustor. *Combustion and Flame*, 159(8):2636–2649, aug 2012. ISSN 00102180. doi: 10.1016/j.combustflame.2012.03.020. URL http://www.sciencedirect.com/science/article/pii/S0010218012001083.

[69] K. Oberleithner, S. Terhaar, L. Rukes, and C. Oliver Paschereit. Why Nonuniform Density Suppresses the Precessing Vortex Core. *Journal of Engineering for Gas Turbines and Power*, 135(12):121506, sep 2013. ISSN 0742-4795. doi: 10.1115/1.4025130. URL http://gasturbinespower.asmedigitalcollection.asme.org/article.aspx?articleid=1742177.

[70] D. G. Crighton and M. Gaster. Stability of slowly diverging jet flow. *Journal of Fluid Mechanics*, 77(02):397, apr 1976. ISSN 0022-1120. doi: 10.1017/S0022112076002176. URL http://journals.cambridge.org/abstract_S0022112076002176.

[71] K. Oberleithner and C. O. Paschereit. MODELING FLAME DESCRIBING FUNCTIONS BASED ON HYDRODYNAMIC LINEAR STABILITY ANALYSIS. In *Proceedings of ASME Turbo Expo 2016: Turbomachinery Technical Conference and Exposition, June 13 - 17, Seoul, South Korea, in press*, 2016.

[72] J. Jeong and F. Hussain. On the identification of a vortex. *Journal of Fluid Mechanics*, 285(-1):69, apr 1995. ISSN 0022-1120. doi: 10.1017/S0022112095000462. URL http://journals.cambridge.org/abstract_S0022112095000462.

[73] H. J. Krediet, W. Krebs, S. Schimek, and C. Paschereit. IDENTIFICATION OF THE FLAME DESCRIBING FUNCTION OF A PREMIXED SWIRL FLAME FROM LES. In *MCS, Chia Laguna, Cagliari, Sardinia, Italy, September 11-15*, 2011.

[74] H. J. Krediet, C. H. Beck, W. Krebs, S. Schimek, C. O. Paschereit, and J. B. W. Kok. Identification of the Flame Describing Function of a Premixed Swirl Flame from LES. *Combustion Science and Technology*, 184(7-8):888–900, jul 2012. ISSN 0010-2202. doi: 10.1080/00102202.2012.663981. URL http://www.mendeley.com/research/identification-flame-describing-function-premixed-swirl-flame-les/.

[75] H. Krediet, C. Beck, W. Krebs, and J. Kok. Saturation mechanism of the heat release response of a premixed swirl flame using LES. *Proceedings of the Combustion Institute*, 34(1):1223–1230, jan 2013. ISSN 15407489. doi: 10.1016/j.proci.2012.06.140. URL http://www.sciencedirect.com/science/article/pii/S1540748912002489.

[76] S. Terhaar, B. Cosic, C. O. Paschereit, and K. Oberleithner. Impact of Shear Flow Instabilities on the Magnitude and Saturation of the Flame Response. *Journal of Engineering for Gas Turbines and Power*, 136(July):071502, 2014. ISSN 0742-4795. doi: 10.1115/1.4026530. URL http://gasturbinespower.asmedigitalcollection.asme.org/article.aspx?doi=10.1115/1.4026530.

[77] B. Ćosić, S. Terhaar, J. P. Moeck, and C. O. Paschereit. Response of a swirl-stabilized flame to simultaneous perturbations in equivalence ratio and velocity at high oscillation amplitudes. *Combustion and Flame*, 162(4):1046–1062, apr 2015. ISSN 00102180. doi: 10.1016/j.combustflame.2014.09.025. URL http://www.sciencedirect.com/science/article/pii/S001021801400306X.

[78] C. O. Paschereit, S. Terhaar, B. Ćosić, and K. Oberleithner. Application of linear hydrodynamic stability analysis to reacting swirling combustor flows. *Journal of Fluid Science and Technology*, 9(3):JFST0024–JFST0024, sep 2014. ISSN 1880-5558. doi: 10.1299/jfst.2014jfst0024. URL https://www.jstage.jst.go.jp/article/jfst/9/3/9_2014jfst0024/_article.

Associated Publications

Further publications are associated with the work of the author in this document. The following list gives an overview of these publications.

[1] J. P. Moeck, A. Lacarelle, and C. O. Paschereit. Subcritical Thermoacoustic Instabilities in a Premixed Combustor. *14th AIAA/CEAS Aeroacoustics Conference (29th AIAA Aeroacoustics Conference)*, (May):1–18, 2008. doi: 10.2514/6.2008-2946.

[2] S. Schimek, J. P. Moeck, and C. O. Paschereit. Design of a combustion test rig with high amplitude forcing capabilities for nonlinear flame transfer function measurements. In *Proceedings of the 16th International Congress on Sound and Vibration*, 2009.

[3] S. Schimek, J. P. Moeck, and C. O. Paschereit. AN EXPERIMENTAL INVESTIGATION OF THE NONLINEAR RESPONSE OF AN ATMOSPHERIC SWIRL-STABILIZED PREMIXED FLAME. In *Proceedings of ASME Turbo Expo 2010: Power for Land, Sea and Air, June 14 - 18, Glasgow, Scotland*, 2010.

[4] H. J. Krediet, W. Krebs, S. Schimek, and C. Paschereit. IDENTIFICATION OF THE FLAME DESCRIBING FUNCTION OF A PREMIXED SWIRL FLAME FROM LES. In *MCS, Chia Laguna, Cagliari, Sardinia, Italy, September 11-15*, 2011.

[5] S. Schimek, J. P. Moeck, and C. O. Paschereit. Experimental investigation of the influence of high amplitude forcing and swirl fuctuations on the flow field and the transfer function of a swirl-stabilized flame. In *47th AIAA/ASME/SAE/ASEE Joint Propulsion Conference and Exhibit, San Diego, California, Jul 31 – Aug 3 , AIAA paper no. 2011-5702*, 2011.

[6] S. Schimek, S. Göke, C. Schrödinger, and C. O. Paschereit. Analysis of flame transfer functions for blends of CH4 and H2 at different humidity levels. In *50th AIAA Aerospace Science Meeting, AIAA-2012-0932*, 2012. doi: 10.2514/6.2012-932.

[7] S. Schimek, S. Göke, C. Schrödinger, and C. O. Paschereit. Flame Transfer Function Measurements With CH4 and H2 Fuel Mixtures at Ultra Wet Conditions in a Swirl Stabilized Premixed Combustor. In *Proceedings of ASME Turbo Expo 2012, 1-10*. ASME, jun 2012. ISBN 978-0-7918-4468-7. doi: 10.1115/GT2012-69788. URL http://proceedings.asmedigitalcollection.asme.org/proceeding.aspx?articleid=1693939.

[8] S. Schimek, B. Ćosić, J. P. Moeck, S. Terhaar, and C. O. Paschereit. Amplitude-Dependent Flow Field and Flame Response to Axial and Tangential Velocity Fluctuations. In *Proceedings of ASME Turbo Expo 2012: Power for Land, Sea and Air, June 11 - 15, Copenhagen, Denmark*. ASME, jun 2012. ISBN 9780791844687. doi: 10.1115/GT2012-69785. URL http://proceedings.asmedigitalcollection.asme.org/proceeding.aspx?articleid=1693938.

[9] W. Krebs, H. Krediet, S. Hermeth, T. Poinsot, P. E., S. Schimek, and C. O. Paschereit. Comparison of Nonlinear to Linear Thermoacoustic Stability Analysis of a Gas Turbine Combustion System. In *Proceedings of ASME Turbo Expo 2012: Power for Land, Sea and Air, June 11 - 15, Copenhagen, Denmark*, 2012.

[10] H. J. Krediet, C. H. Beck, W. Krebs, S. Schimek, C. O. Paschereit, and J. B. W. Kok. Identification of the Flame Describing Function of a Premixed Swirl Flame from LES. *Combustion Science and Technology*, 184(7-8):888–900, jul 2012. ISSN 0010-2202. doi: 10.1080/00102202.2012.663981. URL http://www.mendeley.com/research/identification-flame-describing-function-premixed-swirl-flame-les/.

[11] K. Oberleithner, S. Schimek, and C. O. Paschereit. On the Impact of Shear Flow Instabilities on Global Heat Release Rate Fluctuations: Linear Stability Analysis of an Isothermal and a Reacting Swirling Jet. In *Proceedings of ASME Turbo Expo*. ASME, 2012. ISBN 978-0-7918-4468-7. doi: 10.1115/GT2012-69774. URL http://proceedings.asmedigitalcollection.asme.org/proceeding.aspx?doi=10.1115/GT2012-69774.

[12] W. Krebs, H. Krediet, S. Hermeth, T. E. P. Poinsot, S. Schimek, and C. O. Paschereit. Comparison of Nonlinear to Linear Thermoacoustic Stability Analysis of a Gas Turbine Combustion System. *Journal of Engineering for Gas Turbines and Power*, 135(8): 081503 (8 Pages), 2013. ISSN 0742-4795 (online), 1528-8919 (print). doi: 10.1115/1.4023887.